AD-A215 395

REPORT DOCUMENTATION PAGE

Form Approved
OMB No. 0704-0188

1. AGENCY USE ONLY (Leave blank)	2. REPORT DATE	3. REPORT TYPE AND DATES COVERED
	August 21, 1982	Annual (March 1, 1981- May 31, 1982

4. TITLE AND SUBTITLE

STRUCTURAL AND KINETIC PROPERTIES OF GRAPHITE INTERCALATION COMPOUNDS

5. FUNDING NUMBERS

61102F
2306/D2

6. AUTHOR(S)

D.D.L. Chung

7. PERFORMING ORGANIZATION NAME(S) AND ADDRESS(ES)

Department of Metallurgical Engineering and Materials Science, Carnegie-Mellon University, Pittsburgh, PA 15213

8. PERFORMING ORGANIZATION REPORT NUMBER

AFOSR-TR- 89-1630

9. SPONSORING/MONITORING AGENCY NAME(S) AND ADDRESS(ES)

AFOSR
BLDG 410
BAFB DC 20332-6448

10. SPONSORING/MONITORING AGENCY REPORT NUMBER

AFOSR-78-3536

11. SUPPLEMENTARY NOTES

12a. DISTRIBUTION/AVAILABILITY STATEMENT

Approved for public release;
distribution unlimited.

12b. DISTRIBUTION CODE

13. ABSTRACT (Maximum 200 words)

(OVER)

14. SUBJECT TERMS	15. NUMBER OF PAGES	16. PRICE CODE
	113	

17. SECURITY CLASSIFICATION OF REPORT	18. SECURITY CLASSIFICATION OF THIS PAGE	19. SECURITY CLASSIFICATION OF ABSTRACT	20. LIMITATION OF ABSTRACT
unclassified	unclassified		

NSN 7540-01-280-5500

Standard Form 298 (890104 Draft)
Prescribed by ANSI Std. 239-18

AFOSR-TR- 85-1530

20. ABSTRACT (Continue on reverse side if necessary and identify by block number)

We report the first TTT-diagram for the intercalation of graphite. The TTT-curves were C-shaped. Within the temperature range where a given stage was stable, the reaction rate increased with increasing temperature at low temperatures (suggesting a diffusion-controlled mechanism) and decreased with increasing temperature at high temperatures (suggesting an interface-controlled mechanism). Also reported is a TCT-diagram describing the dependence of theintercalation kinetics on the external intercalate concentration (i.e., Br_2 concentration in the Br_2-CCl_4 solution containing the sample). The finalstage decreased in discrete steps with increasing Br_2 concentration in the Br_2-CCl_4 solution containing the sample, but the rate of intercalation increased linearly with increasing Br_2 concentration in the solution. Although bromine intercalation by immersion in pure bromine at room temperature appears to involve direct formation of the final stage of 2, the actual progressive stage decrease toward the final stage was clearly observed by altering the relative intercalation rates of different stages by either raising the temperature or by lowering the Br_2 concentration in the Br_2-CCl_4 solution containing the sample. The intercalate front first observed by surface profilometry was found by x-ray diffraction and x-ray absorption to delineate a central region which was nearly pure graphite (except near the c-face surface) and an edge region which contained a very small amount of pure graphite.

In-plane intercalate ordering was observed for the first time in intercalated graphite fibers. This observation was made in stage 1 and stage 2 graphite-ICl based on Thornel P-100 graphite fibers and prepared by the two-bulb method, in which liquid ICl was at 95°C while graphite was at 100°C for stage 1 and 130°C for stage 2. As shown by the transmission Laue x-ray diffraction technique, the in-plane ordering was the same for stage 1 and stage 2 fibers, and for stage 1 HOPG. The unit cell was monoclinic and commensurate with graphite, as previously found by Ghosh and Chung by single crystal x-ray diffraction.

By x-ray diffraction, exfoliated graphite-Br_2 was found to exhibit the same in-plane superlattice ordering as intercalated graphite prior to exfoliation. This ordering persisted even after heating for an hour at 1700°C. By dilatometry, a single exfoliation event was found to consist of multiple expansion spurts, which occurred at ~150°C and ~240°C for first exfoliation, and ~100°C and ~240°C for subsequent cycles. The amount of expansion was found to increase with decreasing intercalate activity during intercalation. With exfoliation cycles to higher temperatures or longer times, the amount of residual expansion after the collapse on cooling increased until no second exfoliation was observed on reheating. Due to intercalate desorption, the amount of expansion for concentrated samples increased with increasing sample width; desorbed samples showed little width dependence. Acoustic emission was observed before appreciable expansion during the first exfoliation cycle; it was not observed during the collapse of subsequent exfoliation cycles. A model of exfoliation involving intercalate islands is proposed.

STRUCTURAL AND KINETIC PROPERTIES OF GRAPHITE INTERCALATION COMPOUNDS

(AFOSR-78-3536)

ANNUAL TECHNICAL REPORT

TO THE

AIR FORCE OFFICE OF SCIENTIFIC RESEARCH

BY THE

DEPARTMENT OF METALLURGICAL ENGINEERING & MATERIALS SCIENCE

CARNEGIE-MELLON UNIVERSITY

PITTSBURGH, PENNSYLVANIA 15213

Grant Period: March 1, 1981 -- May 31, 1982

Deborah Chung

Dr. D. D. L. Chung
Principal Investigator

August 21, 1982
Date

RESEARCH OBJECTIVE

The research objective is to gain a basic understanding of

(i) the process of intercalation of graphite,

(ii) the process of exfoliation of intercalated graphite.

Emphasis is given to the kinetic and the structural effects.

TABLE OF CONTENTS

STATUS OF THE RESEARCH EFFORT

Summary

We report the first TTT-diagram for the intercalation of graphite. The TTT-curves were C-shaped. Within the temperature range where a given stage was stable, the reaction rate increased with increasing temperature at low temperatures (suggesting a diffusion-controlled mechanism) and decreased with increasing temperature at high temperatures (suggesting an interface-controlled mechanism). Also reported is a TCT-diagram describing the dependence of the of the intercalation kinetics on the external intercalate concentration (i.e., Br_2 concentration in the Br_2-CCl_4 solution containing the sample). The final stage decreased in discrete steps with increasing Br_2 concentration in the Br_2-CCl_4 solution containing the sample, but the rate of intercalation increased linearly with increasing Br_2 concentration in the solution. Although bromine intercalation by immersion in pure bromine at room temperature appeared to involve direct formation of the final stage of 2, the actual progressive stage decrease toward the final stage was clearly observed by altering the relative intercalation rates of different stages by either raising the temperature or by lowering the Br_2 concentration in the Br_2-CCl_4 solution containing the sample. The intercalate front first observed by surface profilometry was found by x-ray diffraction and x-ray absorption to delineate a central region which was nearly pure graphite (except near the c-face surface) and an edge region which contained a very small amount of pure graphite.

In-plane intercalate ordering was observed for the first time in intercalated graphite fibers. This observation was made in stage 1 and stage 2 graphite-ICl based on Thornel P-100 graphite fibers and prepared by the two-bulb method, in which liquid ICl was at 95°C while graphite was at 100°C for stage 1 and 130°C for stage 2. As shown by the transmission Laue x-ray diffraction technique, the in-plane ordering was the same for stage 1 and stage 2 fibers, and for stage 1

HOPG. The unit cell was monoclinic and commensurate with graphite, as previously found by Ghosh and Chung by single crystal x-ray diffraction.

A. Intercalation Methods

Intercalation mostly occurs on exposure of graphite to the intercalate vapor or liquid; this is known as spontaneous intercalation[1]. For some intercalates, intercalation can be made to occur electrolytically by using graphite as an electrode. Spontaneous intercalation is by far more versatile than electrolytic intercalation, although there are some intercalates which require electrolytic intercalation. During the past years, a number of spontaneous intercalation methods have emerged, so that it is of value to systematize them.

Listed in Table 1 are the various intercalation methods, which differ in the parameter(s) used to control the eventual stage. These methods are described below.

1. Temperature method

In the temperature method, either the sample temperature or the intercalate reservoir temperature (which controls the intercalate vapor pressure) or both is/are varied to control the eventual stage.

(a) Two-bulb method I

In the two-bulb method I, the sample temperature is varied to control the eventual stage, while the intercalate vapor pressure is fixed. This is the most popular method, which was originally developed for the intercalation of alkali metals[2]. The sample temperature should be kept higher than the intercalate reservoir temperature to avoid condensation of the intercalate on the sample.

(b) Two-bulb method II

In the two-bulb method II, the intercalate vapor pressure is varied by changing the temperature of the intercalate reservoir. This variation is used to control the eventual stage. This method was originally developed

for the intercalation of alkali metals, but has also been applied to the intercalation of Br_2[3], $FeCl_3$[4], AsF_5[5], etc.

(c) One-bulb method

In the one-bulb method, both the sample and the intercalate reservoir are kept at the same temperature. Thus, an increase in sample temperature necessarily increases the intercalate vapor pressure. This method is experimentally simpler than the two-bulb methods because it requires only one temperature. It has been applied for the intercalation of $FeCl_3$[6], SbF_5[7], AsF_5[8], MF_6 (M=Os, Ir, As)[9], etc. In this work, the one-bulb method was applied for the first time to prepare various stages of graphite-Br_2.

2. Solution method

In the solution method, the intercalate is dissolved in a certain solvent which does not intercalate. The concentration of the intercalate in the solvent is used to control the eventual stage. This method was first used by Hennig to prepare graphite-Br_2 residue compounds with Br_2-CCl_4 solution.[3] In this work, the use of this method to prepare various stages of graphite-Br_2 was established. The solution method has also been applied for the intercalation of HNO_3 (with fuming nitric acid + concentrated nitric acid)[10] and Li (with Li-Na alloy)[11].

3. Limited reactant method

In the limited reactant method, the amount of intercalate (reactant) used is limited to a specific value to give a chosen eventual stage. This method has been applied to the intercalation of K[12], $SnCl_4$[13], etc. Two means of excitation have been used to initiate intercalation. The more common way is heating, as used for K intercalation[12]. The newer way is the use of light (i.e., the photochemical method), as used for $SnCl_4$ intercalation[13].

4. Limited time method

In the limited time method, the time of intercalation is limited to a specific value in order to give a chosen stage, which forms prior to the eventual stage. This method is mostly used for AsF_5 intercalation[14]. Because of the possible coexistence of stages prior to the formation of the final stage, this method often does not give a pure stage.

In the case of Br_2 intercalation, the two-bulb method II is perhaps the most popular, but it suffers from its slow kinetics. In this method, the Br_2 vapor pressure is controlled by the temperature of the Br_2 reservoir, while the sample temperature is typically room temperature. The vapor pressure P_{Br_2} of pure bromine is given by[15]

$$\log_{10} P_{Br_2} = \begin{cases} 5.82 - \dfrac{638.25}{T + 158.006} & -48°C<T<58.2°C \\ 7.583 - \dfrac{1562.26}{T + 273.78} & 70°C<T<110°C, \end{cases} \quad (1)$$

where P_{Br_2} is pressure in mm Hg and T is temperature in °C.

Closely related to this method is the solution method, in which the Br_2 vapor pressure is controlled by the concentration of Br_2 in a Br_2-CCl_4 solution. Both the solution and the sample are typically at room temperature. The relatively fast kinetics of the solution method is because the sample is usually immersed in the solution (i.e., liquid-phase intercalation) rather than being exposed in the vapor only (i.e., vapor-phase intercalation). The vapor pressure P_{sol} above the Br_2-CCl_2 solution is related to the vapor pressure P_{Br_2} of pure bromine and the mole fraction X of Br_2 in the solution by the relation[16]

$$\ln \left(\frac{P_{sol}}{P_{Br_2} X} \right) = 1.197 (1-X)^2 - 0.493 (1-X)^3 \quad (2)$$

Shown in Fig. 1 are x-ray diffraction patterns obtained with Cuka radiation showing the 00ℓ lines in various stages prepared from highly oriented pyrolytic graphite (HOPG) by the solution method. The second stage was prepared by immersion in pure liquid bromine (X=1) at room temperature; the third stage was prepared by immersion in Br_2-CCl_4 with X=0.2 at room temperature; the fourth stage was prepared by immersion in Br_2-CCl_4 with X=0.15. The c-axis periodicity was thus found to be 10.38 Å, 13.73 Å and 16.9±0.2 Å for stages 2, 3 and 4, respectively. These values are in agreement with those of corresponding stages prepared by the two-bulb method II.[17]

In the solution method, the eventual stage number increases with decreasing X and the rate of intercalation also decreases with decreasing X, so the preparation of high stages takes quite a long time (e.g., a few days for samples that are a few m wide). On the other hand, in the one-blub method, the eventual stage number increases with increasing temperature and the rate of intercalation also increases with increasing temperature, so the preparation of high stages takes even less time than the lowest stage. Therefore, the one-blub method is particularly convenient for high stages. In this work, the one-bulb method was applied for the first time to prepare various stages of graphite-br_2. Shown in Fig. 2 are x-ray diffraction patterns obtained with CuKα radiation showing the 00ℓ lines in samples prepared by the one-bulb method. The second stage was prepared by immersion in pure liquid bromine at room temperature; the third stage was prepared by immersion in pure bromine in 105°C. The c-axis periodicity was 10.38 Å and 13.73 Å for stages 2 and 3, respectively. These values are close to those of the corresponding stages prepared by the solution method.

It is possible to combine the solution method and the one-blub method by adjusting both the temperature and X. Shown in Fig. 3 is the x-ray diffraction

pattern of stage 4 prepared by immersion in Br_2-CCl_4 (X=0.5) at 105°C. This combined method allows investigation of the dependence of the eventual stage on the sample temperature and the vapor pressure. Such an investigation will yield the pressure-temperature phase diagram, which can be analyzed to give the enthalpy and entropy of the transformation from one stage to another. The determination of the phase diagram is presently in progress.

Also shown in Fig. 3 is the x-ray diffraction pattern of pure graphite (HOPG). Comparison of the linewidths of the diffraction peaks of various samples in Fig. 1-3 shows that the linewidths of the superlattice lines and the pure graphite lines (at similar 2θ angles) are approximately the same for stage 2, and that the linewidths of the superlattice lines increase slightly with increasing stage number. The linewidths thus indicate that the graphite-Br_2 samples prepared by both the solution method and the one-blub method are well-staged.

B. Intercalation Kinetics

An extensive investigation has been carried out on the kinetics of intercalation of bromine in HOPG. This section considers (i) intercalate fronts, (ii) stage evolution, and (iii) mechanism.

Intercalate Fronts

Revealed by optical microscopy

An indication of the progress of intercalation is the deformation of the sample shape or surface profile during intercalation. The shape deformation known as the "ash tray effect" accompanies the intercalation of graphite for most intercalates. This effect involves the sharp bending of the graphite layers at the intercalate front due to the large thickness increase in the region behind the intercalate front.[18]

As the deformation of the basal surface does represent the presence of intercalation,[19] we have used this deformation to observe in situ the growth of the intercalation compound by using an optical microscopy. For this observation, the solution method was used at room temperature in the vapor phase. The sample was positioned in a glass bottle containing a Br_2-CCl_4 solution such that the c-face was perpendicular to the incident light beam. The bottle was sealed and placed under an optical microscope. The sample surface was photographed in situ at different times of intercalation. Due to the specular surface of HOPG, under perpendicular lighting, undeformed regions reflect the light back upon itself while deformed regions scatter the light out of the field of view. In short, flat regions are bright and bent regions are dark. Figure 4 shows optical micrographs of a sample after different times of intercalation at X=0.15, together with the schematic surface profiles. The eventual stage was 4. By this optical method, the deformed region was quite sharply delineated and could be seen to propagate toward the center of the sample.

Figure 5 is a plot of the width of the deformed (edge) region behind the intercalate front as a function of time during intercalation. It can be seen from Fig. 5 that the deformed region grew quickly initially, followed by a region where growth was of apparently constant velocity, in agreement with the results of ex situ surface profilometry.[18] The constant velocity suggests interface-controlled growth.[18,20] On the other hand, these data can be plotted as a function of the square root of time, as shown in Fig. 6. That this plot is quite linear suggests the intercalate growth to be diffusion-controlled. Comparison of Fig. 5 and Fig. 6 indicates that the overall linear fit is better in Fig. 6, so that the diffusion-controlled mechanism is probably the case for this intercalation condition. However, based on these figures alone, the interface-controlled mechanism cannot be ruled out. To better elucidate the mechanism, a study of the temperature dependence of the intercalation rate was performed, as described later in this section, where the TTT-diagram was found to support the diffusion-controlled mechanism for intercalation at room temperature.

Revealed by x-ray absorption

The x-ray absorption technique gives more information than the optical microscopic observation of the intercalate front. This is because the amount of x-ray absorbed is related to the bromine concentration. Due to the large difference in atomic mass between carbon and bromine, x-ray absorption gives a rather accurate determination of the bromine concentration. The absorption measurement was performed in the transmission geometry. Hence, the whole sample thickness was analyzed at any one time, irrespective of the surface topography.

The x-ray radiation used was CuKα. The x-ray beam was collimated by a slit of size 0.01mm x 2mm. The sample was mounted so that the middle

of its long edge intersected the beam. It was translated through the beam on a motor driven micrometer stage, such that the direction of translation was along the long edge of the sample. The transmitted beam intensity was measured as the total number of counts detected within a counting interval. Counting started before the beam impinged upon the sample and continued after the sample left the beam in order to determine the incident beam intensity. A 0.1mm receiving slit was located behind the sample. A graphite monochromator tuned to CuKα was located behind this slit.

Shown in Fig. 7(a) is the intercalate concentration profile across the c-face obtained after 297 hr of room temperature intercalation in liquid bromine. This intercalation condition yields a final stage of 2. The sample was of size 12mm x 12mm x 0.15mm and weighed 50 mg before intercalation. The intercalation was interrupted intermittantly for x-ray analysis. The average weight loss due to intercalate desorption was 2 mg during each interruption, which typically lasted ~1.5 hr. The vertical axis in Fig. 7(a) describes the intercalate concentration in terms of the stage number. For example, the intercalate concentration corresponding to that of pure stage 2 is labeled "2" in the vertical axis; similarly the intercalate concentration corresponding to that of pure stage 3 is labeled "3" in that axis. Figure 7(a) shows that the concentration changed from a region of nearly pure stage 2 to a region of negligible intercalate concentration over a narrow spatial region. This front moved inward as intercalation proceeded. This is consistent with the surface deformation of the sample during intercalation.

Revealed by x-ray diffraction

X-ray diffraction was performed by using a θ-2θ x-ray powder diffractometer. The 00ℓ diffraction pattern was obtained from the basal plane, with the

rectangular cross-section of the x-ray beam perpendicular to the long edge of the sample. The CuKα radiation was used. For diffraction at selected areas of a sample, lead or tantalum foil was used to mask the area at which diffraction was not desired. For a typical sample of width 4mm, the diffraction pattern of the central 2-mm wide portion of the sample was obtained by masking the remaining regions near the two long edges of the sample. Similarly, the diffraction pattern of the two edge regions (each edge region being 1mm wide) was obtained by masking the central 2-mm wide portion of the sample. Diffraction patterns were typically taken for a 2θ range of 15 to 25°C. This range allowed the diffraction run to be obtained in a reasonable length of time while showing the strongest superlattice lines not coincident with the graphite lines. Though a monochromator was used, the graphite (002) line due to the K_β radiation was quite pronounced. No attempt was made to measure the graphite (002) K_α line because its intensity was so high that it overloaded the detector.

To indicate the relative depths from the basal surface of different stages present within a sample during intercalation, diffraction patterns were obtained with both CuKα and MoKα radiations on a 12mm x 12mm x 0.15mm HOPG sample, which was intercalated in pure bromine at room temperature and removed for analysis intermittantly. The MoKα radiation, having a higher energy than CuKα, yields a greater penetration distance. Hence phases farther from the surface can contribute more to the diffraction pattern obtained with MoKα than is the case with CuKα. Selected area x-ray diffraction was also done on this sample; masking was such as to allow observation of either 4mm of the center region or 4mm of the two edge regions combined (i.e., 2mm of each edge region).

X-ray diffraction patterns obtained from the "center" and "edge" regions are shown in Fig. 7(b) and (c) for CuKα and MoKα radiations, respectively. The widths of the center and edge regions are indicated in Fig 7(a). Each diffraction peak in Fig. 7(b) and (c) is labeled by the ℓ index of the (00ℓ) Miller indices with the subscript indicating the stage (G indicating graphite) and the superscript, if present, indicating the $K\alpha_1$, $K\alpha_2$ or KS component. The difference between Fig. 7(b) and (c) illustrates the depth dependence of the stage distribution. Figure 7(b) and (c) show that the edge region is predominantly stage 2, whereas the center region is predominantly graphite, except that the center region near the surface has a considerable amount of stage 2. In other words, there is a significant depth dependence of the stage distribution in the center region.

Effect on weight measurement

Shown in Fig. 8 is the plot of weight uptake against the square root of time during room temperature intercalation by immersion of the samples in Br_2-CCl_4 solutions of various concentrations ranging from 5 mol % Br_2 to 50 mol % Br_2. The weight measurement was carried out ex situ by using a Perkin-Elmer AD-2Z Autobalance. X-ray analysis was performed on the samples immediately after each weight measurement. The curves in Fig. 5 are quite linear for the first half of the time axis and they deviate from linearity at long intercalation times. This deviation from linearity is attributed to be due to the meeting of the intercalate fronts at the center of the sample. When the fronts met, the intercalation rate changed. The meeting of the fronts was indeed observed by x-ray absorption at roughly the times when the weight curves deviate from linearity.

Stage Evolution

The stage evolution that leads to the formation of a pure eventual stage is fundamental to elucidation of the kinetics of intercalation. This process has been investigated for (i) the solution method, and (ii) the one-bulb method.

Solution method

Shown in Fig. 9 are representative intercalate concentration profiles (obtained by x-ray absorption) and x-ray diffraction patterns of the edge and center regions at different times during intercalation by immersion in a 50 mol % Br_2 Br_2-CCl_4 solution at room temperature. After 34 hr of intercalation, there was not much evidence for appreciable intercalation in the center region, which was ahead of the intercalate front, although some weak stage 3 and stage 4 superlattice (00ℓ) lines were observed. On the other hand, the edge region was mainly stage 2, which coexisted with smaller quantities of stage 3, stage 4 and graphite. After 210 hr of intercalation, the fronts had met, the stage 4 and graphite components in the edge region had disappeared, the stage 4 and stage 3 components in the center region had grown, a stage 2 component had appeared in the center region, and the graphite component had greatly diminished in the center region. After 1187 hr of intercalation, the concentration profile was flat, indicating that intercalation was essentially complete. Furthermore, both the edge and center regions were almost pure stage 2, which was the final stage for this intercalation condition. In addition to the major intercalate front (also referred to as "the first front") ahead of which was mainly pure graphite, a second front was observed behind the first front as shown in Fig. 9. Both the first and second fronts moved toward the center during intercalation, but they progressed at different rates. Of interest is that the shoulder in the concentration profile between the first and second fronts occurred at a concentration roughly corresponding to that of pure stage 3. Also note that

the maximum in each concentration profile approximately corresponds to the concentration of pure stage 2. It is probable that the shoulder was due to the completion of intercalating the whole sample thickness to stage 3, so that the region between the maximum and the shoulder consisted of a mixture of stages 2 and 3. However, x-ray diffraction at this small area was not carried out to confirm this hypothesis. In some cases, a third front was also observed, though it was not as clear as the first and second fronts.

Representative concentration profiles and diffraction patterns obtained after 600 hr of intercalation in various concentrations of Br_2-CCl_4 solutions at room temperature are shown in Fig. 10. After 600 hr of intercalation in a 15 mol % Br_2 solution, stage 4 was the main phase present. Because the first fronts had not met, pure graphite was also present in the center region. After 600 hr of intercalation in a 25 mol % Br_2 solution, stage 3 was dominant in the edge region and stage 4 was dominant in the center region. Because the fronts had met, pure graphite was absent. After 600 hr of intercalation in a 30 mol % Br_2 solution, stage 3 was dominant in both the center and the edge regions. Note the presence of the second front in Fig. 10. The second front was clearest for external intercalate concentrations near the limits for giving a certain final stage, such as 40 mol % Br_2 (final stage = 2) and 15 mol % Br_2 (final stage = 3). The latter is one of the concentrations shown in Fig. 10. Refer to Table 3 for these limits.

The stage evolution during intercalation is illustrated in Table 2 for two representative external intercalate concentrations (50 and 20 mol % Br_2). The table lists the stages present in the edge and center regions at various intercalation times, together with the percentage weight gain at each time. The symbol denoting the main phase (indicated by the stage number or G for graphite) was underlined. Note that the center region was always taken as the central 2-mm wide region, irrespective of the front

position. For the case of the 50 mol % Br_2 solution, stage 2 was the final stage, which was attained as a pure stage after 663-1182 hr of intercalation. Before this, stages 3 and 4 and pure graphite were also observed. Stage 2 was the dominant stage at all times in the edge region, whereas stages 4, 3 and 2 were successively dominant in the center region. The pure graphite phase was dominant in the edge region for the first 15-24 hr of intercalation, whereas it was dominant in the center region for the first 140-210 hr of intercalation. For the case of the 20 mol % Br_2 solution, stage 3 was the final stage, which was attained as a pure stage after 667-1812 hr of intercalation. Before this, stages 4 and 5 and pure graphite were also observed. Pure graphite, stage 4 and stage 3 were successively the dominant stage in both the edge and center regions. However, the pure graphite phase was dominant in the edge region for the first 63-66 hr of intercalation, whereas it was dominant in the center region for the first 355-667 hr of intercalation. Shown in Table 2 is the coexistence of stages higher than the eventual stage. This behavior is in contrast to that in K intercalation, where little stage coexistence occurs during the progressive stage decrease toward the eventual stage.[21]

Table 3 compares the stage obtained after 468 - 689 hr of intercalation for various external intercalate concentrations. Also indicated in Table 2 are the final stages for the various concentrations. For a final stage of 2, concentrations above ~40 mol % Br_2 is required; for a final stage of 3, concentrations from 15 to 30 mol % Br_2 are appropriate.

Both Table 2 and Fig. 7 show that the intercalation involved a progressive decrease in the stage number rather than the direct formation of the final stage. However, the higher the external intercalate concentration, the more it appears to be direct final stage formation.

The dependence of the intercalation rate on the external intercalate concentration is summarized in the temperature-concentration-transformation (TCT) diagram in Fig. 11. The curves there give the times for a certain stage to start forming and to finish forming, so that the curves separate regions in the diagram corresponding to the coexistence of different combinations of phases, which are indicated by the stage number or G for the pure graphite phase. To see how the phases evolve during intercalation at a particular external intercalate concentration, the TCT-diagram should be read horizontally from left to right. The normalized time in the horizontal scale in Fig. 11 is the time divided by the square of the width behind the first front, so that its unit is s/cm^2. For example, at a mole fraction of 0.2 for the Br_2 concentration in the Br_2-CCl_4 solution, stage 4 began forming after $\sim 7 \times 10^4$ s/cm^2, stage 3 began forming after $\sim 2 \times 10^5$ s/cm^2, stage 4 finished forming after $\sim 4 \times 10^7$ s/cm^2 and stage 3 finished forming after $\sim 3 \times 10^8$ s/cm^2. As a result, pure graphite was the only phase observed before $\sim 7 \times 10^4$ s/cm^2, stage 4 and graphite coexisted from $\sim 7 \times 10^4$ s/cm^2 to $\sim 2 \times 10^5$ s/cm^2, stage 3, stage 4 and graphite coexisted from $\sim 2 \times 10^5$ s/cm^2 to $\sim 4 \times 10^7$ s/cm^2, stages 3 and 4 coexisted (without graphite) from $\sim 4 \times 10^7$ s/cm^2 to $\sim 3 \times 10^8$ s/cm^2, and stage 3 (the final stage) was present alone after $\sim 3 \times 10^8$ s/cm^2, which was when intercalation was complete. The horizontal bands in Fig. 11 separate the different ranges of mole fraction which give different final stages. These ranges are also given in Table 3. Because of the significant error involved in measuring the time when a certain stage higher than the final stage just began to form, the error bars for such data points probably extend to the left more than indicated, as implied by the arrows pointing to the left for such error bars in Fig. 11. The other curves are more accurate; each error bar covers the data points obtained from the results of x-ray diffraction, x-ray absorption and optical microscopy.

One-bulb method

X-ray diffraction and x-ray absorption were also used ex situ to follow the intercalate concentration profiles and stage evolution during intercalation at various constant temperatures from room temperature to 140°C. Intercalation was performed by immersion of the sample in pure bromine sealed in a Monel ampoule, such that the sample and bromine were at the same temperature, which was controlled by a water bath.

Shown in Fig. 12 are a series of x-ray diffraction patterns obtained after 2 hr of Br_2 intercalation at various temperatures toward a final stage of 2. Samples were intercalated in liquid bromine. They were 4 mm x 14 mm x 0.5 mm and mounted so that the full 4 mm width was in the x-ray beam. Due to the deformation caused by intercalation, quantitative intensity measurements could not be made. Nonetheless, the dependence on temperature can be clearly seen in Fig. 12 . At 25°C, essentially only stage 2 was observed after 2 hr; above 30°C, increasing amounts of stage 3 were observed, till at 50°C, no stage 2 peak was evident after 2 hr. However, the final stage was pure stage 2 for all the temperatures from 25°C to 50°C, as shown by x-ray diffraction after a week of intercalation. This dependence on temperature is further illustrated in Fig. 13, where the relative integrated intensities of the stage 2 (003) peak and the stage 3 (004) peak after 2 hr of intercalation are shown as a function of the temperature. Therefore, the higher the intercalation temperature, the faster the kinetics of stage 3 formation compared to that of stage 2 formation, even though the final stage is 2 for all these temperatures.

We have also allowed samples (4.5 x 12 mm; thickness: 0.1 - 0.25 mm) to be intercalated in liquid bromine for 2 hr at 72°C, 81°C, 90°C and 100°C. Note that the intercalation conditions are the same as those used in Fig. 12 except that these temperatures are higher. After 2 hr of intercalation at 72°C, a weight increase of 24 %(1.9 mole % Br_2) was observed; after 2

hr of intercalation at 81°C, a weight incrased of 34 % (2.6 mole % Br_2) was observed; after 2 hr of intercalation at 90°C, a weight increase of 43 % (3.3 mole % Br_2) was observed; after 2 hr of intercalation at 100°C, a weight increase of 54 % (4.1 mole % Br_2) was observed. Shown in Fig. 14 are superlattice x-ray diffraction peaks obtained at the region behind the intercalate front (the edge region) by masking the center region with a 3 mm wide lead foil for the 72°C sample and with a 2 mm wide lead foil for the 81°C and 90°C samples. No mask was used for the 100°C sample. Corresponding intercalate concentration profiles across the whole sample width obtained by x-ray absorption are shown in Fig. 15, which indicates that the intercalation rate increased with increasing temperature and that intercalation was close to completion after 2 hr of intercalation at 100°C. Formation of stage 4 in addition to the final stage of 3 was observed after 2 hr of intercalation at 72, 81 and 90°C. Figure 14 shows that the higher was the temperature, the smaller was the proportion of the stage 4 component. This trend is a consequence of the fact that the stage 3 was the final stage and that the intercalation rate increased with increasing temperature, so that, after 2 hr of intercalation, intercalation was far from complete at 72°C but was relatively close to completion at 100°C, as shown by the concentration profiles in Fig. 15. The final stage was pure stage 3 for all the temperatures from 72°C to 100°C, as shown by x-ray diffraction after about 2 weeks of intercalation.

The relative integrated intensities of the stage 3 (003) peak, the stage 4 (004) peak and the graphite (002) Kβ peak after 1 hr of intercalation are shown in Fig. 16. These particular superlattice lines were chosen for these stages because they were strong and well-resolved from one another. It should be emphasized that these intensity data only give qualitative trends of the phase quantities as a function of the temperature. Separately

indicated in Fig. 16 are the relative intensities obtained in the center region and the edge region; the center region was the central 2-mm wide region whereas the edge region was the remaining areas of the 4-mm wide sample. The final stage was 3 at all these temperatures. It was attained as a pure stage for both the center and edge regions after 1 hr of intercalation at 100°C. The intermediate phase of stage 4 was observed to be strongest at an intermediate time not too close to the beginning nor the completion of intercalation. As a result, it was strongest after 1 hr of intercalation at 80°C compared to the other temperatures shown in Fig. 16. The graphite phase decreased while stage 3 increased with increasing temperature because the intercalation rate increased with increasing temperature.

Similar measurements were made after various intercalation times at various temperatures. The results are summarized in the form of a time-temperature-transformation (TTT) diagram in Fig. 17. The diagram shows the phase evolution as a function of time during intercalation at various constant temperatures. The horizontal bands mark the temperature limits for obtaining particular final stages. For a final stage of 2, the temperature should be below $\sim 72^{\circ}C$; for a final stage of 3, the temperature should be between $\sim 72^{\circ}C$ and $\sim 140^{\circ}C$; for a final stage of 4, the temperature should be above $\sim 140^{\circ}C$. Note that intercalation was by immersion in pure bromine at all temperatures. That the final stage increased by increasing the temperature was predicted by the reaction enthalpies and entropies measured by Aaronson et al.[22] for graphite-alkali metals and by Sasa[23] for graphite-bromine, and was experimentally shown by Bach et al.[24] for graphite-bromine by weight measurement.

Fig. 17 shows that the rate of stage 2 growth increases with increasing temperature from $\sim 20^{\circ}C$ to $\sim 58^{\circ}C$, suggesting diffusion-controlled kinetics for this temperature range whereas it decreases with increasing temperature from $\sim 58^{\circ}C$ to $\sim 72^{\circ}C$ ($\sim 72^{\circ}C$ is the upper temperature limit for stage 2 stability),

suggesting interface-controlled kinetics for this temperature range. A similar C-shaped TTT-curve was obtained for the time for the completion of growth of stage 3, indicating diffusion-controlled kinetics at ~72 - ~110°C and interface-controlled kinetics at ~110 - ~140°C. Of interest is that the C-shaped curves for stage 2 and stage 3 completion are roughly parallel to each other for both temperature regimes.

Mechanism

The x-ray absorption observation of the intercalate fronts was made for various external intercalate concentrations from 0.05 to 1.00 in Br_2 mole fractions. Figure 18shows the plot of the square of the width of the region behind the first front as a function of time during intercalation for various external intercalate concentrations. This plot yielded quite good linear fits to each set of data points, whereas a plot of the width (not squared) versus time did not give good linear fits. This is consistent with the optical microscopy results shown in Fig. 5 and 6. Hence, a parabolic growth rate seems to apply to the progress of the first front, indicating a diffusion-controlled growth. On the other hand, the second front does not follow a parabolic rate law, but rather shows a better fit to a linear rate. Because of the large scatter of the data for the second front compared to the first front, the rate of movement of the second front did not allow quantitative analysis. The slope of the plot in Fig.18 gives the growth rate, which is the same as 4 times the diffusion coefficient D. This rate is plotted against the external intercalate concentration in Fig. 19. Included in Fig. 19 are growth rates determined by x-ray absorption and optical microscopy. As mentioned earlier in this section, optical microscopy observation of the front position was made at various external intercalate concentrations. Figure 19 shows that the dependence of the

growth rate on the concentration is approximately linear. This dependence suggests that the intercalation reaction may be best understood as a reaction involving a single intercalate layer, while staging is more or less imposed by other constraints in the system, such as elastic or electrostatic stresses.

Based on the diffusion-controlled mechanism for the intercalation process for all the external intercalate concentrations at room temperature (23°C), we calculated the diffusion coefficients D from results of optical microscopy, x-ray absorption and weight measurement. The D values are listed in Table 4 for various external intercalate concentrations. The D values obtained from the three experimental techniques are in good agreement with one another. Moreover, the D value of 2.36×10^{-8} cm^2/s which we obtained for pure bromine liquid at 23°C is in close agreement with the D value of 2.45×10^{-8} cm^2/s reported by Dowell and Badorrek[25] for near-saturated bromine vapor at 30°C. Table 4 shows that D increases with increasing external intercalate concentration.

Although the room temperature results support a diffusion-controlled model, a study of the dependence of the kinetics on temperature is important for a better understanding of the mechanism. For this purpose, the TTT-diagram (Fig. 17) is of great value, as discussed below.

If we consider the reaction of bromine with an nth stage graphite-bromine intercalation compound to form an (n+1)st stage compound, we may write

$$A\ C_{n8}\ Br_2(s) + Br_2(g) \underset{k_r}{\overset{k_f}{\rightleftarrows}} B\ C_{(n+1)8}\ Br_2(s), \qquad (3)$$

where k_f is the rate constant for the reaction in the forward direction and k_r is the rate constant for the reverse reaction. Hence, the rate of the reaction in the forward direction is

$$r_f = k_f\ a^A_{C_{n8}}\ Br_2\ a_{Br_2} \qquad (4)$$

and in the reverse direction

$$r_r = k_r \, a^B_{C_{(n+1)8}\,Br_2} \quad , \tag{5}$$

where r_f = forward rate

$a_{C_{n8}\,Br_2}$ = activity of $C_{n8}\,Br_2$

a_{Br_2} = activity of $Br_2(g)$

$a_{C_{(n+1)8}Br_2}$ = activity of $C_{(n+1)8}\,Br_2$

At equilibrium, the rate of product formation is equal to the rate of reactant lost. Thus,

$$k_f \, a^A_{C_{n8}\,Br_2} \, a_{Br_2} = k_r \, a^B_{C_{(n+1)8}\,Br_2} \quad .$$

Hence, the equilibrium constant K is

$$K = \frac{k_f}{k_r} = \frac{a^B_{C_{(n+1)8}\,Br_2}}{a^A_{C_{n8}Br_2} \, a_{Br_2}} \quad . \tag{6}$$

Eq. (6) can be rewritten as

$$\frac{a^A_{C_{n8}\,Br_2} \, a_{Br_2}}{a^B_{C_{(n+1)8}\,Br_2}} - \frac{1}{K} = 0 \tag{7}$$

Taking the activity of a solid as 1, the Eq. (6) can be rewritten as

$$K = \frac{1}{p^{eq}_{Br_2}} \quad , \tag{8}$$

where the activity of bromine is taken as the bromine partial pressure at equilibrium condition. Assume that the reduced temperature (T/T_c) and pressure (P/P_c) are small, since for Br_2, T_c = 302°C and P_c = 126 atm.

At non-equilibrium conditions, the rate will be proportional to the deviation from equilibrium. Hence,

$$v \propto \left[\left(P^{act}_{Br_2} - P^{eq}_{Br_2}\right) = \left(P^{act}_{Br_2} - \frac{1}{K}\right) = \left(P^{act}_{Br_2} - \exp\left[\frac{\Delta G}{RT}\right]\right)\right], \qquad (9)$$

where $P^{act}_{Br_2}$ is the actual Br_2 vapor pressure.

If we consider that the reaction is occurring within a solid, we can write the proportionality constant as the probability of a jump across the interface. Thus,

$$v = \upsilon\lambda \exp\left[\frac{-E_i}{RT}\right]\left(P^{act}_{Br_2} - \exp\left[\frac{\Delta G}{RT}\right]\right) \quad , \qquad (10)$$

where υ = vibrational frequency of Br_2, λ = distance across the interface, E_i = energy required to cross the interface.

Since the reaction is occurring within a solid, one also has to take into account the diffusion rate. Since the TTT-curves (C-curves) are plotted as a function of time, the appropriate form is

$$t = \frac{x^2}{D} + \frac{x}{v} \, , \qquad (11)$$

where x = distance of the reaction front from the sample edge, D = diffusion coefficient.

Consider the effect of temperature on the intercalation time. The intercalation time is proportional to the reciprical of the velocity and the diffusion coefficient. At low temperatures the diffusion coefficient is small and determines the appearance of the TTT-curve. At temperatures where ΔG approaches zero, the interface reaction controls the velocity and is responsible for the upper branch of the C-curve. At intermediate temperatures (the nose of the C-curve), diffusion is fast and there is still considerable driving force for the reaction. In this region the velocity term again dominates but the velocity will be governed by the jump probability and the bromine vibrational frequency. The most significant term here is the vibrational frequency while the probability term determines the temperature dependence of the C-curve nose. An increase in the vibrational frequency causes the diffusion coefficient to dominate the transformation curve up to higher temperatures and the nose of the C-curve would move to shorter times. In the probability term, a decrease in E_i would cause a blunter nose on the

C-curve.

By using Eq.(11), TTT-curves have been calculated to fit the experimental curves in Fig. 17, which shows the theoretical curves as dotted lines. The theoretical curves were obtained with the following experimentally determined values:

$$\left.\begin{aligned} \Delta H &= -10.9 \text{ kcal/mol} \\ \Delta S &= -31.9 \text{ cal/mol K} \\ \text{for stage 2, and} & \\ \Delta H &= -10.6 \text{ kcal/mol} \\ \Delta S &= -30.0 \text{ cal/mol K} \end{aligned}\right\} \text{(from prelimary P vs 1/T phase diagram)}$$

for stage 3, and the diffusion coefficient

$$D = 4.12 \times 10^{5} \frac{cm^2}{sec} \exp\left[-18.1 \text{ kcal mol}^{-1}/RT\right] \quad (12)$$

(for thermogravimetric results during desoprtion)

E_i was approximated by the energy for the movement of an interstitial, which was estimated by Thrower and Loader as 692 cal mol^{-1} (0.03 eV). The $\upsilon\lambda$ term was taken as 10^{-5} cm/sec for fitting the experimental curve.

Experimentally there has not been much work done in determining the rate controlling parameters involved in intercalation. Hooley et al[27-29], Dowell[30] and Ubbelohde[31-33] have investigated the effects of pressure and graphite structure on the reaction rate of bromine intercalation, but until rather recently little other work has been done other than to establish conditions whereby a given intercalation compound can be formed, which other investigators then use with apparently small concern for optimizing the reaction conditions. Nonetheless, some work has been done in investigating intercalation kinetics and, in a related vein, thermodynamics involved with intercalation. Aronson et al.[22] have determined a phase diagram for the alkali metal compounds based on electrochemically determined enthalpies and entropies of reaction. Sasa et al.[17] have investigated the graphite-Br_2 system and determined entropy and enthalpy

for the reaction forming second stage graphite-bromine from third stage. Metz and Siemsgluss[34], in the case of $FeCl_3$, and Dowell[25], for Br_2, HNO_3 and $PdCl_2$, have investigated rates of intercalation to determine diffusion coefficients. Bardhan et al.[18,20] have investigated the kinetics of bromine intercalation and interpreted their findings in terms of an interface-controlled reaction. Flandrois et al.[35] have investigated the kinetics of intercalation in the $NiCl_2$ system. Hamwi et al.[21] have elegantly followed the course of intercalation of a graphite-potassium compound.

The overall results of these experiments can allow one to draw some interesting conclusions. Diffusion appears to be quite rapid, based on measurement in the case of Br_2, HNO_3 and $PdCl_2$[25], and suggested in the metal halide compounds by the observation that a uniform intercalate concentration is established in quite a short time in terms of the amount of intercalate which has been absorbed[25 34.35]. In several cases, i.e., HNO_3[36], and K[21], it is observed that several stages are formed before the final lowest stage. In fact, in the study of K, Hamwi et al. were unable to positively identify the highest initial stage which formed. $NiCl_2$ and Br_2[17] have been reported to directly form the lowest stage, 2, upon intercalation. Recently, reports have been made that in the case of Br_2, some higher stages are formed prior to the formation of the second stage compound[19]. In this work we have found that x-ray diffraction of the inner, apparently unintercalated region does indicate the presence of higher stages though x-ray absorption suggests that the amount present is very small. In studies made on K[21], $FeCl_3$[34], and $NiCl_2$[35], all the investigators came to the conclusion that the reaction was controlled by processes outside the graphite, probably condensation and adsorption of intercalate onto the graphite surface. At the same time, the intercalate concentration within the sample remains fairly uniform though steadily increasing with time as would be predicted by a reaction

whose rate is determined by a slow reaction rate step followed by a fast diffusion step. In the case of bromine on the other hand, the intercalated region is pronouncedly distinct from the unintercalated region. In the work at hand, it also seems unlikely that the adsorption step is significantly slow given the immersion in a liquid as compared to the vapor phase method used for K, $NiCl_2$, and $FeCl_3$.

While several stages are present in the case of Br_2 intercalation, a contrast should be made with the sort of progressive staging observed in K. In K, the staging is a rather deliberate situation, even to the extent of having plateaus in the intercalate uptake versus time curves, which indicate that the one stage has nearly saturated the sample before the next stage appreciably has begun. Such is not the case for Br_2 where a well-defined intercalate front exists. Rather, weight versus time curves are smooth, and the concentration profiles indicate the shoulders in the opposite sense, i.e., growth of the next lower stage is evident well before intercalation of the previous stage is complete. Furthermore the instances where a difference in stage is pronounced are those at high temperatures and low concentrations, instances where the reaction rate of the lowest stage may be expected to decrease for thermodynamic reasons. This is less clear in the case of low concentrations since the diffusion rate is also decreasing as a function of concentration. At high temperatures, however, the increase in the diffusion rate is quite dramatic while the decrease in reaction rate for a low stage is equally apparent. It may be pointed out that the shape of the C-curves, i.e., the sharpness of them, indicates that for most temperatures, the reaction rate at the internal interface is considerable faster than the diffusion step.

C. Intercalation of Graphite Fibers

Intercalated graphite fibers have recently received considerable attention because of their use in polymer-matrix composites for high electrical conductivity applications.[37] The intercalation of graphite fibers with HSO_3F, AsF_5 or SbF_5 gave an up to 50 times increase in the electrical conductivity.[38] X-ray diffraction showed the formation of stage 2 graphite-AsF_5 in high modulus ex-PAN graphite fibers (eg. Union Carbide TP 4104B).[39,40] Formation of stage 1 graphite-K in fibers was shown by x-ray diffraction[40] and the appearance of the gold color.[40,41] Absorption of Br_2 and ICl in graphite fibers was indicated by weight uptake measurement,[42,43] but confirmation of intercalation by using x-ray diffraction had not been reported. Warner et al.[42] interpreted the absorption as not being intercalation, but rather plasticization, whereas Hooley and Deitz[43] interpreted the absorption as intercalation. Desorption of brominated graphite fibers resulted in a stable material having an electrical conductivity higher than that of pristine graphite fibers[40,44] Similar treatment with ICl gave an even higher value of the electrical conductivity[40] In this work, we have obtained the first x-ray diffraction evidence of intercalation of ICl in graphite fibers. Furthermore, we have shown that the in-plane unit cell of ICl-intercalated fibers is the same as that of ICl-intercalated single crystal graphite or highly oriented pyrolytic graphite (HOPG).

Synthesis

The graphite fibers used in this work are listed in Table 5. Intercalation was carried out by exposure of the fibers to ICl vapor in equilibrium with ICl liquid at 95°C; this temperature was chosen for the ICl liquid because ICl boils at 97.4°C. The purity of ICl was 95+%, as supplied by Alfa Products. While the ICl liquid was held at 95°C, the fibers (typically

~1.0 cm long) were held at a temperature ranging from 100°C to 135°C. The reaction vessel was made of Pyrex glass and was sealed without evacuation. The intercalation time investigated ranged from 8 hours to 24 hours.

Staging and in-plane structure

X-ray diffraction was used to characterize the crystal structural effects of intercalation. The Transmission Laue method was used, with MoK$_\alpha$ radiation and a specimen-to-film distance of 6 cm. The intercalated fibers were removed from the reaction vessel, cut to a typical length of ~2 mm, and then sealed in a glass capillary of 1 mm I.D. and 0.01 mm wall thickness; this procedure took typically ~ 1 min. The fiber axes thus had a preferred orientation along the capillary axis. The set-up allowed d-values ranging from 0.8 Å to ~6 Å to be measured. The exposure time was 6 hr for every sample.

Figure 20 shows the x-ray diffraction photographs of the three types of pristine graphite fibers listed in Table 5. The Thornel P-100 fibers gave the largest number of diffraction lines, as listed in Table 6. The Celion GY-70 fibers gave fewer lines, but they are as sharp as those of Thornel P-100. On the other hand, the Panex 30 fibers gave only a few relatively diffused lines. Hence, the crystalline perfection of the graphite fibers decreased in the order (1) Thornel P-100, (2) Celion GY-70, and (3) Panex 30.

Figure 21 shows the x-ray diffraction photographs of (a) HOPG, (b) Thornel P-100, (c) Celion GY-70, and (d) Panex 30 after exposure to ICl. The HOPG sample was intercalated by exposure to ICl vapor at room temperature for 1 day, and resulted in a stage 1 compound (Fig. **21** (a)); the indexing of the diffraction lines is shown in Table 7 . All three types of fibers were

treated identically by holding the fibers at 130°C and the ICl liquid at 95°C for 8 hr. After the treatment, the Thornel P-100 fibers (Fig. **21(b)**) showed superlattice diffraction lines, which were absent in Fig. **20(a)**. Indexing of the pattern in Fig. **21**(b) showed that the intercalated Thornel P-100 fibers were predominantly stage 2. (The indexing of the pattern for stage 2 Thornel P-100 fibers is given later in this paper). The same treatment for Celion GY-70 and Panex 30 fibers did not yield any superlattice lines. It should be mentioned that room temperature exposure of any type of fibers to ICl did not yield any superlattice lines, although such treatment of HOPG resulted in stage 1. Thus, Fig. **21** shows that the ease of intercalation of the various graphite materials decreases in the order (1) HOPG, (2) Thornel P-100, (3) Celion GY-70, and (4) Panex 30. In fact, no diffraction evidence of ICl intercalation was obtained for Celion GY-70 and Panex 30 fibers, although intercalation was clearly shown for Thornel P-100.

Figure 22 shows x-ray diffraction patterns of intercalated Thornel P-100 fibers after various lengths of desorption time (0 min, 10 min, 2 hr, 1 week). Intercalation was performed by holding the fibers at 130°C and the ICl liquid at 95°C for 24 hr. Desorption was allowed to occur in air at room temperature. Fig. **22**(a) shows the pattern obtained after a negligible length of desportion time (0 min); the indexing of this pattern is shown in Table 4. Note that the second stage (00ℓ) type lines were observed for ℓ = 2,3,5,6,8,9. The (001) line was not observed because its large d value caused it to be blocked by the beam stop. The absence of (00ℓ) lines for ℓ=4,7 is probably systematic due to the space group, which is presently not known since the positions of the intercalate molecules within a unit cell has not been determined. In addition to the (00ℓ) lines, (hk0), (h0ℓ) and (0kℓ) lines were observed. The in-plane superlattice was thus found to be the same as that of

stage 1 graphite-ICl based on single crystal graphite. The in-plane unit cell of stage 1 graphite-ICl as determined by Ghosh and Chung[45] by single crystal x-ray diffraction is shown in Fig. 23. The unit cell is monoclinic and commensurate with the graphite lattice, with in-plane lattice constants a=4.92 Å, and b=42.68 Å, and the angles $\alpha=\beta=90°$ and $\gamma=93.3°$. Desorption resulted in a gradual decrease of the intensities of the superlattice lines without shifting any line. This means that the initial stage (stage 2) was maintained during desorption. The presence of superlattice diffraction lines even after a week of desorption indicates that (i) desorption of intercalated fibers results in a material which is still intercalated, and (ii) desorption of intercalated fibers occurs over an appreciably long time.

By lowering the sample temperature to 100°C, with the ICl liquid maintained at 95°C, stage 1 graphite-ICl (mixed with small quantities of stages 2 and 3) was obtained in Thornel P-100 graphite fibers. Although we were able to obtain relatively pure stage 2, we have not yet been able to obtain pure stage 1. The in-plane superlattice of stage 1 was also found to be the same as that shown in Fig. 23.

The ICl intercalation method used in this work is based on the two-bulb method developed for potassium intercalation.[46] In contrast, previous work on intercalation of ICl in fibers involved exposure to ICl vapor at room temperature.[42,43] We have found that the two-bulb method used in this work gave graphite-ICl of specific stages, whereas room temperature exposure to ICl did not lead to superlattice formation.

The ease of intercalation was found to increase with increasing crystal perfection of the graphite material, such that the crystal perfection decreases in the order (1) HOPG, (2) Thornel P-100, (3) Celion GY-70, and (4) Panex 30. In fact, Thornel P-100 was the only type of fibers which

could be intercalated with ICl using our method, as indicated by the superlattice formation. Note that we consider superlattice formation to be conclusive evidence for intercalation. In this work, the first such evidence was obtained for the intercalation of ICl in graphite fibers.

Of significance is that we have observed for the first time in-plane intercalate ordering in intercalated graphite fibers. Moreover, we have found that the in-plane unit cell of stage 1 and stage 2 ICl-intercalated fibers is the same as that of stage 1 graphite-ICl single crystal graphite[9] and that of stage 1 graphite-ICl HOPG. In addition to the in-plane superlattice, staging was observed.

The Transmission Laue method used in this work was found to be more suitable for fiber material compared to the Debye-Scherrer method and the diffractometer method. This is because the preferred orientation of the fibers results in incomplete Debye rings, which might be missed by the film in the Debye-Scherrer method. Moreover, the need of a small sample quantity, the availability of thin-walled capillaries for sealed samples, and the possibility of a long exposure time make the Transmission Laue method more attractive than the diffractometer method.

Density and Stoichiometry

Density measurement provides a good determination of the intercalate concentration and is superior to weight uptake measurement, which is unreliable for fibers due to their low density and small size. The intercalate concentration is related to the stoichiometry. Of interest is the comparison between the stoichiometry of intercalated graphite fibers and that of intercalated single crystals of the same stage.

The density of graphite fibers before and after intercalation was measured by allowing the fibers to float in an agueous solution of Cs_2SO_4 of the appropriate matching specific gravity.[47]

A supersaturated solution of Cs_2SO_4 in distilled water was prepared and allowed to stand overnight to precipitate out any extra salt. 100μℓ of this solution was placed at the bottom of a centrifuging tube. The remaining solution was diluted to 90% of its original density by adding an appropriate amount of distilled water. Then 100μℓ of this solution was placed on top of the previous liquid without disturbing the previous liquid. Four successive layers were placed on top of each other, with similarly decreasing densities. Then the fibers, very finely cut, were added to the tube. Upon centrifuging at 90000 r.p.m. (190,000 g-force) for a few hours, a density gradient was set up in the tube, with the fibers floating in the tube and their position determined by their density. A very small quantity of liquid (∿5μℓ) was withdrawn with a micropipette from the region where the fibers were floating. Its refractive index was measured and the density was read off from well established tables of refractive index vs. density for Cs_2SO_4.

The refractive index of the drop of liquid could be measured to quite a good accuracy (three significant digits). The biggest source of error was in the visual judgement of where the fibers were floating in the tube, which was 4 mm I.D. and 2.5 cm long. The fibers floated in a range of ∿4 mm, mainly due to variation in the density of fibers as supplied. After intercalation, an added problem arose. If the fibers were cut up very small, they tend to deintercalate faster, thus affecting the density. If they were cut up in large pieces (∿2-3 mm long), one would have an uncertainty in position added to the already existing variation in density. Moreover, a long stay in an aqueous medium affects the water, coloring it brown and changing the composition, due to deintercalation, thus affecting the reliability of the tables of refractive

index vs. density. Therefore, the above procedure was used to obtain a rough upper bound on the density, whereas a different procedure was used to determine the density more accurately, as described below.

A solution of Cs_2SO_4 with a density corresponding to the upper bound obtained by the previous method was prepared. A quantity of 1000 μℓ of the solution was placed in a small test-tube and the sample was floated on the top of the solution. Then 10μℓ quantities of water were added step-by-step and the whole liquid was stirred by a vibration pad after each addition, until a large number of fibers went into suspension. For example, after adding 30μℓ, most of the fibers were still floating on top. After adding 40μℓ, a substantial amount of fibers went into suspension. Thus two bounds in the density were obtained. Let initial upper bound = $\rho_{max.}$ Then the density ρ_{fibers} of the fibers is given by ,

$$\rho_{max} \times \frac{1000}{1030} \geq \rho_{fibers} \geq \rho_{max} \times \frac{1000}{1040} .$$

The accuracy obtained in ρ_{fibers} was ∿0.5%, if any density change due to deintercalation was disregarded. (The effect of deintercalation is expected to be small, since it takes about 5 minutes to finish the operation.)

Another source of error was due to the autopipetting instrument used. When measuring quantities as small as 10μℓ, it had an error of ±0.1μℓ. However, this amount was added to ∿1000μℓ of solution, so this error is insignificant.

The maximum density measurable by this method is 2.3 gm/cc.

Shown in Table 9 are the densities measured on Thornel P-100 graphite fibers intercalated by keeping the ICl reservoir at 95°C and the sample at 120°C. This combination of temperatures gave a final stage of 2 (essentially pure) after 24 hr of intercalation, for which the density corresponded to a stoichiometry of $C_{19.2}ICl$ This stoichiometry corresponds to a lower intercalate concentration than the calculated graphite-ICl (stage 2) stoichiometry of $C_{17.8}ICl$, suggesting

the presence of regions not completely intercalated, perhaps due to the imperfect graphitic structure in the fibers.

References

1. G. R. Hennig, Prog. Inorg. Chem. 1 (F.A. Cotton, ed.), Wiley (Interscience), New York, 1959, p. 125.

2. A. Herold, Bull. Soc. Chim. France 187, 999 (1955).

3. G. R. Hennig, J. Chem. Phys. 20, 1438 (1952).

4. C. Underhill, S. Y. Leung, G. Dresselhaus and M. S. Dresselhaus, Solid State Commun. 29, 769 (1979).

5. L. V. Interrante, R. S. Markiewicz and D. W. McKee, Synth. Met. 1, 287 (1979/80).

6. W. Rudorff and H. Schulz, Z. Anorg. Chem. 245, 121 (1940).

7. Jean M. Lalancette and Jeannine Lafontaine, J. C. S. Chem. Commun. 815 (1973).

8. Lin Chun-Hsu, H. Selig, M. Rabinovitz, I. Agranat and S. Sarig, Inorg. Nucl. Chem. Lett. 11, 601 (1975).

9. N. Bartlett, E. M. McCarron and B. W. McQuillan, Synth. Met. 1, 221 (1979/80).

10. A. R. Ubbelohde, Proc. Roy. Soc. A 309, 297 (1969).

11. D. Billaud, E. McRae and A. Herold, Mat. Res. Bull. 14, 857 (1979).

12. D. M. Ottmers and H. F. Rase, Carbon 4, 125 (1966).

13. P. Bowen, W. Jones and J. M. Thomas, J. C. S. Chem. Commun. 677 (1981).

14. E. R. Falardeau, L. R. Hanlon and T. E. Thompson, Inorg. Chem. 17, 301 (1978).

15. S. Ohe, Computer Aided Data Book of Vapor Pressures, Data Book Publishing Company, Tokyo, Japan (1976).

16. C. Barthel and M. Dode, Bull. Soc. Chim. 21, 1312 (1954).

17. T. Sasa, Y. Takahashi and T. Mukaibo, Carbon 9, 407 (1971).

18. K. K. Bardhan and D. D. L. Chung, Carbon 18, 313 (1980).

19. S. H. Anderson and D. D. L. Chung, Ext. Abst. Program -- Bienn. Conf. Carbon 15, 361 (1981).

20. K. K. Bardhan and D. D. L. Chung, Carbon 18, 303 (1980).

21. A. Hamwi, P. Touzain, L. Bonnetain, A. Boeuf, A. Freund, and C. Riekel, Proceedings of the 3rd International Carbon Conference, Baden-Baden, Germany, July 1980.

22. S. Aronson, F. J. Salzano, and D. Bellafiore, J. Chem. Phys. 49, 434 (1968).

23. T. Sasa, Carbon 11, 497 (1973).

24. B. Bach, M. Bagouin, F. Bloc and A. Herold, Compte Rend., Acad. Sci. (Series C) 257, 681 (1963).

25. M. B. Dowell and D. S. Badorrek, Carbon 16, 241 (1978).

26. P. A. Thrower and R. T. Loader, Carbon 7, 467 (1969).

27. J. G. Hooley, W. P. Garby and J. Valentin, Carbon 3, 7 (1965).

28. J. G. Hooley, and J. L. Smee, Carbon 2, 135 (1964).

29. J. G. Hooley, Carbon 10, 155 (1972).

30. M. B. Dowell, Mater. Sci. Eng. 31, 129 (1977).

31. G. A. Saunders, A. R. Ubbelohde and D. A. Young, Proc. R. Soc. London, Ser. A, 271, 499 (1963).

32. G. A. Saunders, A. R. Ubbelohde and D. A. Young, Proc. R. Soc. London, Ser. A, 271, 512 (1963).

33. A. R. Ubbelohde, Carbon 10, 201 (1972).

34. W. Metz and L. Siemsgluss, Mat. Sci. Eng., 31, 119 (1977).

35. S. Flandrois, J. M. Masson, J. C. Rouillon, J. Gaultier and C. Hauw, Synth. Met., 3, 1 (1981).

36. D. E. Nixon, G. S. Parry, and A. R. Ubbelohde, Proc. R. Soc. (London) A291, 324 (1966).

37. F.L. Vogel, Synth. Met. 1, 279 (1979/80).

38. I.L. Kalnin and H.A. Goldberg, Synth. Met. 3, 159 (1981).

39. I.L. Kalnin and H.A. Goldberg, Ext. Abstr. Program - Bienn. Conf. Carbon 15, 367 (1981).

40. D.D. Dominguez, R.N. Bolster and J.S. Murday, Ext. Abstr. Program - Bienn. Conf. Carbon 15, 365 (1981).

41. M. Sano, N. Sato, H. Inokuchi and S. Tamura, Physica 105B, 296 (1981).

42. S.B. Warner, L.H. Peebles and D.R. Uhlmann, Int. Conf. Carbon Fibers, Their Place in Modern Technology, London (1974).

43. J.G. Hooley and V.R. Deitz, Carbon 16, 251 (1978).

44. M. Endo and T. Koyama, Synth. Met. 3, 177 (1981).

45. D. Ghosh and D.D.L. Chung, Phys. Rev. (to be published)

46. A. Herold, Bull. Soc. Chim. France 187, 999 (1955).

47. J.A. Turnbull and W.T. Eeles, 2nd Conf. Ind. Carbon and Graphite, 1965, Soc. Chem. Ind., London, p. 173.

Table 1 Intercalation Methods

Method	Parameters			
	Intercalate vapor pressure	Sample temperature	Amount of intercalate	Time of intercalate
Temperature method — Two-bulb method I	-	x	-	-
Temperature method — Two-bulb method II	x	-	-	-
Temperature method — One-bulb method	x	x	-	-
Solution method	x	-	-	-
Limited reactant method	-	-	x	-
Limited time method	-	-	-	x

x Varied to control the stage

- Not varied

Table 2 Stage evolution during intercalation for two representative external intercalate concentrations

Mole Fraction Br_2 in Br_2 - CCl_4	Time (hr)	Stages Present		Percent Weight Gain $(\frac{\Delta w}{w_i})$
		Edge	Center	
0.5	15	3 4 G	3 4 G	20
	24	2 3 4 G	2 3 4 G	23
	34	2 3 4 G	2 3 4 G	27
	64	2 3 4	2 3 4 G	34
	114	2 3 4	2 3 4 G	42
	140	2 3 4	2 3 4 G	46
	210	2 3	2 3 4 G	55
	308	2 3	2 3	63
	356	2 3	2 3 4	66
	663	2	2 3	77
	1182	2	2	81
0.2	40	4 G	4 G	16
	46	4 G	4 5 G	17
	63	4 G	4 5 G	18
	66	3 4 G	4 5 G	19
	119	3 4 5	4 5 G	24
	163	3 4	3 4 5 G	27
	311	3 4	3 4 5 G	34
	355	3 4	3 4 5 G	35
	667	3 4	3 4	43
	1812	3	3	53

Table 3 Stages present after 468-689 hr of intercalation for various external intercalate concentrations at 23°C.

Mole fraction Br_2 in Br_2-CCl_4	Final Stage	Stages Present		Percent Weight gain ($\Delta w/w_i$)	Time
		Edge	Center		
0.05	/	6 G	6 G	5	468
0.10	4	4 5	4 6 G	26	491
0.15	3	3 4	3 4 5 G	/	689
0.20	3	3 4	3 4	43	667
0.25	3	3 4	3 4	45	666
0.30	3	3	3 4	50	663
0.40	2	2 3	2 3	63	662
0.50	2	2	2 3	77	663

Table 4 Diffusion coefficients for liquid-phase bromine intercalation at 23°C

Mole Fraction Br_2 in Br_2-CCl_4	Diffusion Coefficient ($10^{-9}cm^2/s$)		
	Optical Microscopy	X-ray Absorption	Weight Increase
1.00	23.6		
0.80	26.4		
0.65	17.2		
0.50		10.83	13.14
0.40		9.18	8.24
0.30		6.75	7.59
0.25	6.35	4.28	5.06
0.20		5.00	4.44
0.15	2.78	3.25	
0.10		1.67	2.68
0.05		0.213	0.250

Table 5 Specifications of Graphite Fibers Used

Manufacturer	Union Carbide Corp.	Stackpole Fiber Co.	Celanese Corp.
Grade	Thornel P-100 Grade VS-0054	Panex 30	Celion GY-70
Precursor	Pitch	PAN	PAN
Tensile modulus (10^6 psi)	100	32	75
Tensile strength (10^6 psi)	0.325	0.375	0.27
Density (g/cm^3)	2.16	1.74	1.97
Electrical resistivity (10^{-4} Ω-cm)	2.5		6.5

Table 6 X-ray diffraction lines obtained from pristine graphite fibers (Thornel P-100)

Line No.	d_{obs} (Å)	d_{cal} (Å)	h	k	ℓ	Strength
1	3.38	3.35	0	0	2	S
2	2.11	2.13	1	0	0	M
3	1.69	1.68	0	0	4	S
4	1.23	1.23	1	1	0	Diffuse
5	1.17	1.15	1	1	2	Diffuse
6	1.13	1.12	0	0	6	M

Table 7 X-ray diffraction lines obtained from stage 1 graphite-ICl based on HOPG

Line No.	d_{obs} (Å)	d_{cal} (Å)(Stage 1)	hkℓ (Stage 1)			Strength
			h	k	ℓ	
1	5.32	5.33	0	8	0	W
2	4.86	4.89	1	0	0	VS
3	4.35	4.35	1	4	0	W
4	4.07	4.02	1	0	1	W
5	3.54	3.53	0	0	2	VS
6	3.38	3.42	0	3	2	W
7	3.19	3.16	0	6	2	W
8	3.09	--	--	--	--	VW
9	2.95	2.86	1	0	2	M
10	2.62	2.62	1	6	2	M
11	2.49	2.45	2	0	0	M
12	2.33	2.35	0	0	3	S
13	2.18	2.18	2	8	0	W
14	2.12	2.13	0	20	0	M
15	2.03	2.04	2	$\bar{1}$	1	W
16	1.93	1.94	2	5	2	VW
17	1.87	1.82	2	$\bar{1}$	2	W
18	1.78	1.76	0	0	4	W
19	1.65	1.63	3	0	0	M
20	1.56	1.58	2	$\bar{1}$	3	Diffuse
21	1.47	1.48	3	0	2	W
22	1.36	1.36	2	$\bar{1}$	4	Diffuse
23	1.32	1.34	3	0	3	W
24	1.18	1.18	0	0	6	S
25	1.14	1.14	1	0	6	M

Table 8 X-ray diffractions lines obtained from graphite fibers intercalated with ICl by holding the fibers at 130°C

Line No.	d_{obs} (Å)	d_{cal} (Å) (Stage 2)	hkl (Stage 2)			Strength
			h	k	l	
1	5.30	5.20	0	0	2	W
2	4.80	4.89	1	0	0	W
3	4.25	4.26	0	10	0	W
4	3.89	3.92	0	10	1	W
5	3.43	3.46	0	0	3	VVS
6	2.86	2.83	1	0	3	W
7	2.13	2.13	0	20	0	S
8	2.07	2.07	0	0	5	M
9	1.84	1.82	0	20	3	Diffuse
10	1.73	1.73	0	0	6	W
11	1.70	1.70	10	$\bar{5}$	6*	W
12	1.63	1.63	3	0	0	W
13	1.31	1.30	0	0	8	W
14	1.26	1.26	2	$\bar{1}$	8	VW
15	1.23	1.23	4	$\bar{2}$	0	S
16	1.16	1.16	0	0	9	W
17	1.12	1.11	2	$\bar{1}$	4	W
18	0.99	0.99	4	0	4	W

* Tentative (hkl) assignment

Table 9 Density of Thornel P-100 Graphite Fibers before and after Intercalation

		Density (gm/cc)	Stoichiometry
Experimental	Pristine fibers	1.82 ± 0.01	/
	After 6 hr of intercalation	1.94 ± 0.01 *	/
	After 24 hr of intercalation	2.01 ± 0.01 *	$C_{19.2}ICl$
Theoretical	Pure graphite	2.27	/
	Stage 2 graphite-ICl	2.59†	$C_{17.8}ICl$

* Lower bound values due to slight deintercalation

† Calculated by assuming that the unit cell in Fig. 23 contains 9 ICl molecules, so that the stoichiometry for stage 2 is $C_{17.8}ICl$. (According to Turnbull and Eeles,[47] the stoichiometry of stage 1 is about C_9ICl.)

FIGURE CAPTIONS

Fig. 1 X-ray diffraction patterns of stages 2, 3 and 4 prepared by immersion of graphite in Br_2-CCl_4 solutions. Each diffraction peak is labeled by the ℓ index of the (00ℓ) Miller indices. An expanded (00n) peak for each stage n compound is offset to the right of the diffraction pattern.

Fig. 2 X-ray diffraction patterns of stages 2 and 3 obtained by immersion of graphite in liquid bromine at 20°C and 105°C.

Fig. 3 X-ray diffraction patterns of graphite prior to intercalation and after intercalation to stage 4 by immersion in a 50 mol % Br_2 Br_2-CCl_4 solution at 105°C.

Fig. 4 In situ optical micrographs and schematic surface profiles of a sample after different times of intercalation at room temperature.

Fig. 5 Width of the deformed region behind the intercalate front versus time during intercalation.

Fig. 6 Width of the deformed region behind the intercalate front versus the square root of time during intercalation.

Fig. 7 X-ray absorption profile and x-ray diffraction patterns of the edge and center regions obtained with CuKα and MoKα radiations after 297 hr of room temperature intercalation in liquid bromine. Each diffraction peak is labeled by the ℓ index of the (00ℓ) Miller indices, with the subscript indicating the stage (G indicating graphite) and the superscript, if present, indicating the $K\alpha_1$,$K\alpha_2$ or Kβ component.

Fig. 8 Percentage weight increases versus the square root of time during room temperature intercalation in Br_2-CCl_4 solutions of various Br_2 concentrations.

Fig. 9 X-ray absorption profiles and x-ray diffraction patterns of the edge and center regions at different times during intercalation by immersion in a 50 mol % Br_2 Br_2-CCl_4 solution at room temperature.

Fig. 10 X-ray absorption profiles and x-ray diffraction patterns of the edge and center regions obtained after 600 hr of intercalation in various constant concentrations of Br_2-CCl_4 solutions at room temperature.

Fig. 11 Time-concentration-transformation (TCT) diagram, showing the times for a given stage to start forming and to finish forming for various external intercalate concentrations. The phases present are indicated by the stage numbers and the symbol G for graphite. The horizontal scale indicates the time divided by the square of the width of the region behind the first front.

Fig. 12 X-ray diffraction patterns obtained after 2 hr of intercalation in liquid bromine at various temperatures. The final stage was 2.

Fig. 13 Relative integrated intensities of the stage 2 (003) peak and the stage 3 (004) peak after 2 hr of intercalation as a function of temperature. The final stage was 2.

Fig. 14 Superlattice x-ray diffraction peaks obtained at the region behind the intercalate front after 2 hr of intercalation at various temperatures. A: 72°C, B: 81°C, C: 90°C, D: 100°C. The final stage was 3.

Fig. 15 X-ray absorption profiles obtained after 2 hr of intercalation at various temperatures. A: 72°C, B: 81°C, C: 90°C, D: 100°C. The final stage was 3.

Fig. 16 Relative integrated intensities of the stage 3 (003), stage 4 (004) and graphite (002) Kβ peak after 1 hr of intercalation as a function of temperature. Stage 3, stage 4 and graphite are indicated by 3, 4 and G, respectively.The contribution due to the edge region is shown by the solid bars; that due to the center region is shown by the empty bars.

Fig. 17 Time-temperature-transformation (TTT) diagram showing the times for a given stage to start forming and to finish forming for various isothermal temperatures. The phases present are indicated by the stage numbers and the symbol G for graphite. The horizontal scale indicates the time divided by the square of the width of the region behind the first front.

Fig. 18 The square of the width of the region behind the first front versus time during intercalation for various external intercalate concentrations.

Fig. 19 The growth rate (slope of Fig. 9) versus the external intercalate concentration.

Fig. 20 X-ray diffraction patterns of pristine graphite fibers: (a) Thornel P-100, (b) Celion GY-70, (c) Panex 30.

Fig. 21 X-ray diffraction patterns of (a) HOPG, (b) Thornel P-100, (c) Celion GY-70, and (d) Panex 30 after exposure to ICl.

Fig. 22 X-ray diffraction patterns of intercalated Thornel P-100 fibers after various lengths of desorption time: (a) 0 min, (b) 10 min, (c) 2 hr, (d) 1 week.

Fig. 23 In-plane unit cell of graphite-ICl (After Ref. 9)

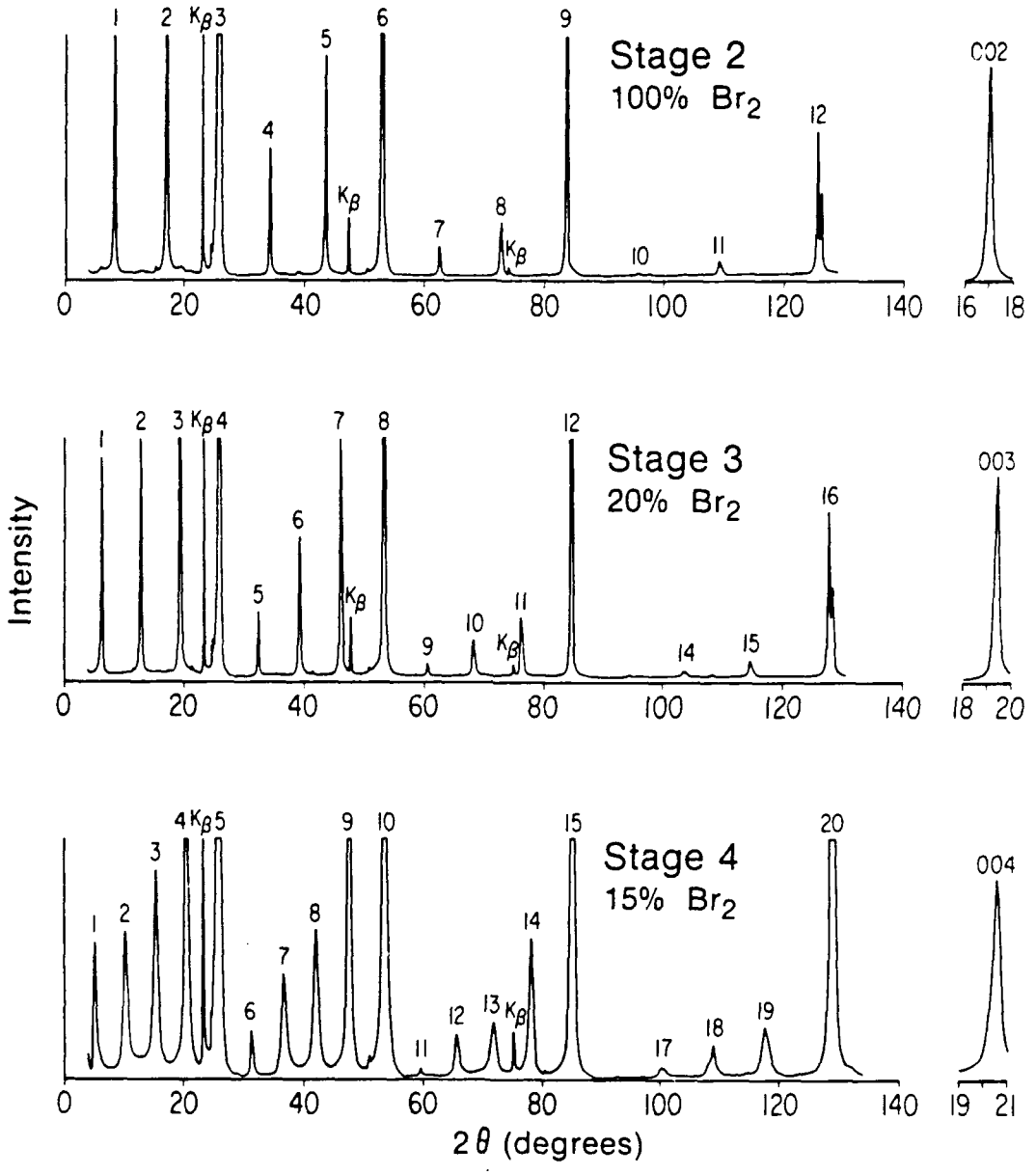
Stage 2
100% Br2
Stage 3
20% Br2
Stage 4
15% Br2
Intensity
2θ (degrees)
002
003
004

Fig. 1

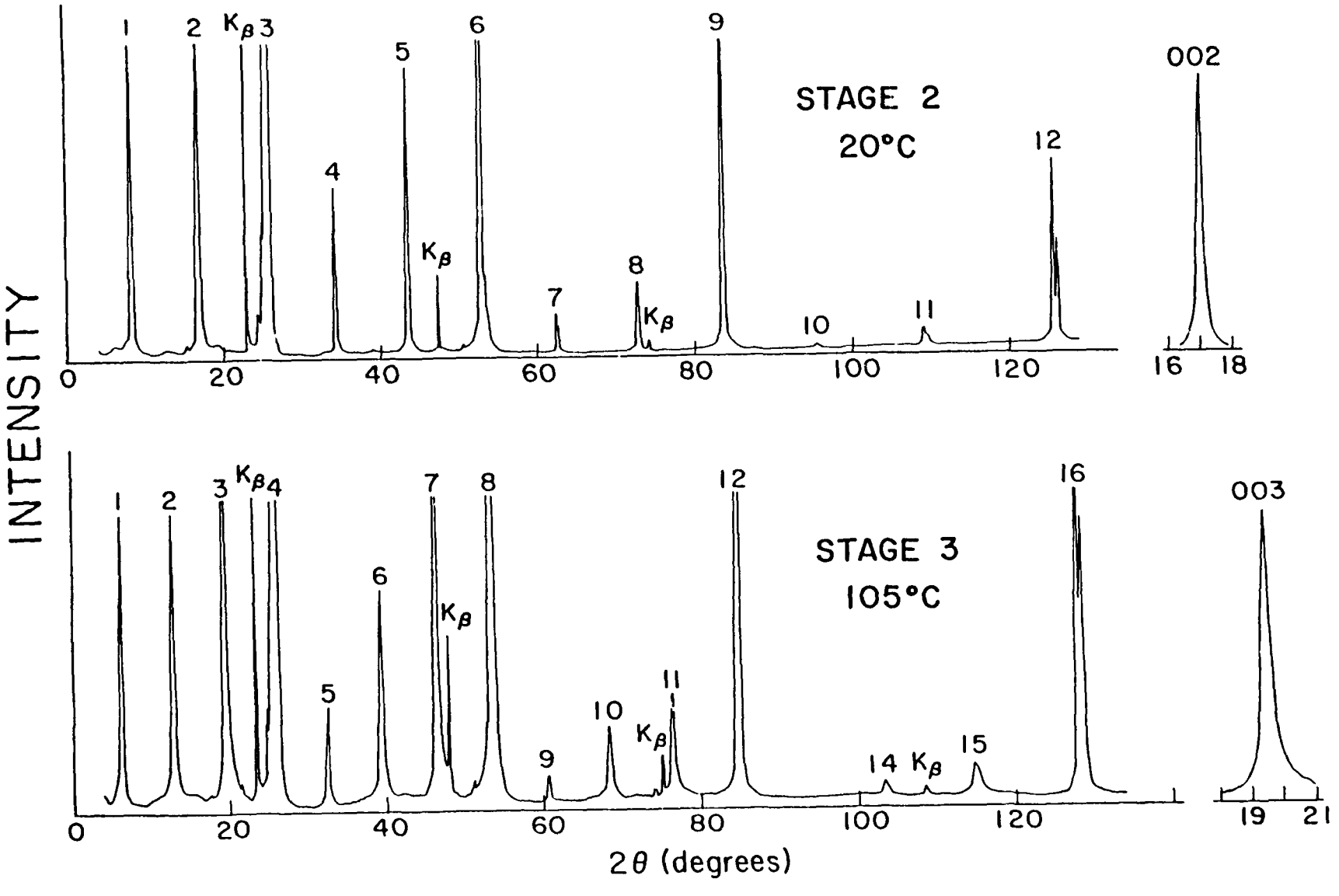
INTENSITY
STAGE 2
20°C
STAGE 3
105°C
002
003
1
2
Kβ
3
4
5
6
7
8
9
10
11
12
14
15
16
0
20
40
60
80
100
120
16
18
19
21
2θ (degrees)

Fig.

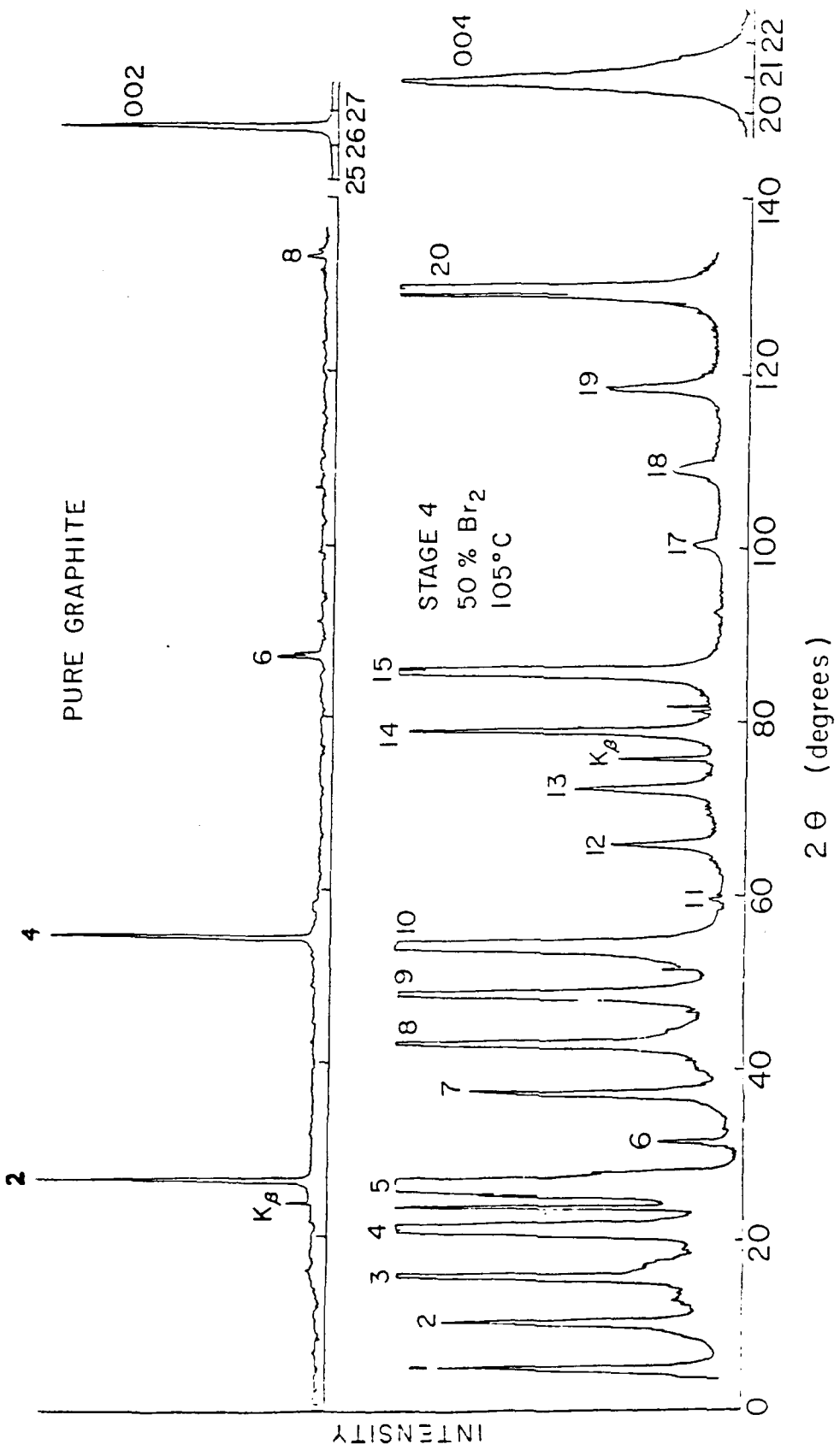
PURE GRAPHITE
STAGE 4
50 % Br2
105°C
002
004
Kβ
INTENSITY
2θ (degrees)
0
20
40
60
80
100
120
140

Fig.

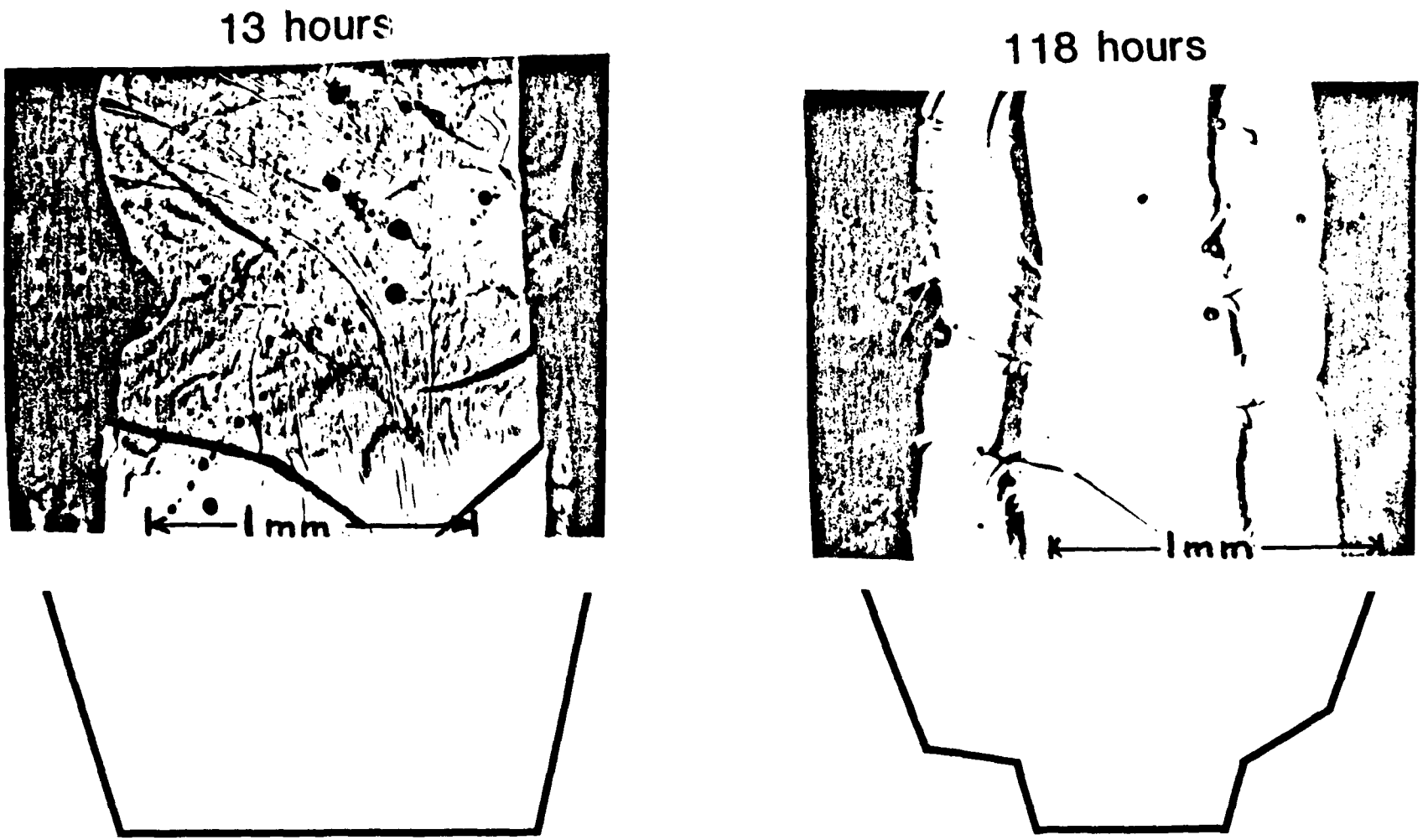

Fig.

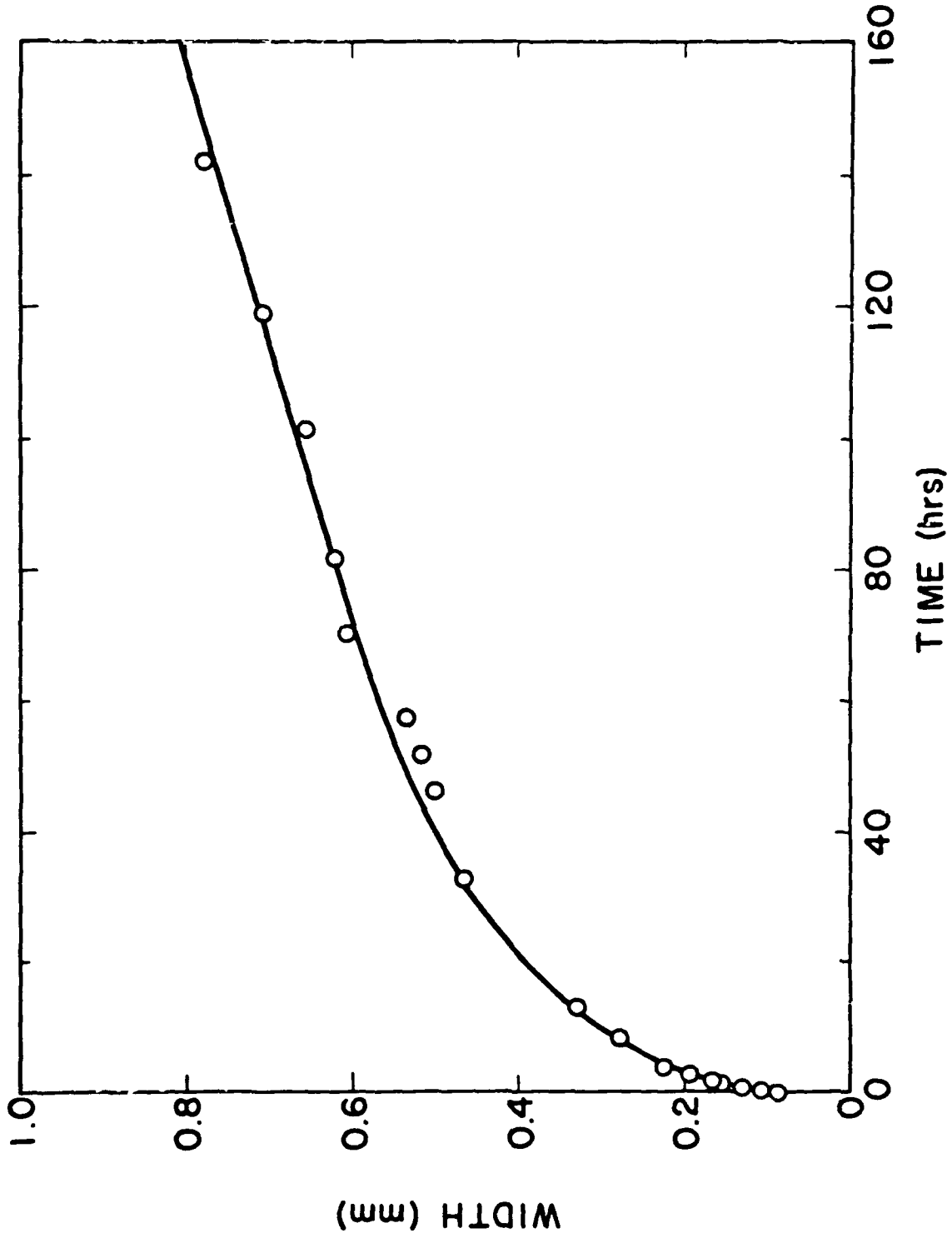

Fig.

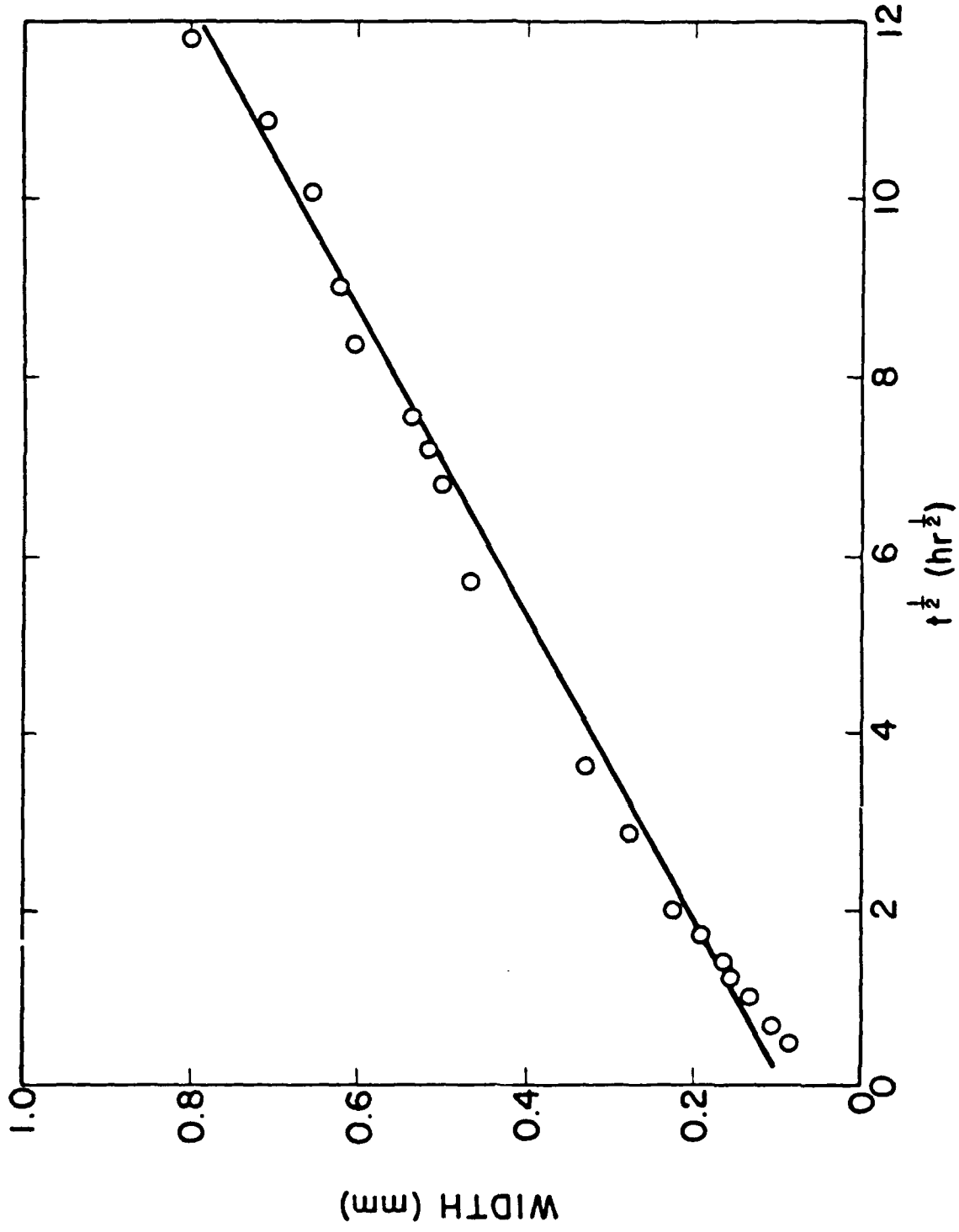

Fig. 6

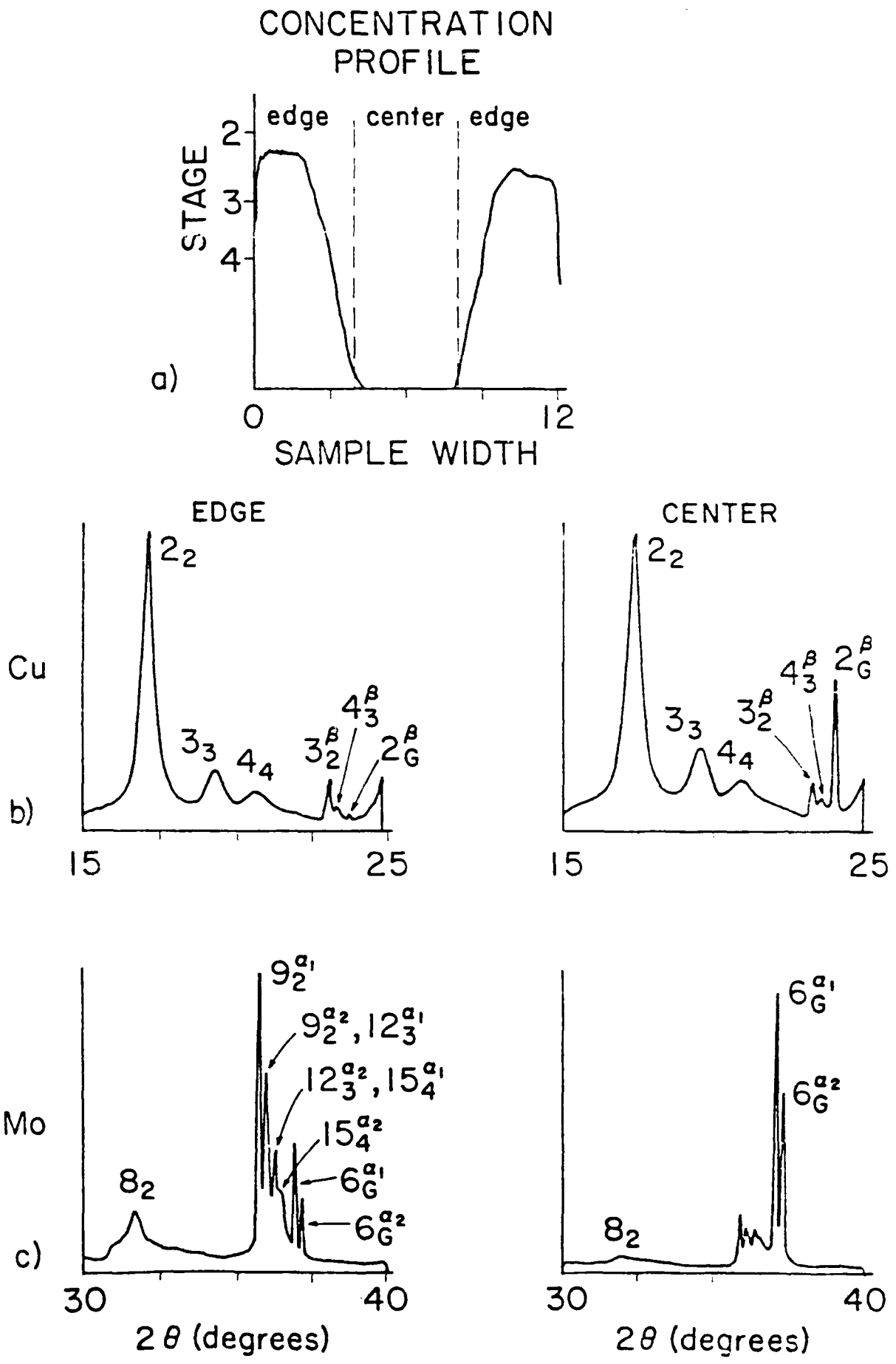
CONCENTRATION PROFILE
edge
center
edge
STAGE
2
3
4
a)
0
12
SAMPLE WIDTH
EDGE
CENTER
Cu
b)
2_2
3_3
4_4
3_2^β
4_3^β
2_G^β
15
25
Mo
c)
$9_2^{a_1}$
$9_2^{a_2}, 12_3^{a_1}$
$12_3^{a_2}, 15_4^{a_1}$
$15_4^{a_2}$
$6_G^{a_1}$
$6_G^{a_2}$
8_2
30
40
2θ (degrees)

Fig. 7

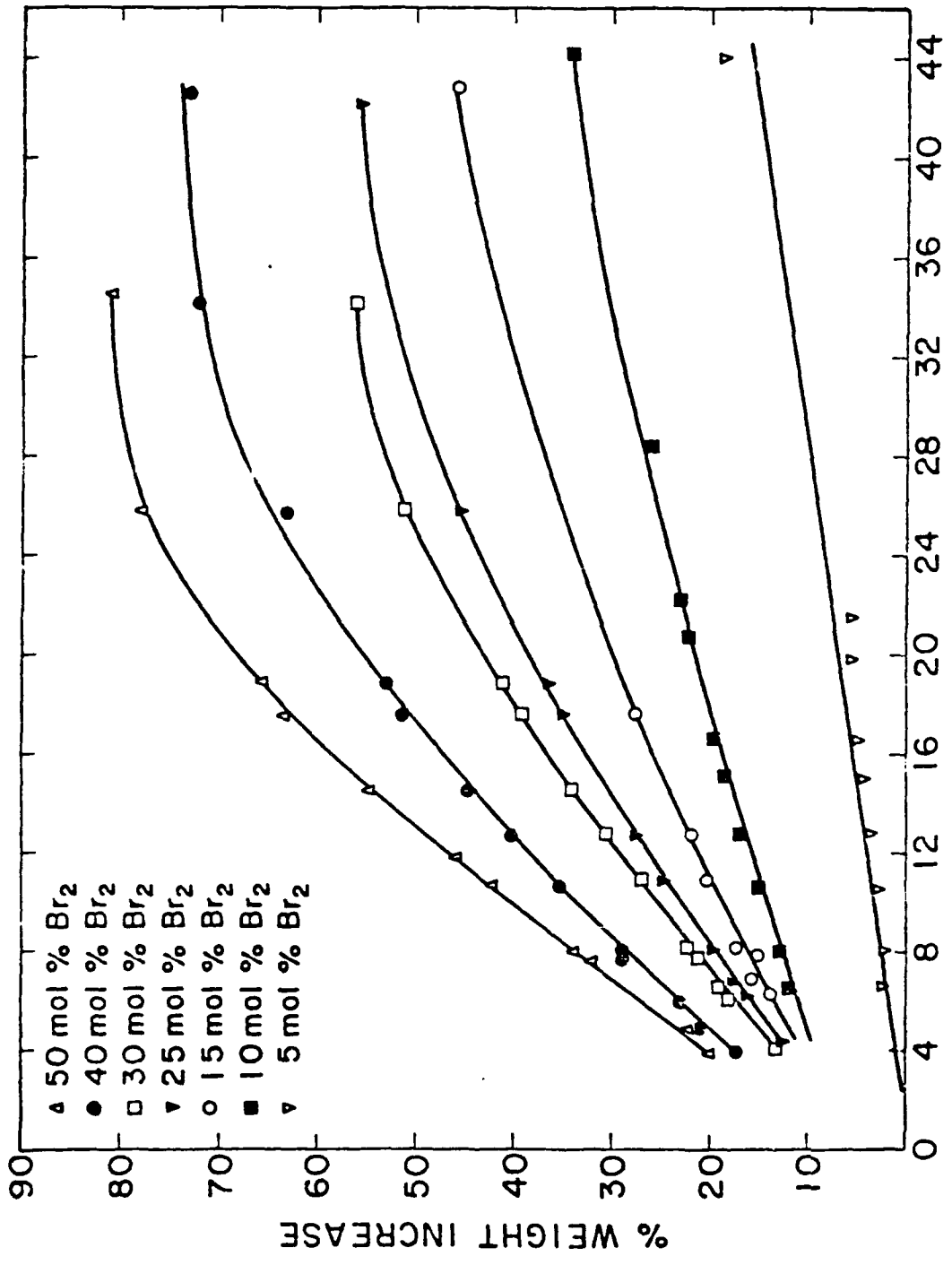
% WEIGHT INCREASE
$t^{1/2}$ (hr)$^{1/2}$
50 mol % Br_2
40 mol % Br_2
30 mol % Br_2
25 mol % Br_2
15 mol % Br_2
10 mol % Br_2
5 mol % Br_2
90
80
70
60
50
40
30
20
10
0
4
8
12
16
20
24
28
32
36
40
44

Fig. 8

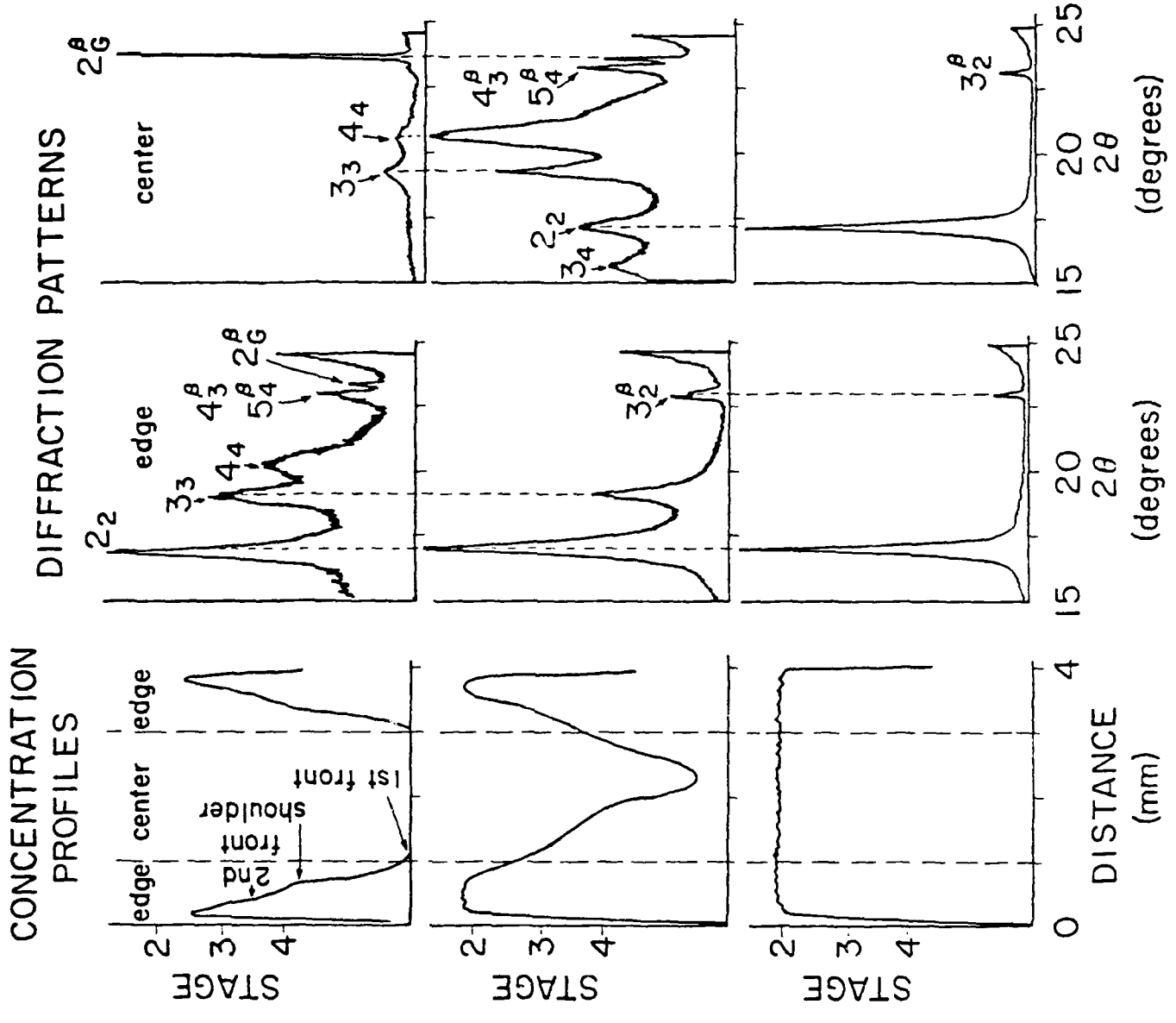
CONCENTRATION PROFILES
DIFFRACTION PATTERNS
34 hrs
210 hrs
1187 hrs
STAGE
edge
center
edge
2nd front shoulder
1st front
center
edge
2_2
3_3
4_4
4_3^β
5_4^β
2_G^β
3_2^β
3_4
2
3
4
0
15
20
25
DISTANCE (mm)
2θ (degrees)

Fig. 9

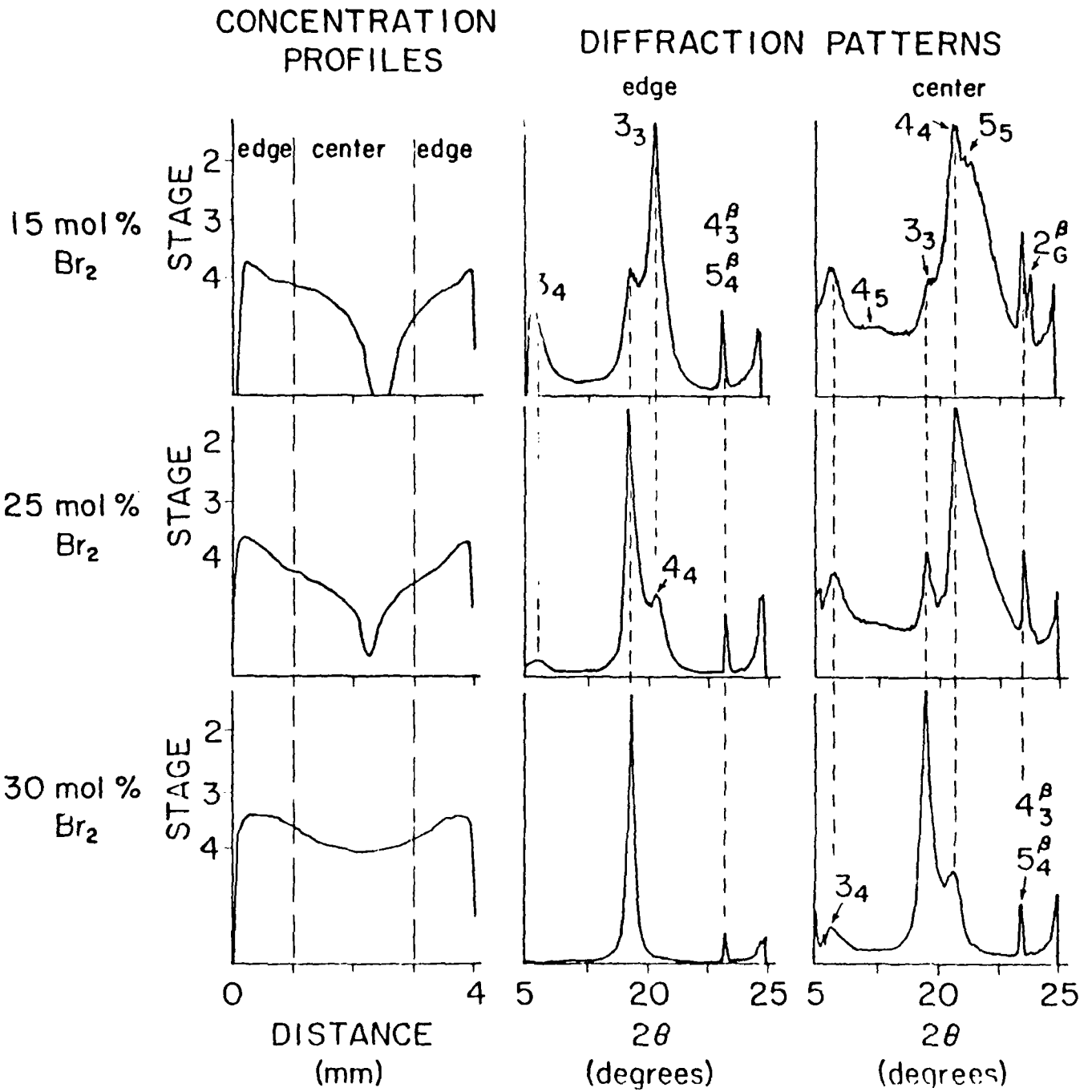
CONCENTRATION PROFILES
DIFFRACTION PATTERNS
edge
center
edge
15 mol % Br2
25 mol % Br2
30 mol % Br2
STAGE
2
3
4
3_3
4_3^β
5_4^β
3_4
4_4
4_4
5_5
3_3
2_G^β
4_5
4_3^β
5_4^β
3_4
0
4
5
20
25
DISTANCE
(mm)
2θ
(degrees)
2θ
(degrees)

Fig. 10

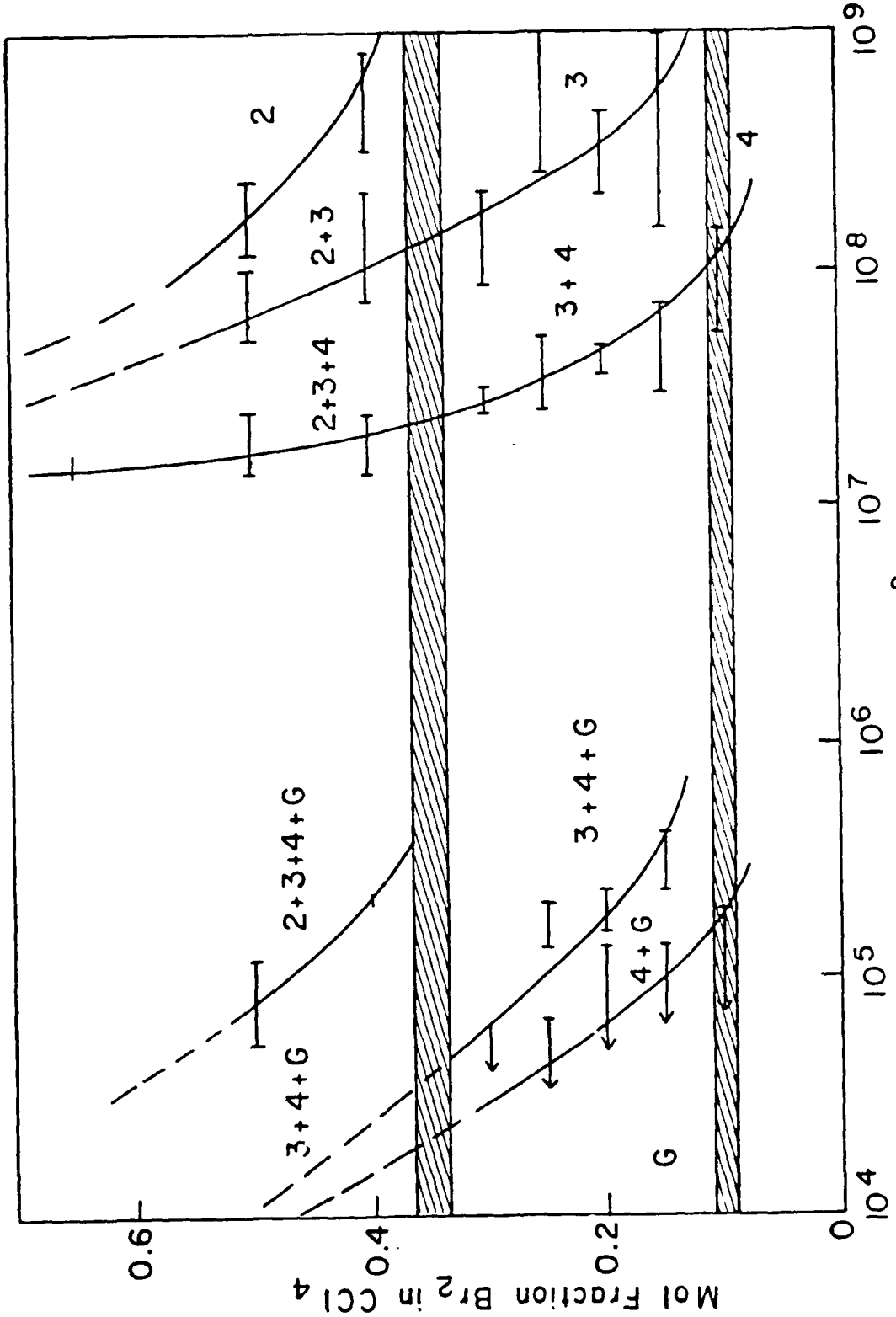
Mol Fraction Br2 in CCl4
0.6
0.4
0.2
0
10^4
10^5
10^6
10^7
10^8
10^9
(s/cm^2)
2
2+3
2+3+4
3
3+4
4
2+3+4+G
3+4+G
4+G
3+4+G
G

Fig. 11

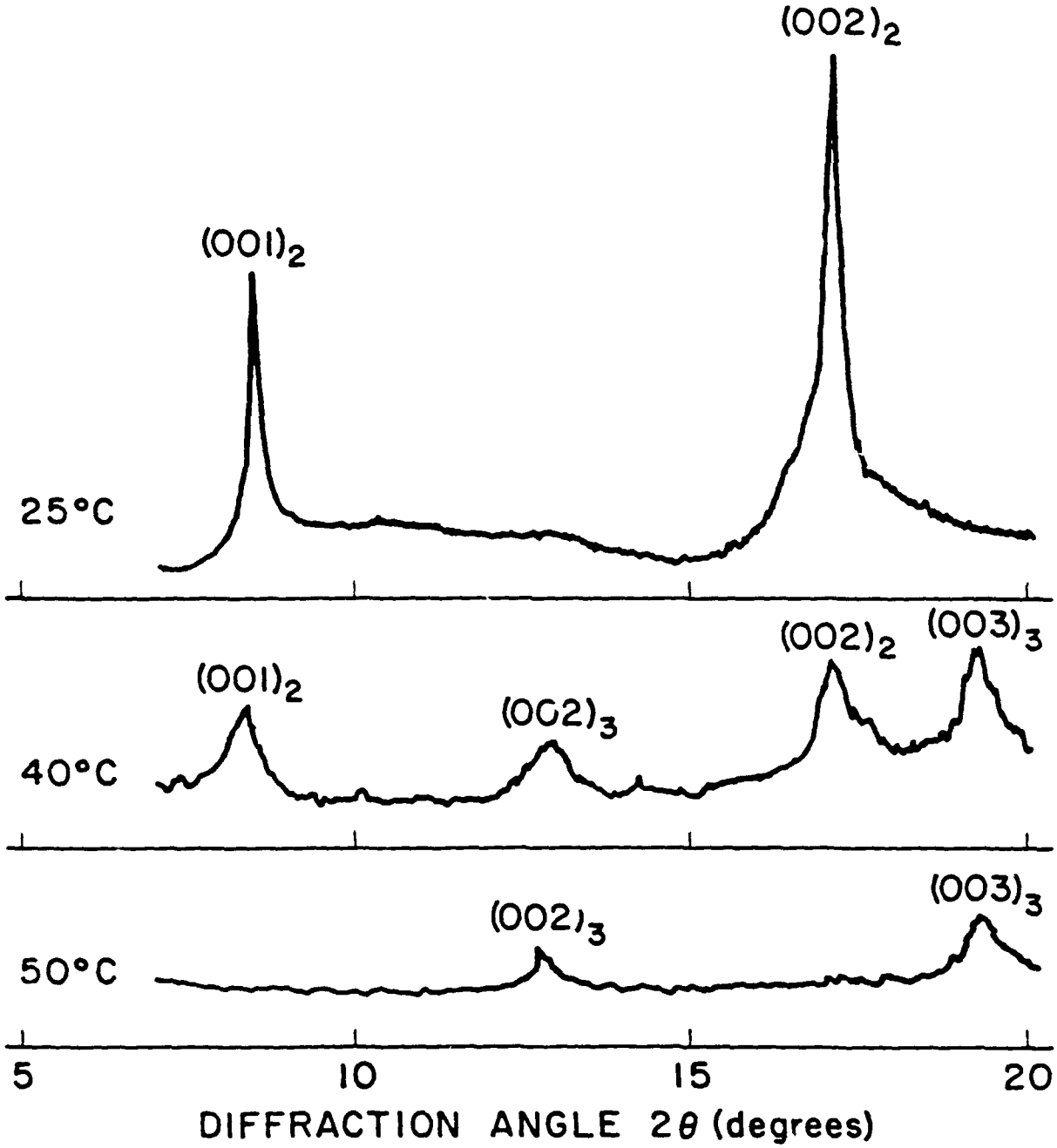
(002)2
(001)2
25°C
(003)3
(002)2
(001)2
(002)3
40°C
(003)3
(002)3
50°C
5
10
15
20
DIFFRACTION ANGLE 2θ (degrees)

Fig. 12

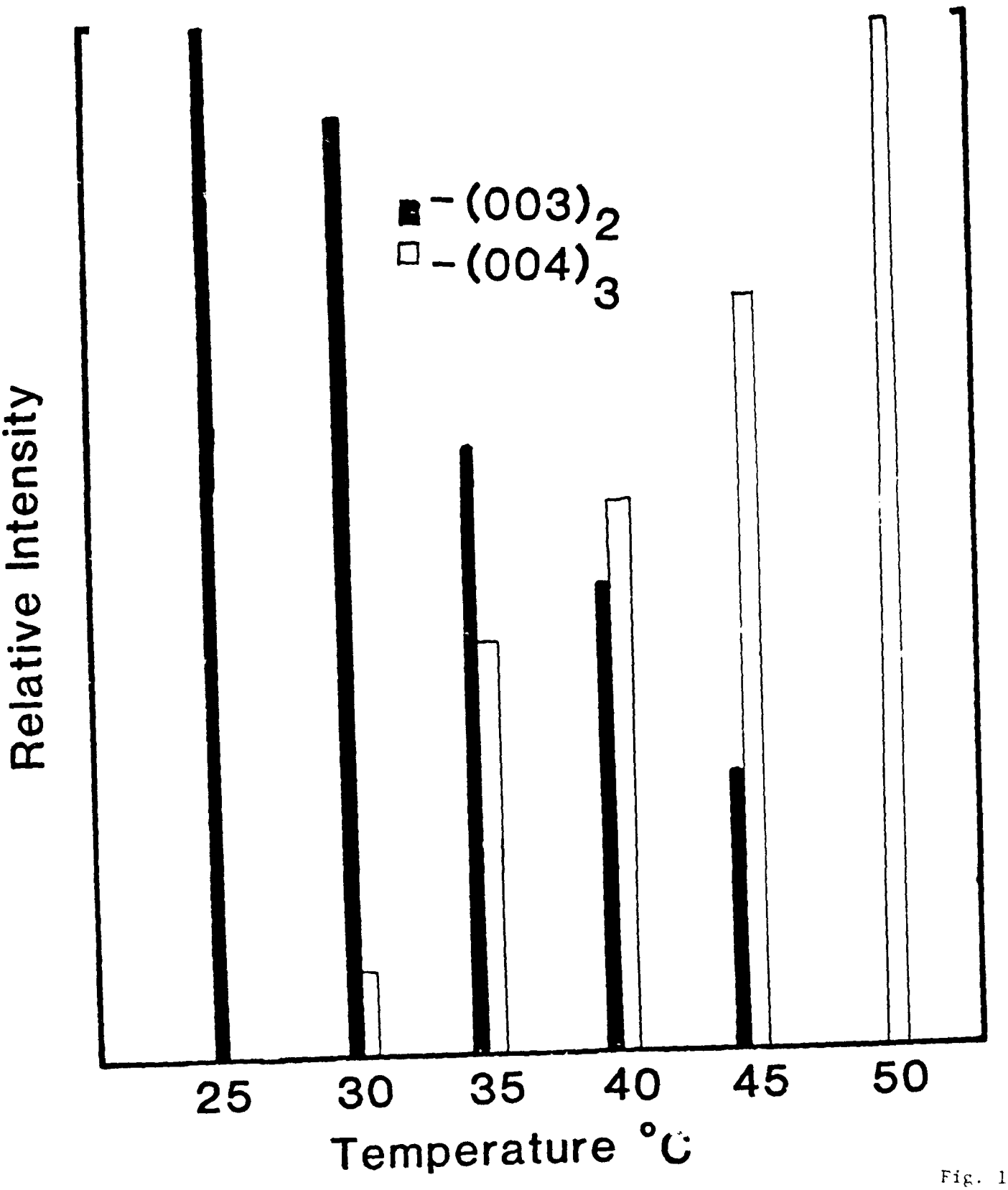

Fig. 13

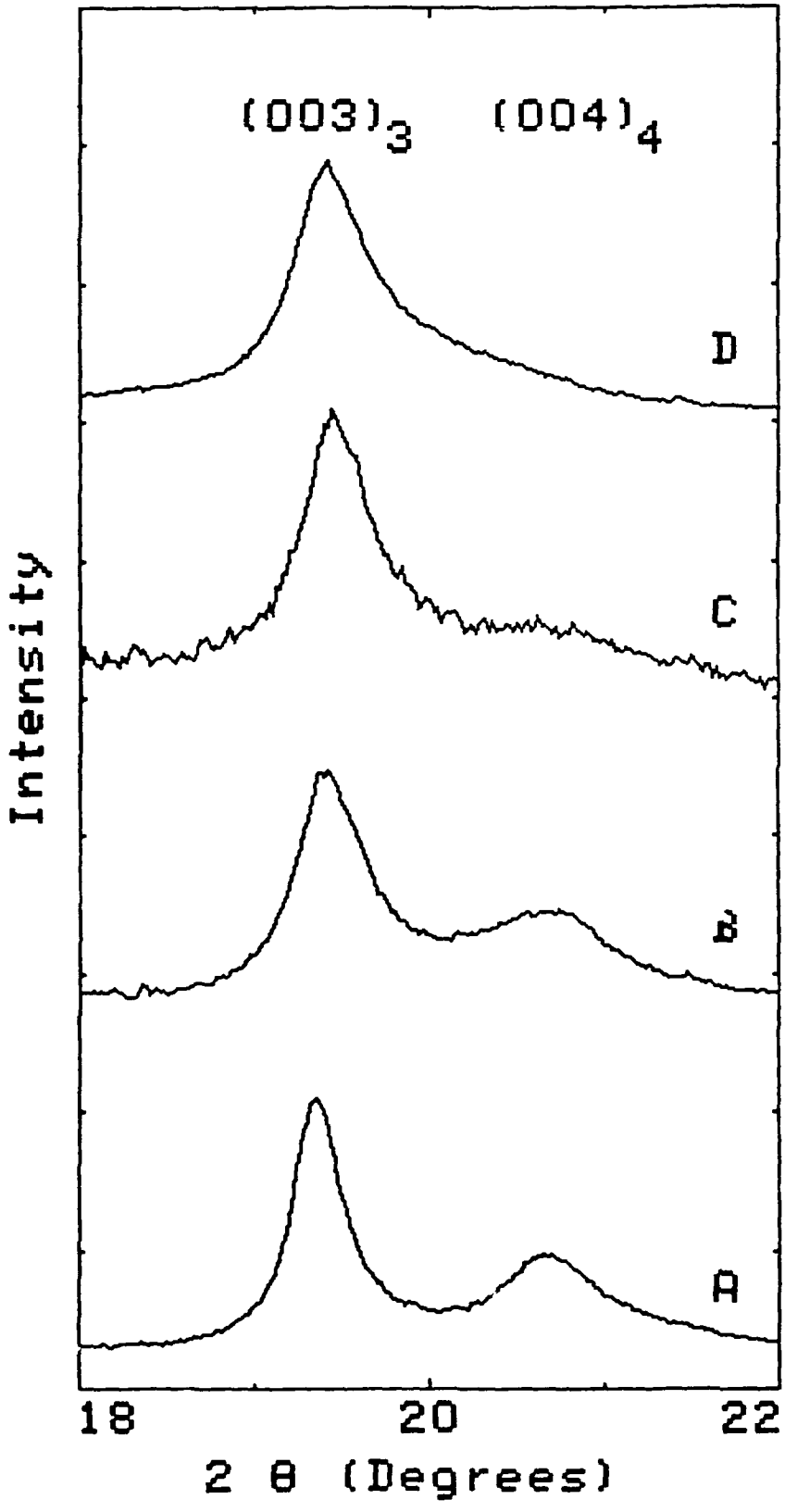

Fig. 14

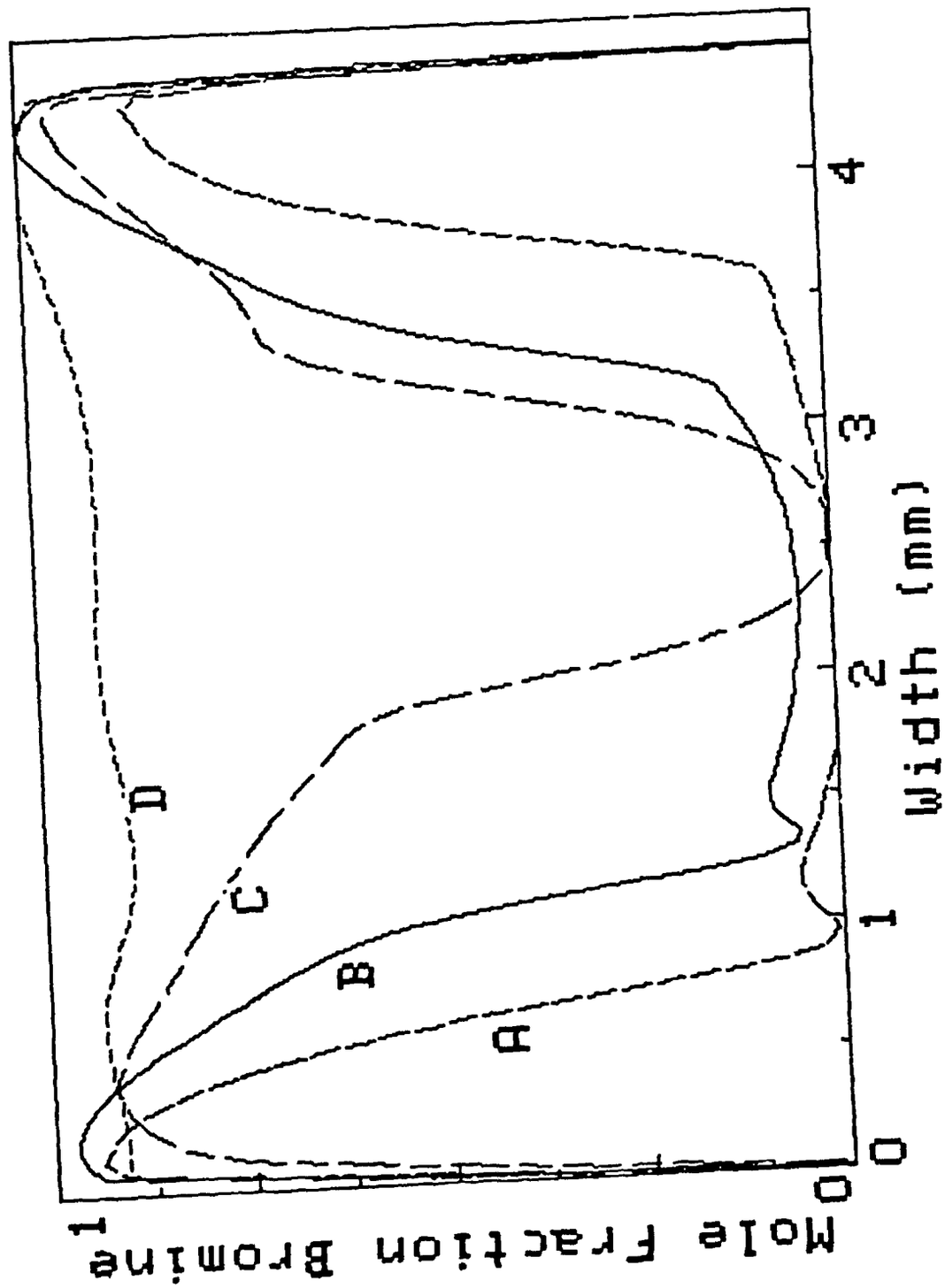

Fig. 15

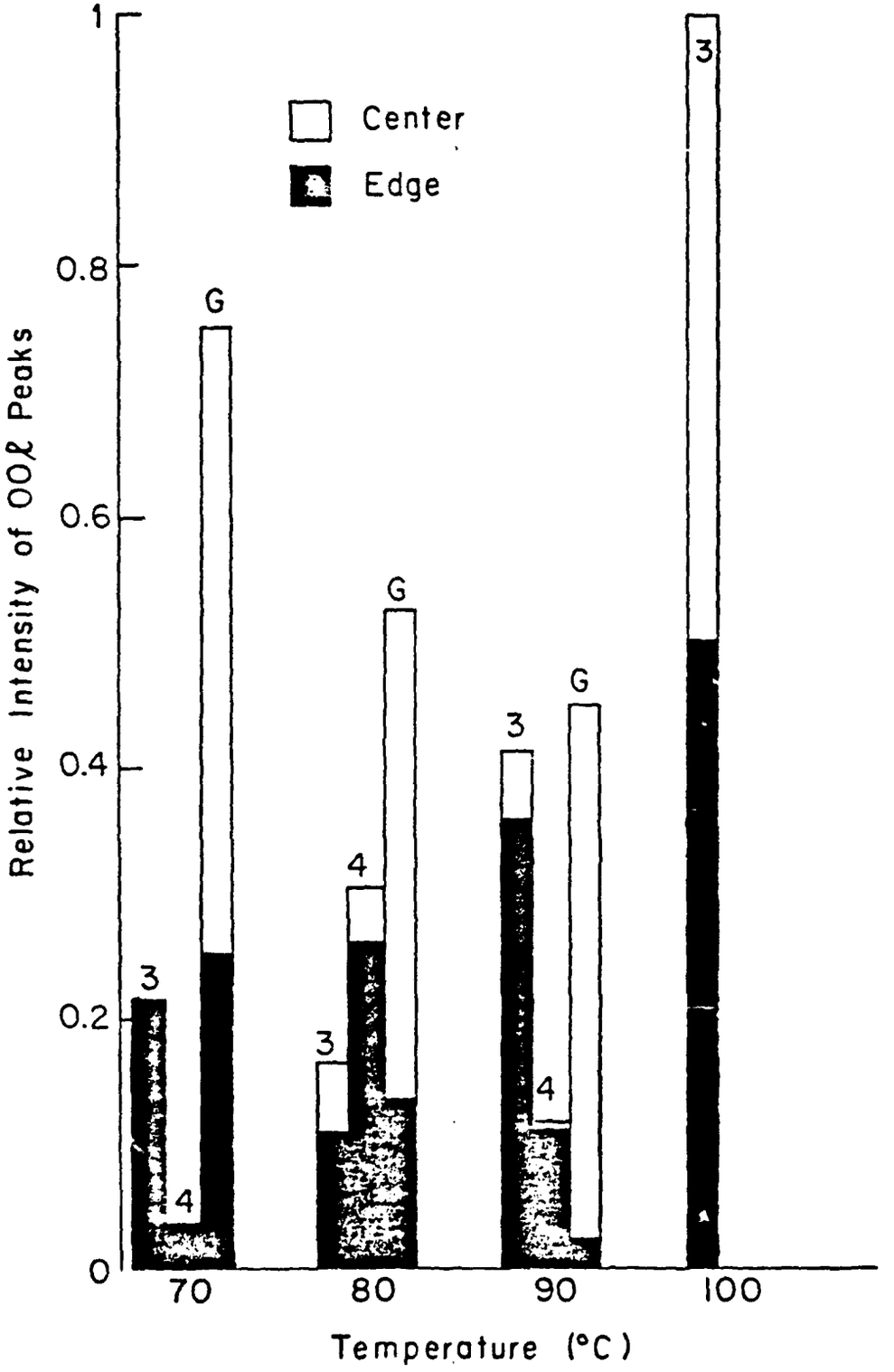
Center
Edge
Relative Intensity of 00ℓ Peaks
Temperature (°C)
0
0.2
0.4
0.6
0.8
1
70
80
90
100
3
4
G

Fig. 16

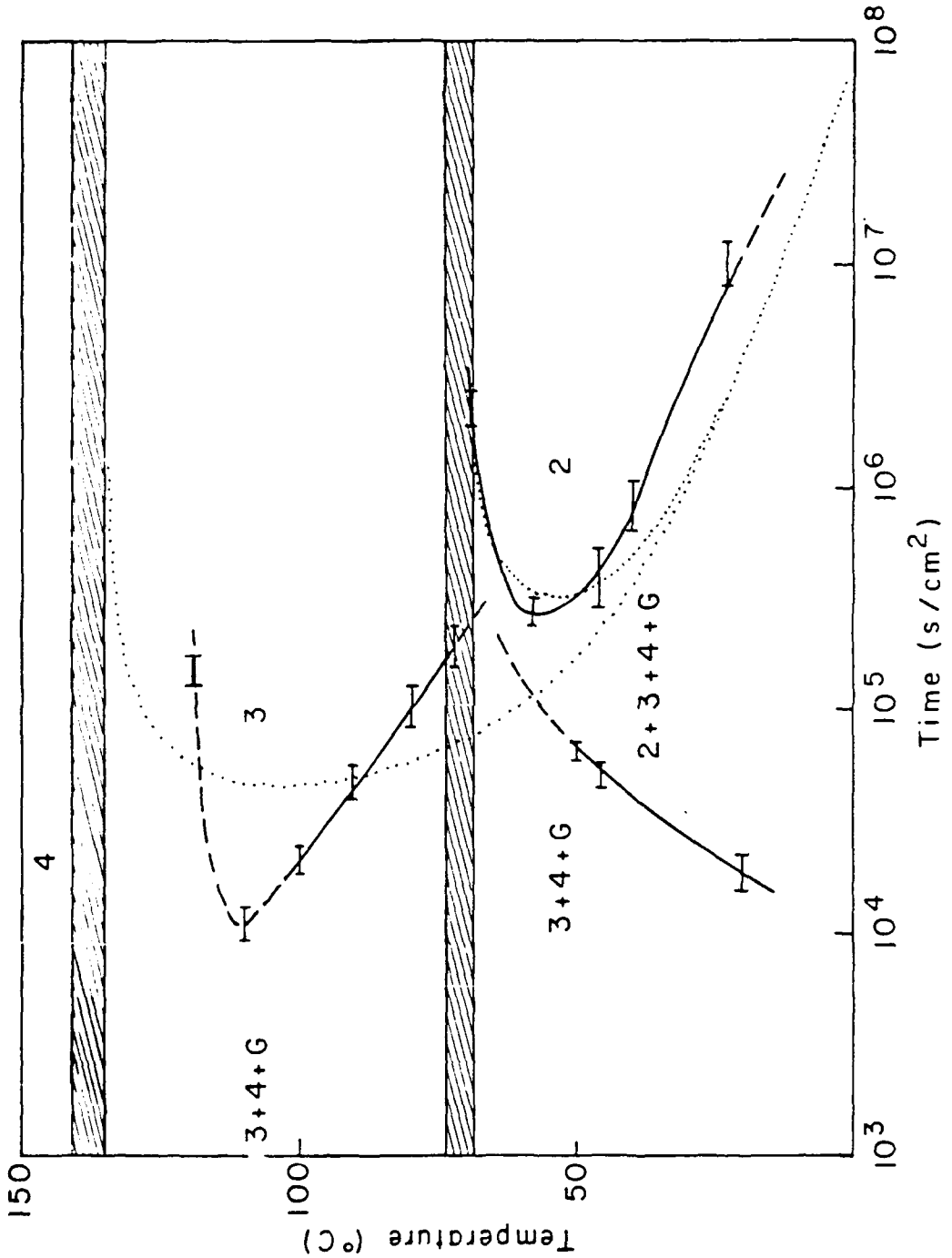
Temperature (°C)
150
100
50
Time (s/cm²)
10³
10⁴
10⁵
10⁶
10⁷
10⁸
4
3
2
3+4+G
3+4+G
2+3+4+G

Fig. 17

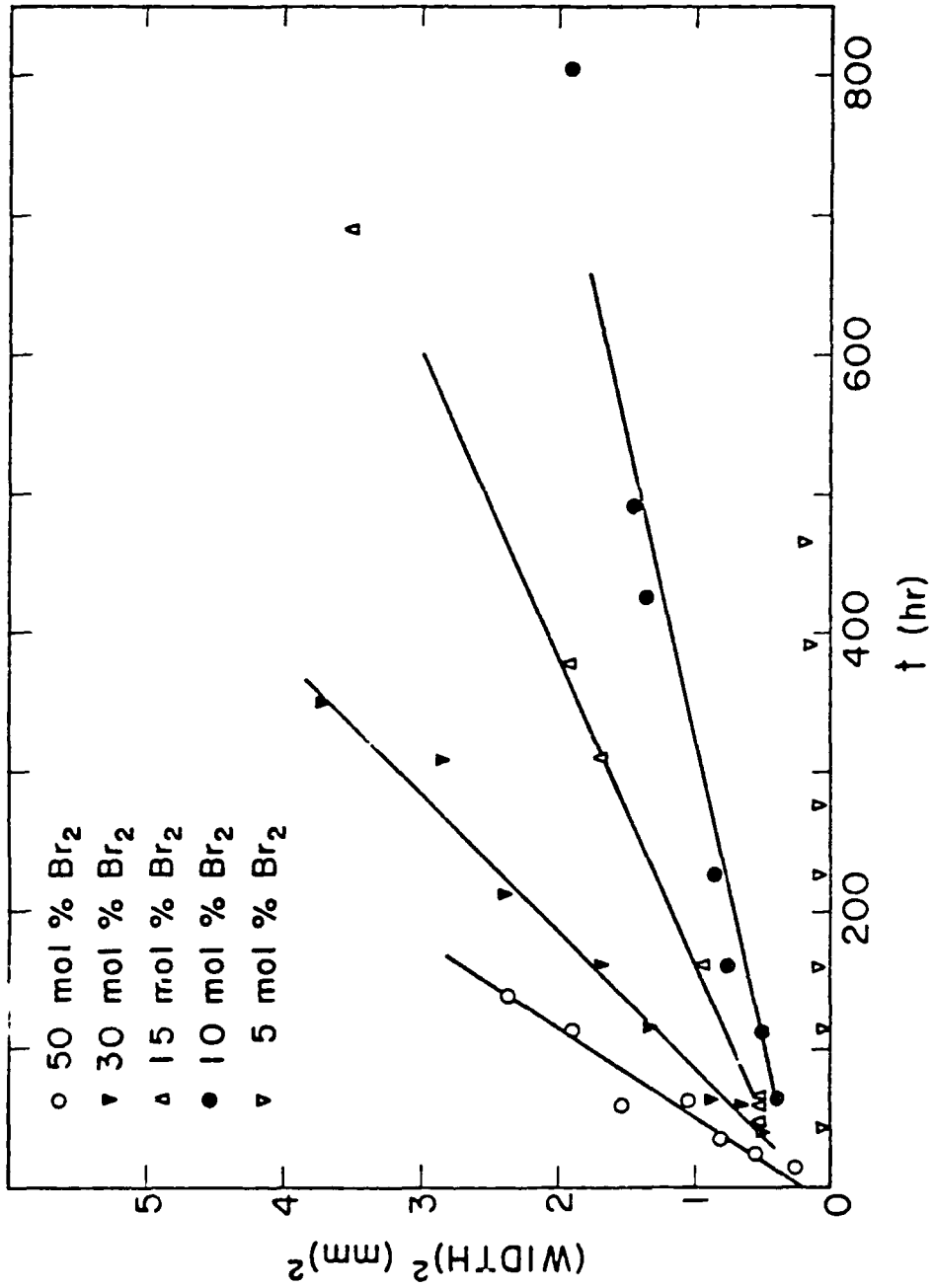
50 mol % Br2
30 mol % Br2
15 mol % Br2
10 mol % Br2
5 mol % Br2
(WIDTH)2 (mm)2
t (hr)
0
1
2
3
4
5
200
400
600
800

Fig. 18

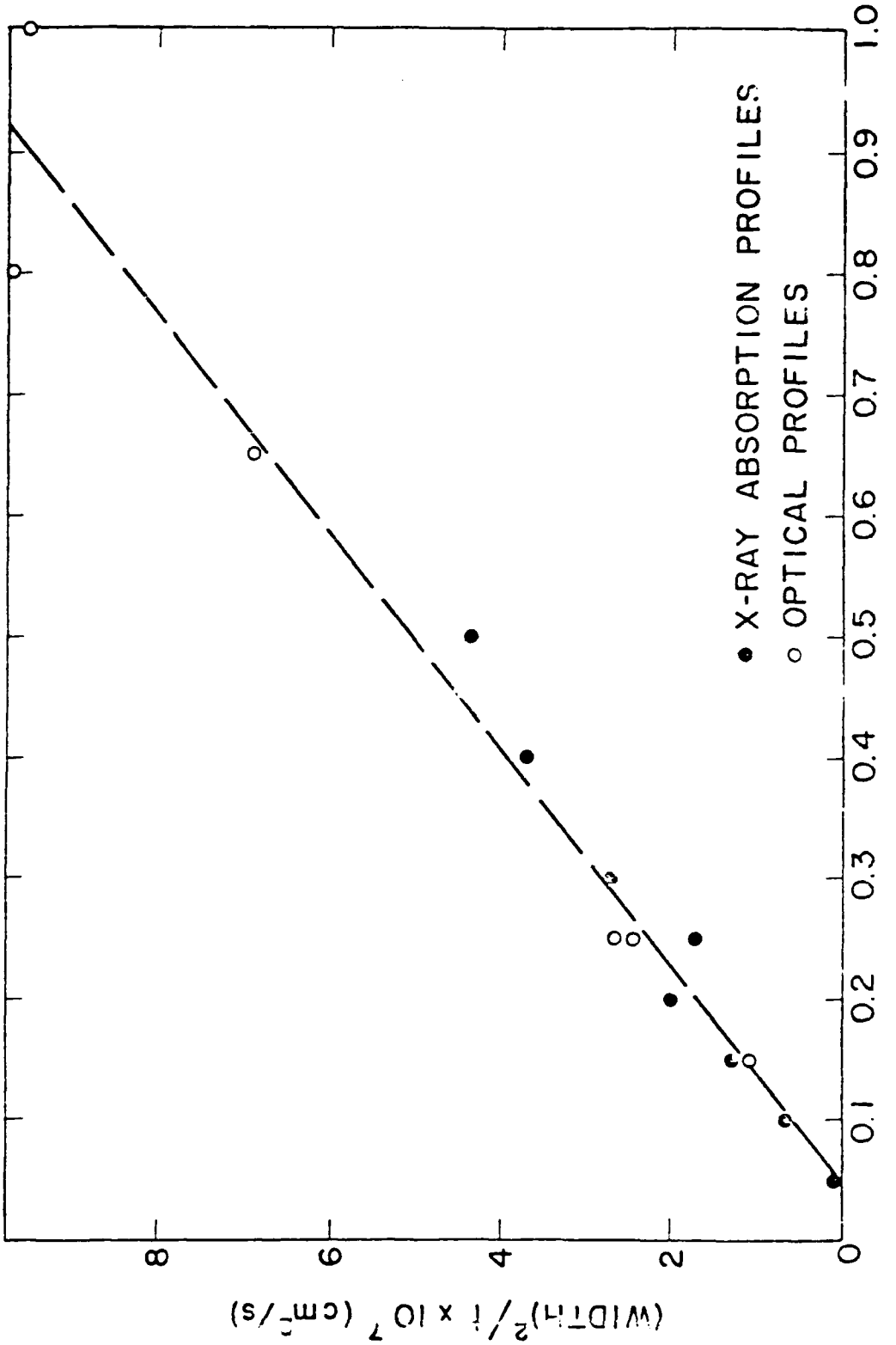
(WIDTH)²/i x 10⁷ (cm⁻²/s)
0
2
4
6
8
0
0.1
0.2
0.3
0.4
0.5
0.6
0.7
0.8
0.9
1.0
MOL FRACTION Br₂ IN CCl₄
● X-RAY ABSORPTION PROFILES
○ OPTICAL PROFILES

Fig. 19

(a) Thornel P-100

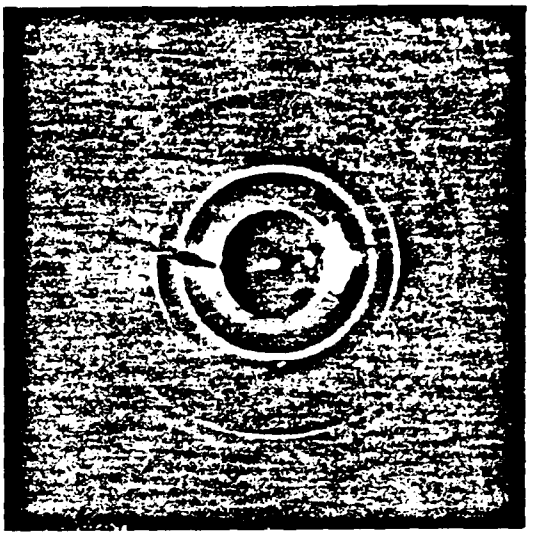

(b) Celion GY-70

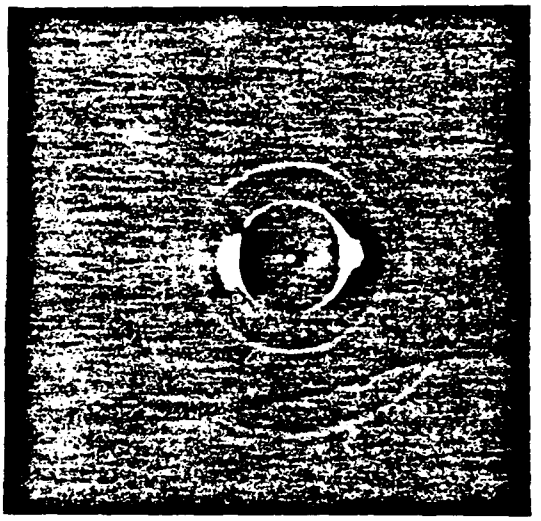

(c) Panex 30

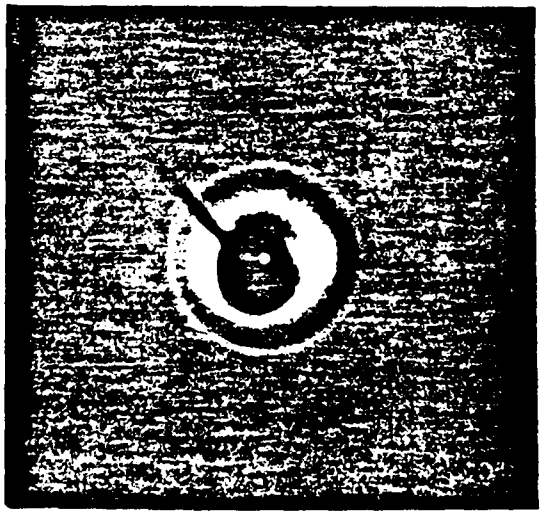

Fig. 20

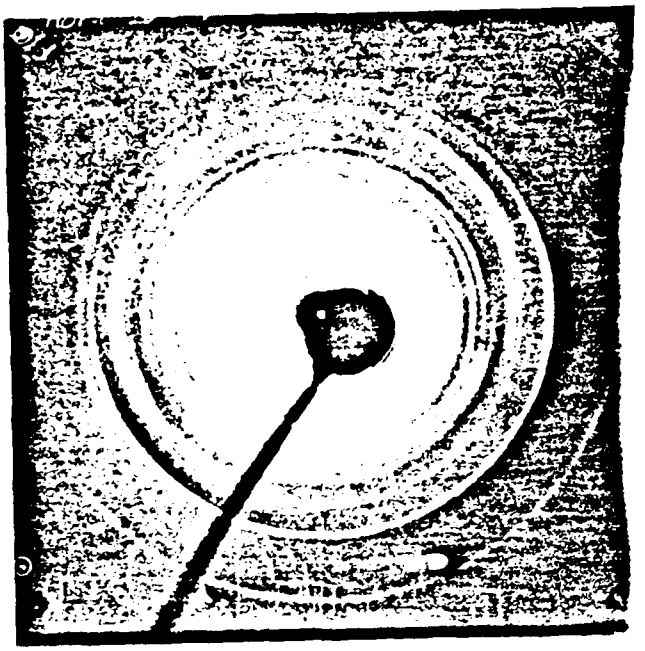

(a) HOPG

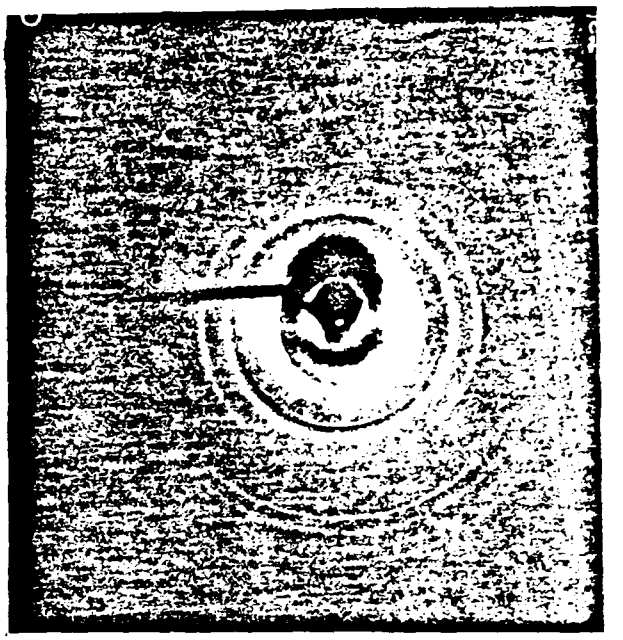

(b) Thornel P-100

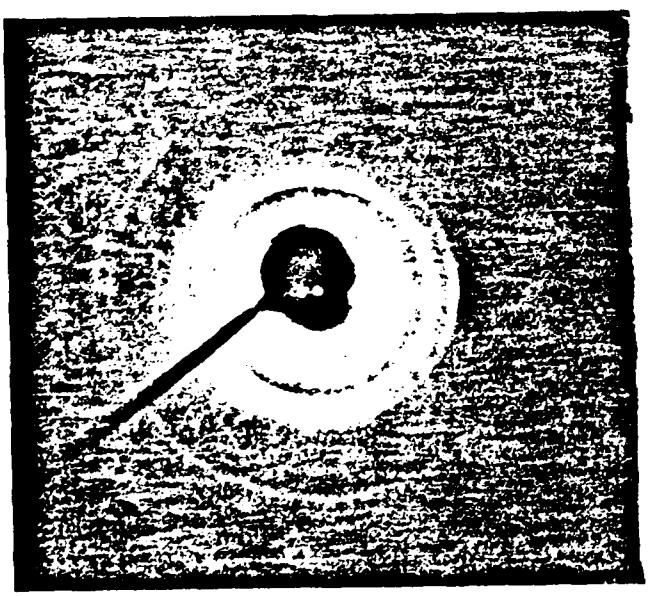

(c) Celion GY-70

(d) Panex 30

Fig. 21

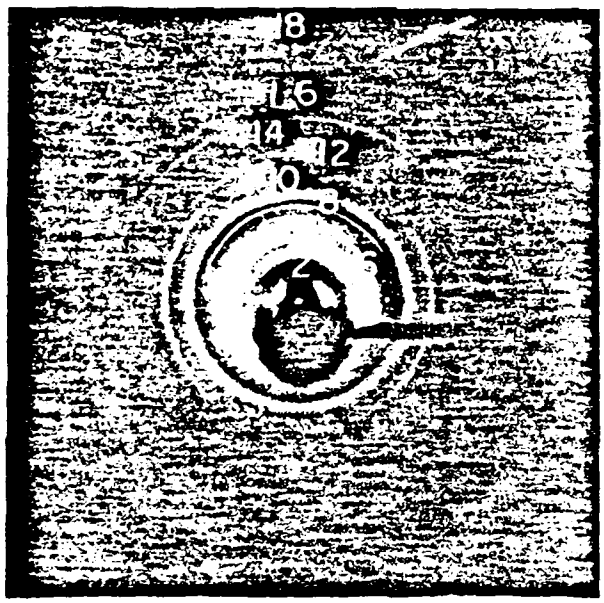

(a) 0 min

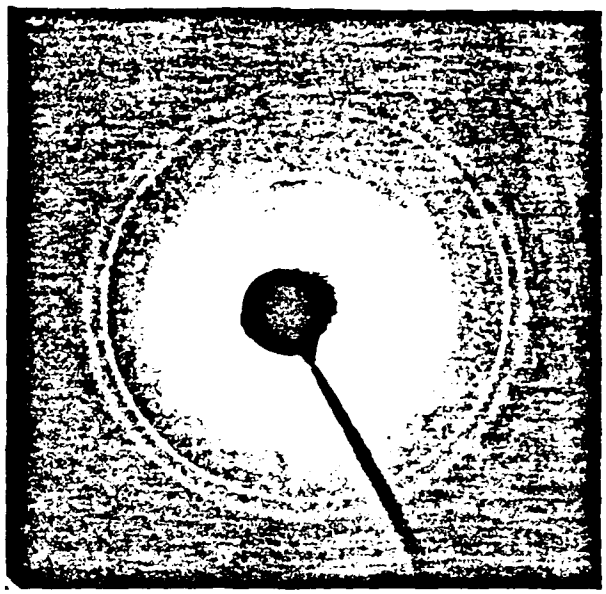

(b) 10 min

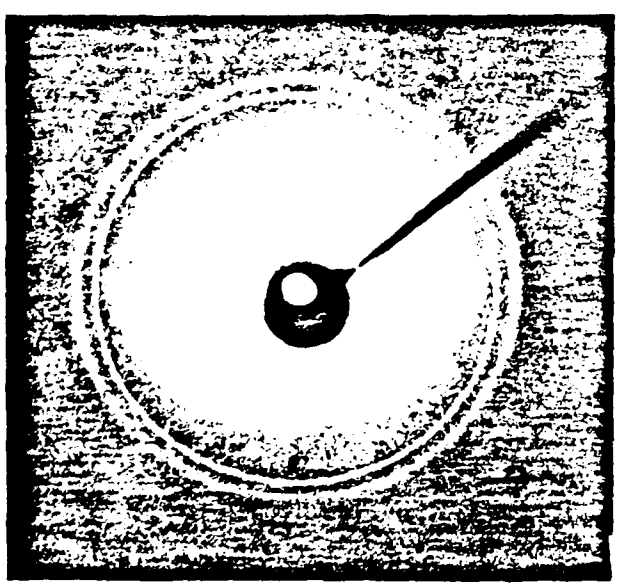

(c) 2 hr

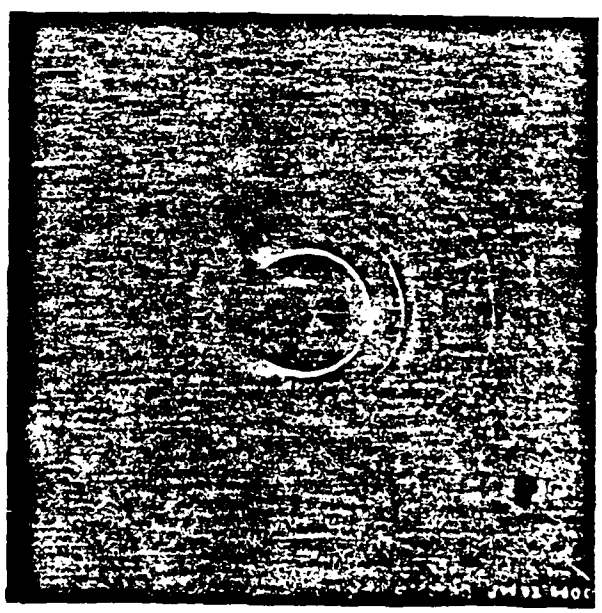

(d) 1 week

Fig. 22

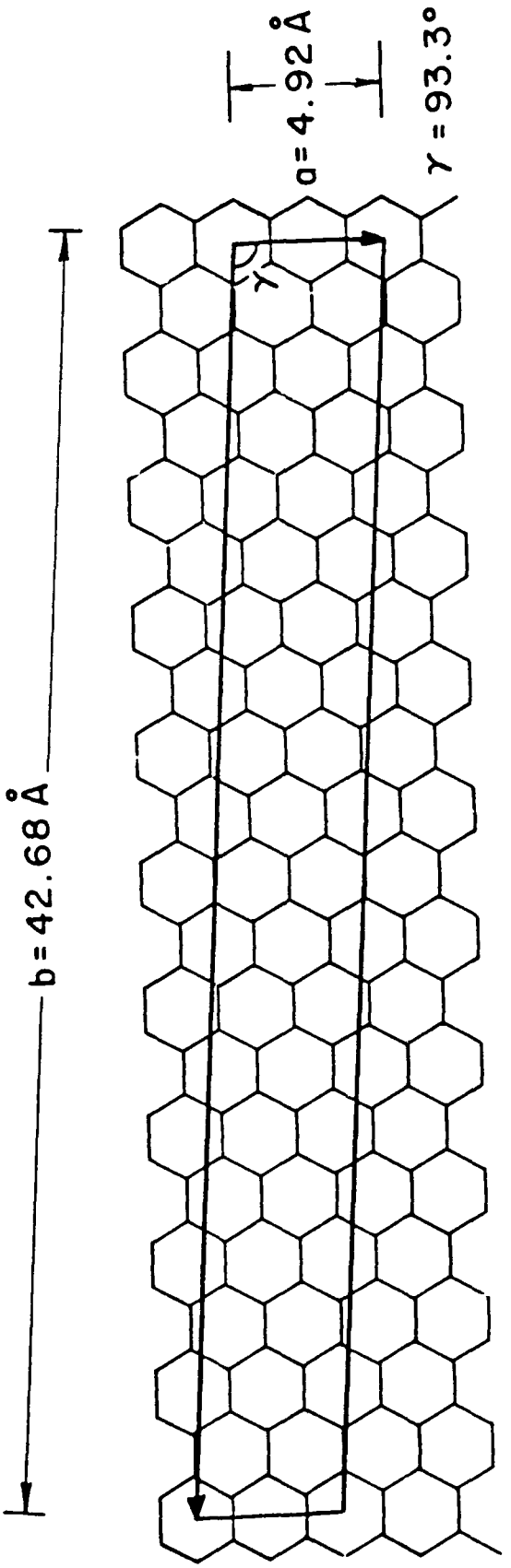

Fig. 23

II. EXFOLIATION OF INTERCALATED GRAPHITE

Summary

By x-ray diffraction, exfoliated graphite-Br_2 was found to exhibit the same in-plane superlattice ordering as intercalated graphite prior to exfoliation. This ordering persisted even after heating for an hour at 1700°C. By dilatometry, a single exfoliation event was found to consist of multiple expansion spurts, which occurred at ~150°C and ~240°C for first exfoliation, and ~100°C and ~240°C for subsequent cycles. The amount of expansion was found to increase with decreasing intercalate activity during intercalation. With exfoliation cycles to higher temperatures or longer times, the amount of residual expansion after the collapse on cooling increased until no second exfoliation was observed on reheating. Due to intercalate desorption, the amount of expansion for concentrated samples increased with increasing sample width; desorbed samples showed little width dependence. Acoustic emission was observed before appreciable expansion during the first exfoliation cycle; it was not observed during the collapse or subsequent exfoliation cycles. A model of exfoliation involving intercalate islands is proposed.

Introduction

When intercalated graphite is heated past a critical temperature, a large expansion along the c-direction occurs, giving the compound a puffed-up appearance. This phenomenon is known as exfoliation.

Brocklehurst[1] observed by dilatometry that desorbed graphite-Br_2 based on polycrystalline artificial extruded graphite began exfoliation at ~300°C upon heating, resulting in an expansion of up to ~2.1 % at 500°C. By similar dilatometric measurement on desorbed graphite-Br_2 based on pyrolytic graphite, Martin and Brocklehurst[2] found that

1. first exfoliation occurred at ~170°C upon first heating,
2. subsequent exfoliation occurred at ~120°C in subsequent heating cycles,
3. collapse occurred at ~110°C upon cooling,
4. second and subsequent exfoliation cycles were reversible,
5. expansion was up to 380 % at 500°C,
6. the exfoliation temperature increased linearly with increasing load.

In contrast to the relatively small amount of expansion observed by Martin and Brocklehurst, Ubbelohde[3] observed an expansion of ~1000 % at 350°C for graphite-Br_2 based on well-oriented graphite. By using differential thermal analysis, optical microscopy and gaseous pycnometry, Mazieres et al.[4] found that desorbed graphite-Br_2 based on pyrocarbons underwent first exfoliation at 160-200°C on heating, second exfoliation at 100-120°C on heating, and collapse at 70-100°C on cooling. Furthermore, they found that thermal cycling decreased the exfoliation tendency progressively and that this effect was more pronounced when the heating was carried out in air. Mazieres et al.[5] observed irreversible exfoliation after heating desorbed graphite-Br_2 based on pyrocarbons to 1000°C and cooling in an argon atmosphere. In addition, they demonstrated that it was possible to intercalate the irreversibly exfoliated material.

Other than graphite-Br_2, exfoliation had also been observed in graphite-ferric chloride[1],

graphite-aluminum chloride[7], and graphite intercalated with a mixture of nitric and sulphuric acids[7].

The tendency for exfoliation depends on the extent of stacking order of the graphite basal planes[5]. Dowell[6] showed that possession of a basal plane stack height, L_c, greater than ~750 Å was necessary for exfoliation.

The exfoliation phenomenon is of technological importance as well as scientific interest. The exfoliation of graphite-ferric chloride has been used to manufacture Grafoil[7], a high temperature thread sealant tape. The exfoliation of graphite-HNO_3-H_2SO_4 has been used for making a thermal insulator for molten metals[11]. The exfoliation of graphite-$FeCl_3$-NH_3 has been used for making blankets for the extinction of metal fires[12]. In addition, exfoliated graphite is being investigated by the U.S. Army for use as a battlefield obscurant[13]. The surface area increase resulting from irreversible exfoliation is attractive for catalytic applications of graphite intercalation compounds[14]. In addition, exfoliation is a phenomenon that affects the thermal stability of graphite intercalation compounds, so understanding of this phenomenon is necessary for the use of graphite intercalation compounds at elevated temperatures.

We have reported that the exfoliation behavior depends more strongly on the parent initial stage than on the intercalate concentration in graphite-Br_2[15]. This paper supports this contention and offers further insight into the exfoliation process. The key issues which are addressed include the following. Is exfoliated graphite intercalated? How reversible is exfoliation? How can the reversibility or irreversibility of exfoliation be controlled? What is the mechanism of exfoliation?

In this work, we have used dilatometry to investigate the dependence of multiple exfoliation and collapse on

1. the stage,

2. the intercalate concentration.

3. the intercalation temperature.

4. the annealing time and temperature after the first exfoliation.

5. the sample size.

6. the intercalate species.

Particular attention was given to the reversibility of exfoliation. In addition, acoustic emission was used to investigate the nature of the exfoliation process and x-ray diffraction was used to study the crystal structure of the exfoliated material.

The main findings of this work are the following

1. Exfoliated graphite exhibits the same in-plane superlattice ordering as intercalated graphite prior to exfoliation. This ordering persists even after heating for an hour at 1700°C.

2. Acoustic emission was observed before appreciable expansion during the first exfoliation cycle. It was not observed during the collapse or subsequent exfoliation cycles.

3. A single exfoliation event consists of multiple expansion spurts, which occur at ~150°C and ~240°C for first exfoliation, and at ~100°C and ~240°C for subsequent cycles.

4. The expansion was found to increase with decreasing intercalate activity during intercalation, such that it increased with decreasing Br_2 concentration in the Br_2-CCl_4 solution and with increasing intercalation temperature.

5. With exfoliation cycles to higher temperatures or longer annealing times, the amount of residual expansion after the collapse on cooling increased until no second exfoliation was observed on reheating, i.e., exfoliation became irreversible.

6. Due to intercalate desorption, concentrated intercalated graphite shows more expansion after first exfoliation than after second exfoliation. However, desorbed intercalated graphite shows less expansion after first exfoliation than after second exfoliation.

7. On repeated exfoliation cycles, concentrated samples show a decrease in the amount of expansion due to desorption during exfoliation, while desorbed samples show little decrease in the amount of exfoliation.

8. Due to intercalate desorption, the amount of expansion for concentrated samples increases with increasing sample width. However, desorbed samples show little width dependence.

Experimental Techniques

Samples were prepared from highly oriented pyrolytic graphite (HOPG) kindly provided by Union Carbide Corporation. Most samples were cut to a size of 4mm x 4mm x 0.5mm and then placed in liquid bromine for intercalation. Samples which were intercalated above room temperature were placed in a constant temperature bath. Times of the order of a minute were required to place a sample in a sample holder, add bromine, seal the sample holder and place it in the water bath. A similar amount of time was necessary to remove the sample from the bath, quench it to room temperature, and remove the sample from the bromine. Fourth stage samples were prepared by placing the samples in a 15 mol% Br_2 bromine-carbon tetrachloride solution. A 12mm x 12mm x 1mm sample of graphite was intercalated in pure bromine for intercalation to second stage and was then cleaved and cut to produce 7mm x 7mm, 5mm x 5mm and 2mm x 2mm samples. Desorption of the lamellar compounds was allowed to occur in air or nitrogen. Stage 1 graphite-ICl was prepared by immersion of HOPG in ICl liquid at room temperature. The stage was characterized by x-ray diffraction using Cu K_α radiation.

Exfoliation was followed with a probe connected to a linear variable differential transducer (LVDT). The sample temperature was measured by a Pt-Pt 10% Rh thermocouple bead in contact with the sample. A heating and cooling rate of 20°C/min was used in the exfoliation cycles. The weight of the probe on the sample was 28 grams. The samples were purged with nitrogen gas in the presence of air during the measurements.

Acoustic emission during exfoliation was detected by using an ultrasonic 1.6 MHz narrow band transducer (Aerotech Gamma) equipped with a high temperature delay line. The transducer signal was amplified and the acoustic emission pulses were counted by using a frequency counter.

Experimental Results

The effect of exfoliation on the intercalate superlattice was investigated by x-ray diffraction. The Transmission Laue Method was used, with Mo K_α radiation and a specimen-to-film distance of 6 cm. The HOPG samples were oriented to yield mainly the (hk0) in-

plane diffraction lines. The set-up allowed d-values ranging from 0.8 A to ~6 A to be measured. The exposure time was ~12 hr for every sample.

Figure 1 shows x-ray diffraction patterns obtained on graphite-Br_2 (i)after desorption from saturation and before exfoliation, and (ii) after exfoliation carried out at ~300°C. The indexing of the diffraction lines are shown in Table 1 for these samples as well as pristine graphite and graphite-Br_2 exfoliated at 1700°C. The in-plane superlattice was the same as that of stage 2 graphite-Br_2 based on single crystal graphite, as determined by Ghosh and Chung [5]. The unit cell is monoclinic and commensurate with the graphite lattice, with in-plane lattice constants a=4.26 A, b=8.87 A, and the angles $\alpha=\beta=90°$ and $\gamma=103.9°$. Due to the mechanical deformation resulting from exfoliation, the diffraction pattern was closer to a powder pattern after exfoliation, as indicated by the complete diffraction rings obtained after exfoliation (Fig.1). For the same reason, certain (hkl) lines not observed before exfoliation were observed afterward.

Figure 2 illustrates the general features of exfoliation which we observed in graphite-Br_2 by dilatometry. The sample had been desorbed from 6.3 mol% Br_2 (stage 2) to 1.6 mol% Br_2 prior to heating. During the initial part of the first heating cycle, expansion occurred very slightly though with a thermal expansion coefficient several times that of graphite. Eventually the sample exfoliated within a relatively narrow temperature range. We have determined a first onset temperature (T_1 for the first exfoliation cycle,T_2 for the second cycle) by extrapolating the line of exfoliation expansion and taking its intersection with the horizontal base line. The expansion rate diminished to form a shoulder (first shoulder) in the curve, and then increased again to form a second shoulder, as shown in Fig. 2, where the second shoulder of the first exfoliation cycle is labeled. No shoulders were observed at higher temperatures up to 600°C in graphite-Br_2. We designate the fractional expansion at the first shoulder as E_1 for the first cycle and E_2 for the second cycle, as determined by the intersection of the line of exfoliation expansion and the expansion line at the shoulder. The second onset temperature

and the fractional expansion at the second shoulder are illustrated in Fig. 2 for the first exfoliation cycle. On cooling, a large degree of hysteresis was evident, with contraction of the exfoliated structure occurring predominantly within a narrow temperature range, resulting in a small residual fractional expansion, E_c. We designate the collapse temperature T_c as the temperature determined by the intersection of lines extrapolated from the contraction region and the linear region of the curve on cooling prior to collapse. On reheating, second exfoliation occurred at about the same temperature at which collapse occurred during cooling, i.e., $T_2=T_c$. It is interesting to note that while T_1 and T_2 were quite separate, the second shoulder was observed at about the same temperature in any exfoliation cycle. The collapse behavior was largely the same for any exfoliation cycle.

The exfoliation behavior of a first stage graphite-ICl is shown in Fig. 3. In general the exfoliation curve is much like that observed for graphite-Br_2. The main difference is that the exfoliation onset temperature T_1 of graphite-ICl is approximately the same as the collapse temperature T_c and the second exfoliation temperatures T_2, whereas in graphite-Br_2, T_1 is generally higher than T_2. It may also by pointed out that T_2 in graphite-ICl is about 100°C higher than that of graphite-Br_2.

In comparing Figures 2 and 3, it can be seen that the amount of expansion which occurred during second exfoliation of graphite-ICl was considerably less than that which occurred in graphite-Br_2. This is probably not an attribute of the intercalate species, but rather a consequence of the amount of desorption which had occurred during first exfoliation. While the graphite-ICl sample was a saturated (first stage) compound just before exfoliation was begun, the graphite-Br_2 sample was a desorbed sample prior to exfoliation. Therefore, desorption was much more significant during first exfoliation of the graphite-ICl sample than the graphite-Br_2 sample. The dependence of exfoliation on desorption is given later in this paper.

Figure 4 illustrates the dependence of expansion on the number, N, of exfoliation cycles

for graphite-Br_2 samples which were, in one case (open circles), allowed to desorb from a second stage parent compound to 1.5 mol% Br_2 before exfoliation and, in the other case (closed circles), not allowed to desorb before exfoliation (i.e., the second stage parent compound). The fractional expansion at the first shoulder (i.e.,E_N, where N is the number of exfoliation cycles) was plotted against N. All samples were 5 mm square. At the end of five exfoliation cycles, each carried out to 290°C, the partially desorbed sample had further desorbed to 0.7 mol% Br_2. For the desorbed sample, E_2 was greater than E_1, and there was only a slight decrease from E_2 to E_5. For the second stage parent compound, the bromine concentration varied from 6.3 mol% Br_2 before the first exfoliation run to 0.6 mol% Br_2 after the fifth exfoliation cycle, each carried out to 340°C. In this case, the expansion behaved as might be expected, i.e.,$E_1>E_2>E_3>E_4>E_5$. In general, we observed $E_1>E_2$ when samples were exfoliated without prior desorption, and $E_1<E_2$ when samples were allowed to desorb to an approximately constant weight before exfoliation.

The extent of desorption during each exfoliation cycle was measured by gravimetry. The results are shown in Fig. 5, where the intercalate concentration (in mol% Br_2) was plotted against the square root of the number, N, of exfoliation cycles. The sample had been desorbed from second stage to 1.4 mol% Br_2 prior to exfoliation. The greatest weight loss occurred during the first and second exfoliation cycles, with the concentration decreased from 1.4 to 1.2 mol% Br_2 after the first exfoliation and from 1.2 to 0.9 mol% Br_2 after the second exfoliation. A similar loss, from 0.9 to 0.7 mol% Br_2 required seventeen additional exfoliation cycles. It is this region from N=2 to N=19 which is shown in Fig. 5. The concentrations after cycles 0 and 1 are not shown because they are too far from the succeeding concentrations. The line drawn is a least square fit of the data with a correlation coefficient of -0.96. The dependence on $\sqrt{N}$ suggests that the weight loss may be treated as a diffusion process with an exfoliation cycle being analogous to a unit of desorption time. The effective overall diffusion coefficient during an exfoliation cycle is probably an average of the diffusion coefficients within the temperature range covered by the exfoliation cycle.

Figure 6 shows the dependence of E_1 on the sample width (the dimension perpendicular to the c-axis) for samples which were initially second stage. The filled circles correspond to samples which were not desorbed prior to exfoliation, and the open circles correspond to samples which were allowed to desorb to ~1.5 mol% Br_2 before the exfoliation cycles. The samples were all square and of approximately the same thickness. For samples which were not allowed to desorb, E_1 increased as the width of the sample increased. The samples which were allowed to desorb did not show this size dependence. Consequently we attribute the apparent width dependence to be actually a concentration dependence, which is appearing as a consequence of desorption during the previous exfoliation cycles. This point is discussed in the next section.

Figure 7 illustrates the effect of the maximum temperature on the exfoliation behavior. Plot A in Fig. 7 shows dilatometric results obtained during two exfoliation cycles carried out to ~200°C; Plot B was obtained during two cycles carried out to ~400°C; Plot C was obtained during two cycles carried out to ~600°C. The main trend indicated in Fig. 7 is that E_c (the residual fractional expansion) increased as the maximum temperature increased. Figure 8 shows similar effects due to isothermal annealing at the maximum temperature during the first heating. Contraction was observed during annealing. After annealing for 0.5 hr at ~600°C, the fractional expansion was only 90 % of the initial 600°C expansion; after a one-hour anneal, the fractional expansion was 80 % of the initial 600°C expansion; after a 3-hour anneal, the fractional expansion was 70 % of the initial 600°C expansion. However, no contraction was observed in samples annealed at 200°C or 400°C. It should be noted that a second exfoliation was not observed in the samples annealed at 600°C. The results of annealing at different temperatures for various lengths of time are summarized in Table 2, where E_c and E_2 are listed relative to E_1 to lower the effect of the error in measuring the initial sample thickness. Whereas E_c/E_1 is affected by annealing, E_2/E_1 appears independent of annealing. While most of the data were obtained at heating rates of 20 C/min, several runs were made at 10 C/min and 40 C/min. Within this range of heating rates, little or no effects were observed which could be attributed to the change in heating rate. This is most

likely due to the fact that even at 40 C/min. the time spent in heating to the exfoliation temperature is long compared to the time needed for desorption.

We have previously reported that the initial stage determines the exfoliation behavior[15]. We have further evidence that the initial intercalating conditions determine the exfoliation behavior. Table 3 illustrates the effect of the initial stage on the subsequent exfoliation behavior. Some samples were allowed to be intercalated, desorbed and reintercalated. Irrespective of the stage after the second intercalation, the samples which were first intercalated to fourth stage in a Br_2-CCl_4 solution of 15 mol% Br_2 had a lower T_1, larger E_1, and larger E_2 than those which were first intercalated to second stage. Within a group of the same initial stage, the sample intercalated twice had a greater E_1 and E_2 than the sample intercalated once, though neither T_1, T_c nor T_2 were affected by reintercalation.

It was interesting to observe that acoustic emission occurred before appreciable exfoliation took place (Fig. 9). The acoustic emission events were observed as a large number of pulses within a short period of time. Very few events were observed once marked expansion had begun. While it may certainly have been the case that once a cellular structure began to form the acoustic pulses were attenuated beyond detection, a gradual reduction in the number of pulses was not observed. Instead, emission was observed at generally one or two distinct temperatures which were separate from the exfoliation onset temperature. On the other hand, acoustic emission occurred during heating in the first exfoliation cycle at about the temperature of the collapse and second exfoliation.

Table 4 is a list of E_1 for samples intercalated in pure bromine at different temperatures (80 - 110°C) to produce third stage compounds. Though all the compounds had the same initial stage, E_1 increased with increasing intercalation temperature. Thus, the initial stage is not the sole factor that determines the exfoliation behavior.

Discussion

Exfoliation is commonly considered to be due to the formation of gas bubbles within an anisotropic matrix. The phenomenon is used to produce expanded graphite products such as Grafoil[10] for gaskets, valve packing and insulation, and expanded mica in the form of vermiculite. Martin and Brocklehurst[2], and Aoki et al.[17] both modeled the exfoliation of graphite-bromine by considering the expansion of gaseous bubbles as Griffiths cracks, though Aoki et al.[17] treated intercalated bromine at room temperature as a solid which vaporized at the breakaway temperature. Both assumed the bubbles to be trapped at defects within the crystal. Setton[4] also modeled the exfoliation of graphite-bromine as the vaporization of a condensed phase, after the migration of bromine to defects. Olsen et al.[18], in a study of the exfoliation of graphite-bisulfate compounds, proposed that a bisulfate compound existed as pockets at grain boundaries, with much of the graphite remaining unaffected. They proposed that the intercalate vaporized on heating, in effect causing the pockets to explode, leaving a low density, "isotropic" material between planar arrays of pyrolytic graphite and voids. Similarly, Stevens et al.[6] viewed exfoliation of graphite-ferric chloride as the forcible rupture of sealed or partially sealed spaces within graphite due to the fact that ferric chloride decomposed to iron and chlorine gas. Dowell[7], in discussing the structures of exfoliated graphite-bisulfate and graphite-aluminum chloride compounds, agreed that the intercalate should diffuse to defects to form three-dimensional aggregates which could vaporize, expanding the structure. He also suggested channels through which the vapor escaped from the sample. We would like to propose the following model for the exfoliation of graphite intercalation compounds, as motivated by the experimental results obtained.

We assume that the precursor of bubbles are intercalate filled penny-shaped cracks distributed within a graphite crystal. If the crystal is heated, the pressure within the cracks will increase as the intercalate takes on a more gaseous character. Higashida and Kamada[19] analyzed the stress distribution around pressurized penny-shaped cracks in graphite near a free surface and concluded that two fracture modes are available. One fracture mode is brittle fracture as a Griffiths crack, i.e., the crack diameter increases when the tensile stress in the c-

direction exceeds the fracture strength. The other fracture mode is the buckling of the walls of the crack, i.e., when large bending moments exist at the crack tip, the flat crack may open to form a bubble. We propose that the latter fracture mode is responsible for the expansion observed in exfoliation. Higashida and Kamada found that the internal pressure necessary for fracture by either mode increased as the crack diameter decreased. Furthermore, the internal pressure necessary for buckling was very sensitive to the depth of the crack below a free surface due to the mechanical constraints involved in bending a thick layer. The parameter h/a, where h is the depth of the crack below a free surface and a is the crack radius, was found to be much less than one when buckling was favored over Griffiths cracking. (It may be of interest to note that, unlike in glass, where brittle fracture is typically catastrophic, the c-direction fracture stress in graphite is low enough that the strain energy is rapidly dissipated into the formation of surfaces, so that the crack growth stops rather than propagating catastrophically to the crystal edge.) Although the analysis of Higashida and Kamada was developed for cracks near a surface, it is reasonable to assume that, due to the interaction of stress fields, an array of cracks can buckle throughout the material. That is, while buckling may initiate near a free surface, another crack a similar depth below it can also buckle. Consequently h may be restated as an average c-direction separation of cracks. In short, heating an intercalated sample increases the pressure in penny-shaped cracks. Griffiths cracking is likely to occur at a critical pressure: this will reduce both the internal pressure within the cracks and the pressure necessary to cause buckling. Eventually the internal pressure and crack diameter will be such that buckling occurs, producing the sudden large expansion characteristic of exfoliation. Our observation of acoustic emission before exfoliation is in agreement with the concept of both fracture modes being active.

We attribute the appearance of shoulders in the exfoliation curve to a distribution of crack sizes prior to exfoliation. Though the size distribution is continuous, the exfoliation response is not necessarily so. Buckling will occur at the lowest pressure for cracks of a certain diameter, a, of which there are a suitable number and distribution. When these cracks buckle, cracks with a subcritical internal pressure (due to a slightly smaller diameter,a') may be induced to

buckle. This in turn will reduce the number of cracks of diameter a', increasing the value of h. Since the necessary internal pressure for buckling is a very strong function of h/a, the next exfoliation cycle is delayed until the internal pressure builds up to an appropriate level. This probably results in the appearance of multiple exfoliation episodes in the exfoliation curve.

The discussion thus far tacitly assumes that the cracks are gas tight, with no net flux in or out. This is not necessarily the case. A pathological example is a crack which propagates to the ambient atmosphere. In that case, the internal pressure does not increase and the walls of such a crack can only buckle due to the buckling of surrounding cracks. A less extreme example would be the diffusion of intercalate between basal planes. If the intercalate mobility and solubility are high, the intercalate species may diffuse out of the gas bubbles and into the matrix in a short time in comparison with the length of time required for the exfoliation cycle. For exfoliation at normal pressures, the loss of intercalate from the gas bubbles may even result in the collapse of the exfoliated structure. Subsequent heating and cooling will then cause negligible expansion. Such collapse during heating in the first exfoliation cycle was observed in this work in graphite-nitric acid (Fig. 10). When diffusion is slower, as in the case of bromine, long periods of time and high temperatures are necessary before appreciable collapse occurs (Fig. 8).

Without a high temperature anneal, graphite-Br_2 and graphite-ICl exhibit cyclic exfoliation. On cooling the structure collapses at a low temperature and re-exfoliates when heated above that temperature. The collapse is attributed to capillary forces due to the condensed intercalate, which returns the gas bubbles to a nearly penny-shaped crack configuration. On reheating, exfoliation occurs again as the intercalate vaporizes, buckling the largest set of cracks at about the same temperature that collapse occurs on cooling. The smaller set of cracks exfoliates at higher temperatures for the same reason as before, i.e., a smaller radius requires a higher pressure. On the other hand, collapse of all cracks is concurrent as condensation occurs at only one temperature; small cracks are forced shut by the larger cracks but must re-open on their own.

If cracks buckle to form an exfoliated structure, one problem is in determining the source of the penny-shaped cracks. One possibility may be defects either pre-existing in the graphite or caused by the intercalating conditions. If pre-existing defects serve as sites for penny-shaped cracks, one might expect the exfoliation behavior to be affected mainly by differences in defect distribution due to the graphitizing process. Once the defects have become saturated with intercalate, there should be little dependence of exfoliation on stage or intercalate concentration. If the defects are not saturated, there should be an intercalate concentration dependence, i.e., with less intercalate, less expansion. If defects produced during intercalation serve as crack sites, one would expect that more severe intercalating conditions should produce more defects, hence more exfoliation. Consequently one would expect a low stage compound to be associated with more defects and a greater degree of exfoliation. Otherwise, for saturated defects only a weak dependence on concentration should be expected. However, neither of these arguments can explain our observation that fourth stage samples exfoliate more than second stage samples.

We propose that the intercalate islands suggested by Daumas and Herold[20], determine the size of the penny-shaped cracks. (The crack size is not necessarily equal to the island size; instead we expect a positive correlation between the island size and the subsequent crack size.) In turn, the size of the intercalate islands is determined by the intercalating conditions. In accordance with nucleation theory, as the reactant activity increases, competition between nucleation sites increases and the subsequent microstructure is finer. Hence, as the intercalate activity is decreased, by dilution or by heating, the intercalate island size is expected to increase. For a compound of a given concentration, increased island size means that exfoliation can occur more easily and to a greater extent. Observation of intercalate islands by electron microscopy[21, 22] shows that the intercalate islands can be treated as interstitial dislocation loops and as such are susceptible to pinning at defect sites. Nonetheless, the islands are mobile and can coalesce. It should be mentioned that measurements of the island size have not been made.

When the intercalating activity was reduced by dilution, as in the initially fourth stage samples listed in Table 3, we observed that the amount of exfoliation was greater than that of an initially second stage sample, even though the actual concentration was approximately the same for various samples. Similarly, if the activity is decreased by heating, the amount of exfoliation was observed to increase with temperature for a given stage (Table 4).

Let us consider the effect of desorption on exfoliation. Bardhan et al.[23] showed that a pronounced weight loss occurred on graphite-Br_2. This is only to be expected given the exponential temperature dependence of the diffusion coefficient. Until exfoliation occurs, bromine diffuses more and more rapidly as the temperature is increased. Isothermal gravimetric results[23] indicate that desorption reduces the concentration to a limiting value of ~1.0 - 1.5 mol% Br_2, up to the temperature where exfoliation occurs. The mass fraction of bromine lost depends on $\sqrt{(Dt/l^2)}$, where D is the diffusion coefficient and l is half the sample width. Profilometry[23] and X-ray absorption studies[24] indicate that the concentration in a desorbing graphite-Br_2 compound decreases at the edge initially while the center retains the semblance of the undesorbed sample. By the time the apparent residue compound has been achieved, the concentration profile across the sample is nearly flat, with little difference in the concentration at the edge or the center. The length of time needed for this to occur can be considered as roughly proportional to l^2/D. Hence,for the same concentration a sample half as wide as a given sample will require roughly a quarter of the time to desorb to an equivalent concentration.

The above argument applies to exfoliation in the following manner. During exfoliation the temperature is steadily rising rather than being isothermal. Consequently the diffusion coefficient should be considered as a composite diffusion coefficient weighted by the mass loss rate at each temperature. In effect, small samples may desorb to a low or even residue concentration during the heating cycle though they may have been concentrated or even saturated prior to heating. In this case the exfoliation behavior will be the same for an initially desorbed sample as for an initially saturated sample. Experimentally this was observed.

as shown by the 3 mm sample shown in Fig. 6. For wider samples, a more and more significant amount of intercalate remains in the center of the sample by the time the exfoliation temperature is reached, with the result that the amount of exfoliation increases as the sample width increases. This is the situation described by the solid circles in Fig. 6. On the other hand, if the samples have been desorbed to a low or residue composition prior to exfoliation, this width dependence becomes negligible, as shown by the open circles in Fig. 6. For the same heating rate, as was the case for all the samples in Fig. 6, the effective (Dt) term is the same for all the samples, so that the intercalate concentration remaining in a large sample at the exfoliation temperature is greater than that in a small sample for the case of an initially concentrated samples. Therefore the amount of exfoliation increases with sample width for initially concentrated samples, as we have observed.

The mobility of the intercalate is quite high at the exfoliation temperatures, and the solubility of the intercalate appears to be quite low. Diffusion of the intercalate out of the sample through the matrix is one mechanism for the loss of excess intercalate and is suggested by the least square fit of the data in Fig. 5. However, it is *not necessarily* the only mechanism. The gas cells themselves may serve as sinks for the excess intercalate. Under such circumstances, the matrix would lose intercalate while the sample as a whole would not. On subsequent exfoliation cycles the enriched cells should expand to a greater degree. The latter possibility is consistent with the observation of $E_2 > E_1$ for samples which are initially desorbed. The diffusion of the intercalate out of the sample is not the only means of losing intercalate. It should be born in mind that the weight losses during the first two exfoliation cycles in Fig. 5 do not fit the least square line. There is considerably more desorption during these two cycles than can be explained by using the same diffusion coefficient which can be applied to the later cycles. It seems far more likely that a certain number of the gas bubbles present are bursting, or are forming an interconnected network which in turn opens to the outside of the sample. The channels suggested by Dowell[7] may be such a network. If so, one would expect that a greater initial concentration would tend to rupture and/or interconnect more of the cells, as a greater concentration would serve as a source of a greater gas volume. Consequently

a greater proportion of the initial concentration would be lost on the first exfoliation cycle of an initially concentrated sample than in one which had been desorbed prior to exfoliation. With such a loss of intercalate, less is available on subsequent cycles so that the amount of exfoliation is decreased as shown by the solid circles in Fig. 4.

Table 5 shows the comparison of the exfoliation temperatures (first onset temperatures) of graphite-HNO_3, graphite-Br_2, and graphite-ICl with the respective intercalate melting temperatures and the respective melting and boiling points of bulk HNO_3, Br_2, and ICl. For graphite-Br_2, the collapse temperature (which is the same as the second exfoliation temperature) is approximately the same as the intercalate melting temperature. Other than this match, the exfoliation and collapse temperatures are different from any of the corresponding critical temperatures listed. Comparison of the trends down the various columns in Table 5 shows a possible relationship between the exfoliation temperature and the bulk melting temperature.

Conclusion

The amount of exfoliation of graphite-Br_2 was found to be determined by the intercalation conditions, namely the Br_2 concentration in the Br_2-CCl_4 solution and the temperature, such that the expansion increased with increasing initial stage number and with increasing temperature. Due to intercalate desorption during heating, annealing was found to increase the amount of residual expansion until exfoliation became irreversible. Desorption also resulted in the increase of the exfoliation expansion with increasing sample width for concentrated samples and the decrease in the expansion with repeated exfoliation cycles for these samples. A single exfoliation event was found to consist of multiple expansion spurts, which occurred at ~150°C and ~240°C for first exfoliation, and at ~100°C and ~240°C for subsequent cycles. Acoustic emission was observed before appreciable expansion during the first exfoliation cycle.

In-plane intercalate ordering was observed by x-ray diffraction in exfoliated graphite-Br_2. A model of exfoliation involving intercalate islands[20] is proposed.

References

1. J.E.Brocklehurst, Nature, London.194 (1962) 247.
2. W.H.Martin and J.E.Brocklehurst, Carbon, 1 (1964) 133.
3. A.R.Ubbelohde, Brit. Coal Util. Res. Assoc. Gaz., 51 (1964) 1.
4. C.Mazieres, G.Colin, J.Jegoudez and R.Setton, Carbon, 13 (1975) 289.
5. C.Mazieres, G.Colin, J.Jegoudez and R.Setton, Carbon, 14 (1976) 176.
6. R.E.Stevens, S.Ross and S.P.Wesson, Carbon, 11 (1973) 525.
7. M.B.Dowell, Ext.Abs.Program-Bienn.Conf. Carbon 12 (1975) 35.
8. H.Thiele, Anorg.Allgem.Chem., 207 (1932) 340.
9. M.B.Dowell, Ext.Abs.Program-Bienn.Conf. Carbon 12 (1975) 31.
10. Union Carbide Trademark.U.S. Patent 3,404,061 (1968)
11. H.Mikami, Kokai(Japan. patent).76 96,793 (1976)
12. CECA S.A., Carbone-Lorraine S.A., Brit. Patent 1,588,876
13. W.L.Garrett, J. Sharma, J.Pinto and H.Prask, Technical Report ARLCD-TR-81008, AD-E400 617; Order No.AD-A100727, May.1981 Avail. NTIS.
14. M.A.M.Boersma, in Adv.Mater.Catal., J.Burton and R.L.Garten, eds., Academic Press, 19[illegible], pp.67-99.
15. S.H.Anderson, H.H.Lee and D.D.L.Chung, Ext.Abs.Program-Bienn.Conf. Carbon 15 (1981) 357.
16. D. Ghosh and D.D.L.Chung, Phys. Rev., to be published.
17. K. Aoki, T. Hirai, and S. Yajima, J. Mat. Sci., 6 (1971) 140.
18. L.C.Olsen, S.E.Seeman and H.W.Scott, Carbon, 8 (1970) 85.
19. Y.Higashida and K.Kamada, J.Nucl.Mater., 73 (1978) 30.
20. N.Daumas and A.Herold, C. R. Acad. Sci., Ser. C268 (1969) 373.
21. M.Heerschap, P.Delavignette and S.Amelinckx, Carbon, 1 (1964) 235.
22. M.Heerschap and P. Delavignette, Carbon, 5 (1967) 383.
23. K.K.Bardhan, J.C.Wu, J.S.Culik, S.H.Anderson, and D.D.L.Chung, Synth. Met. 2 (1980) 57.
24. S.H.Anderson and D.D.L.Chung, Carbon,to be published

Table 1 X-ray diffraction lines of pristine graphite, desorbed graphite-Br_2 and exfoliated graphite-Br_2

hkℓ	Pristine graphite			Graphite-Br_2, desorbed			Graphite-Br_2, exfoliated at 300°C			Graphite-Br_2, exfoliated at 1700°C		
	d_{obs} (Å)	d_{cal} (Å)	Strength	d_{obs} (Å)	d_{cal} (Å)	Strength	d_{obs} (Å)	d_{cal} (Å)	Strength	d_{obs} (Å)	d_{cal} (Å)	Strength
023_G							0.96	0.96	VW			
016_G							0.99	0.99	VW	0.99	0.99	VW
$200_G(260)_S$	1.09	1.07	W	1.09	1.07	W						
112_G							1.15	1.13	S	1.15	1.13	M
$110_G(700)_S$	1.25	1.23	M	1.26	1.23	M	1.23	1.23	W	1.23	1.23	M
011_G							2.03	2.03	VS	2.02	2.03	S
$100_G(130)_S$	2.14	2.13	M	2.14	2.13	M	2.14	2.13	M	2.14	2.13	M
120_S							2.66	2.68	W	2.73	2.68	VW
300_S				2.85	2.87	W	2.88	2.87	W	2.86	2.87	VW
002_G							3.36	3.35	S	3.39	3.35	S
200_S				4.16	4.14	W	4.17	4.14	W			

G = graphite
S = in-plane superlattice

Table 3 Effect of Staging on Exfoliation Behavior

Stage after 1st intercalation			4	4	2	2
Stage after 2nd intercalation			2	/	4	/
Mole % Br_2			1.60	1.39	1.55	1.53
First Exfoliation						
	Temperature T_1 (°C)					
		1st Onset	161	145	185	185
		2nd Onset	239	230	230	223
	Fractional Expansion ($\Delta L/L$)					
		1st Shoulder (E_1)	28	18	8	5
		2nd Shoulder	39	23	20	14
First Collapse						
	Temperature T_c (°C)		101	89	104	105
	Residual Fractional Expansion (E_c)		2.3	1.1	2.1	1.0
Second Exfoliation						
	Temperature T_2 (°C)		100	99	99	108
	Fractional Expansion (E_2)		30	16	15	11

FIGURE CAPTIONS

Fig.1 Transmission Laue x-ray diffraction patterns of graphite-Br_2 (a) after desorption from saturation and before exfoliation, and (b) after exfoliation carried out at ~300°C.

Fig.2 Fractional expansion versus temperature during the first two exfoliation-collapse cycles for graphite-Br_2 which had been desorbed from 6.3 mol% Br_2 to 1.6 mol% Br_2 prior to heating.

Fig.3 Fractional expansion versus temperature during the first one and a half exfoliation-collapse cycles for graphite-ICl which was saturated (stage 1) prior to heating.

Fig.4 Fractional expansion at the first shoulder (E_s) versus the number of exfoliation cycles (N) for graphite-Br_2 which (i) were not desorbed prior to heating and (ii) were desorbed prior to heating.

Fig.5 Gravimetric determination of the intercalate (Br_2) concentration as a function of ℓ/N, where N is the number of exfoliation cycles.

Fig.6 Fractional expansion at the first shoulder during first exfoliation (E_s) versus the sample width perpendicular to the c-axis for graphite-Br_2.

Fig.7 Fractional expansion versus temperature during the first one and a half exfoliation-collapse cycles carried out to three different maximum temperatures for graphite-Br_2.

Fig.8 Fractional expansion of graphite-Br_2 versus temperature during the first one and a half exfoliation-collapse cycles in which isothermal annealing at the maximum temperature (~600°C) during the first heating cycle was carried out for various lengths of time.

Fig.9 Acoustic emission versus temperature superimposed on a curve of fractional expansion versus temperature for one exfoliation-collapse cycle of graphite-Br_2.

Fig.10 Fractional expansion versus temperature during the first two exfoliation-collapse cycles of graphite-nitric acid.

a

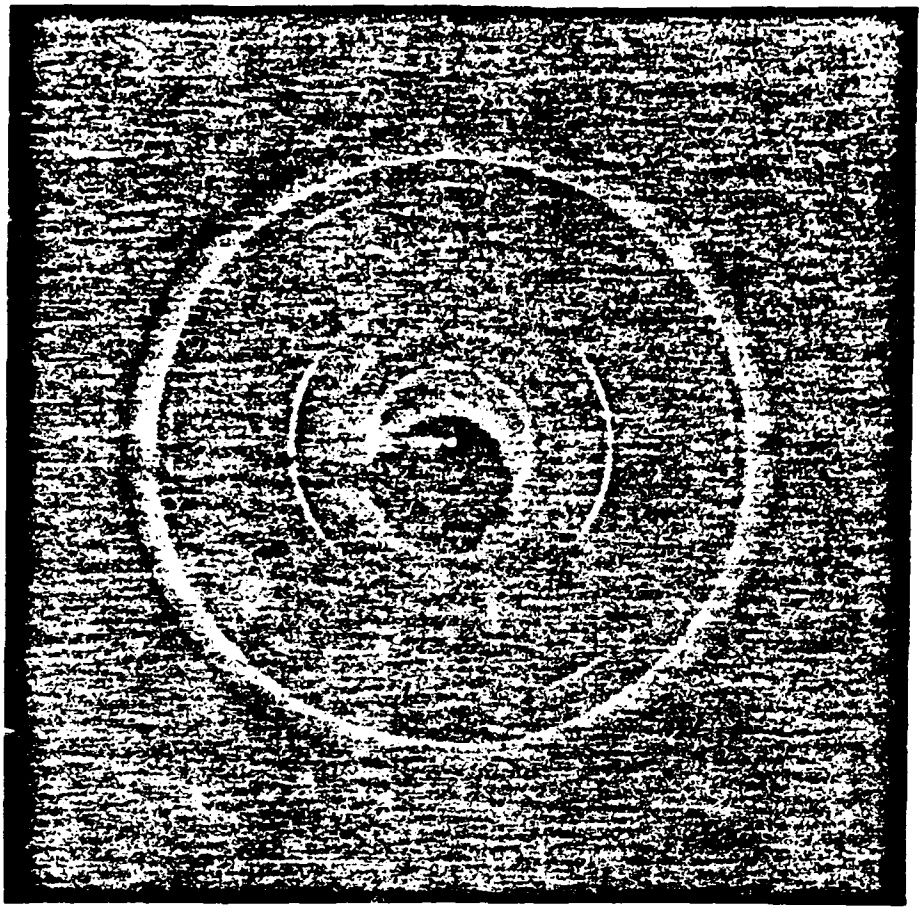

b

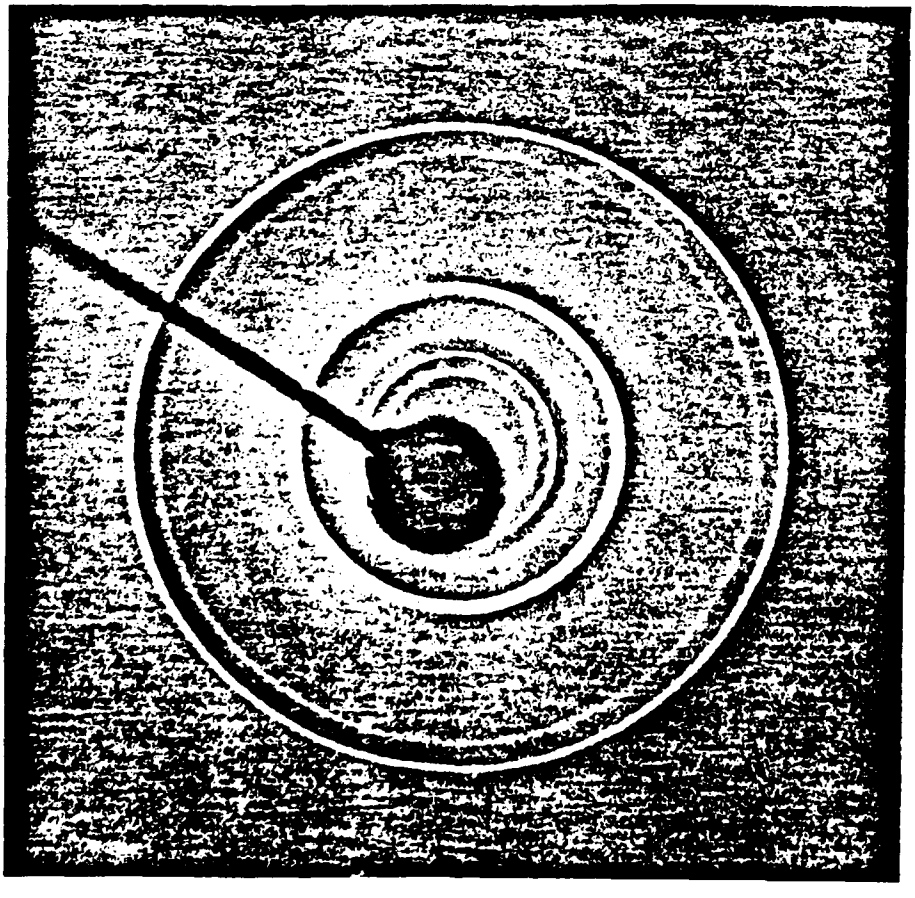

Fig. 1

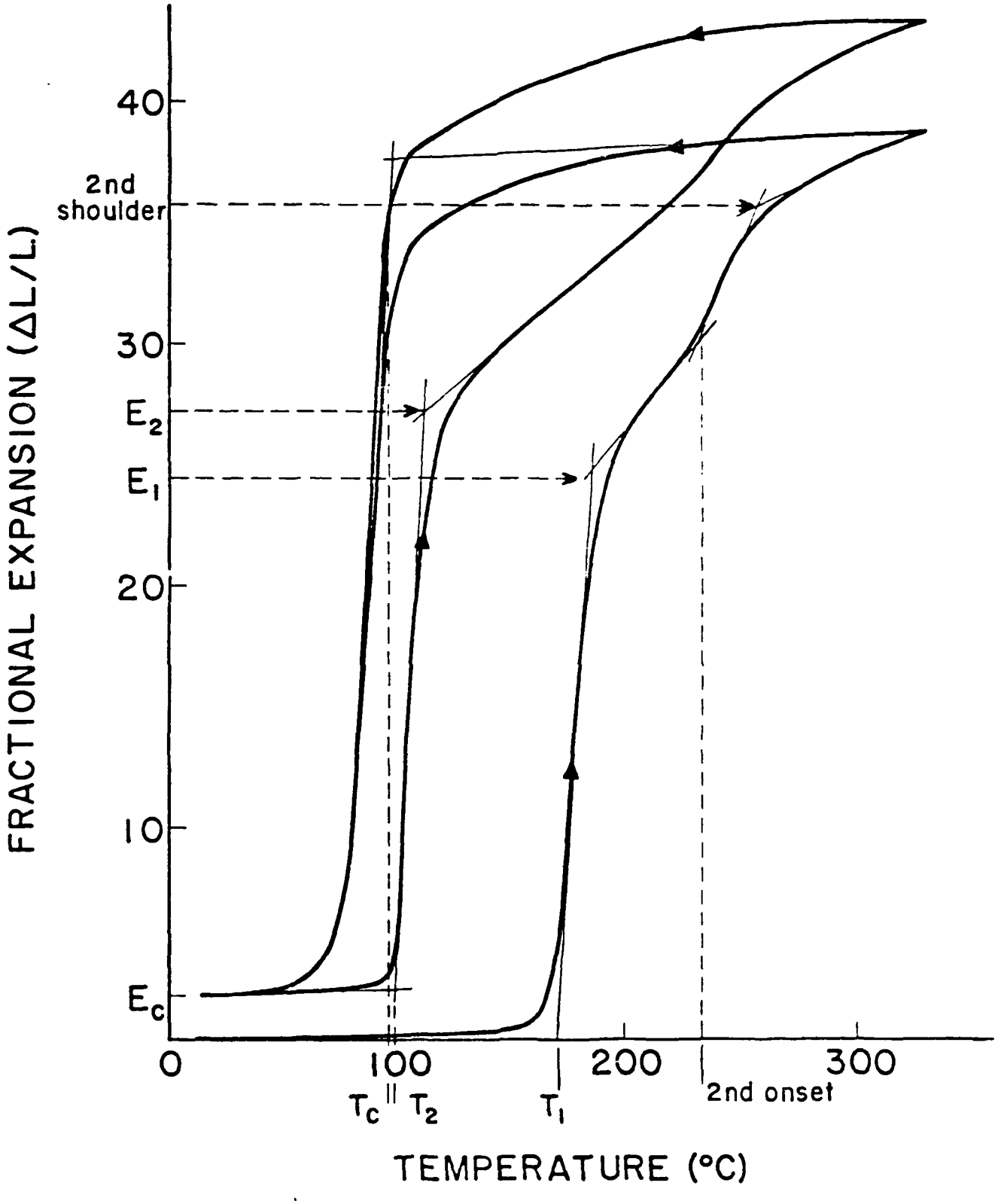
FRACTIONAL EXPANSION (ΔL/L)
40
2nd shoulder
30
E2
E1
20
10
Ec
0
100
200
300
Tc
T2
T1
2nd onset
TEMPERATURE (°C)

Fig. 2

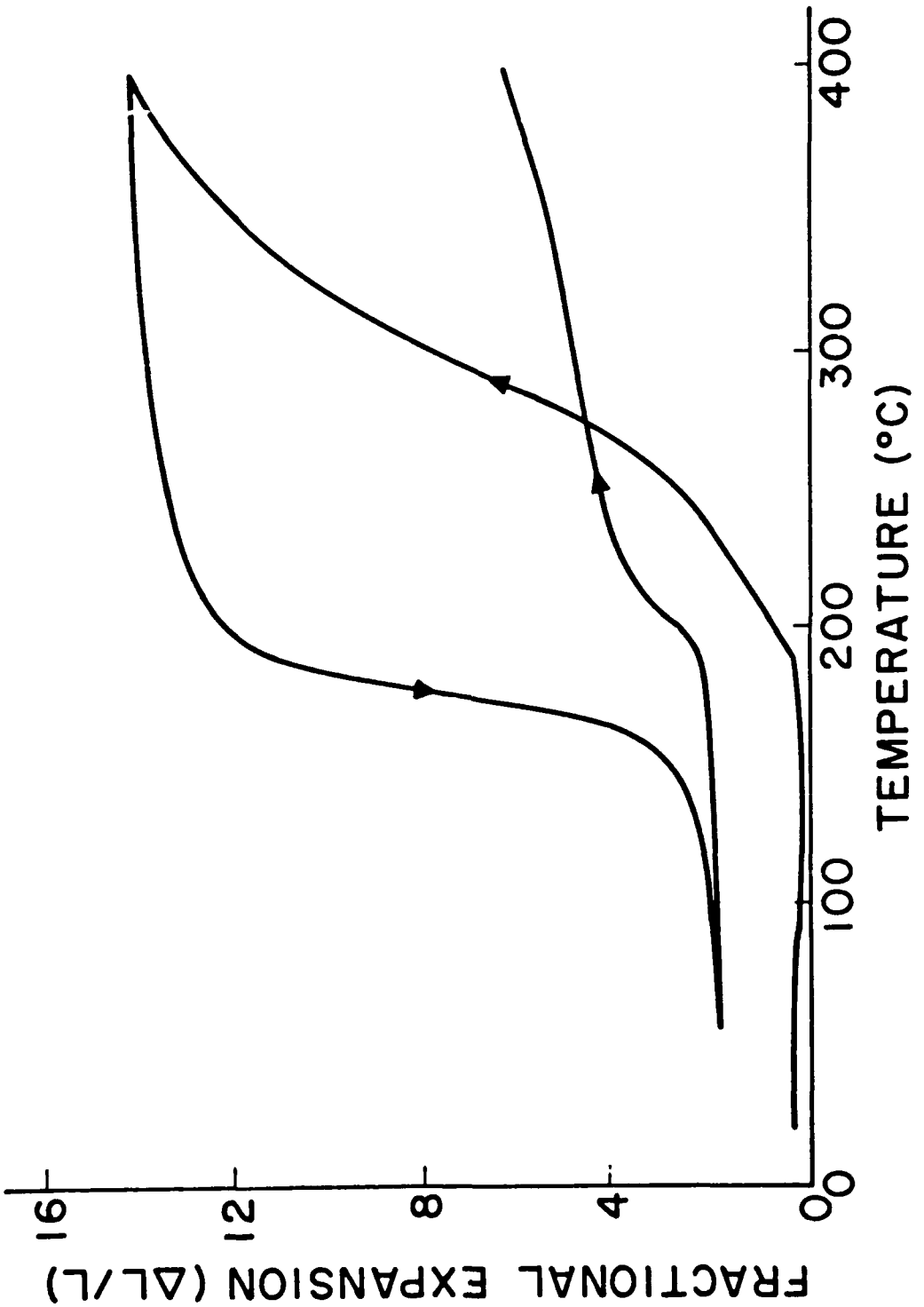
FRACTIONAL EXPANSION (ΔL/L)
0
4
8
12
16
0
100
200
300
400
TEMPERATURE (°C)

Fig. 3

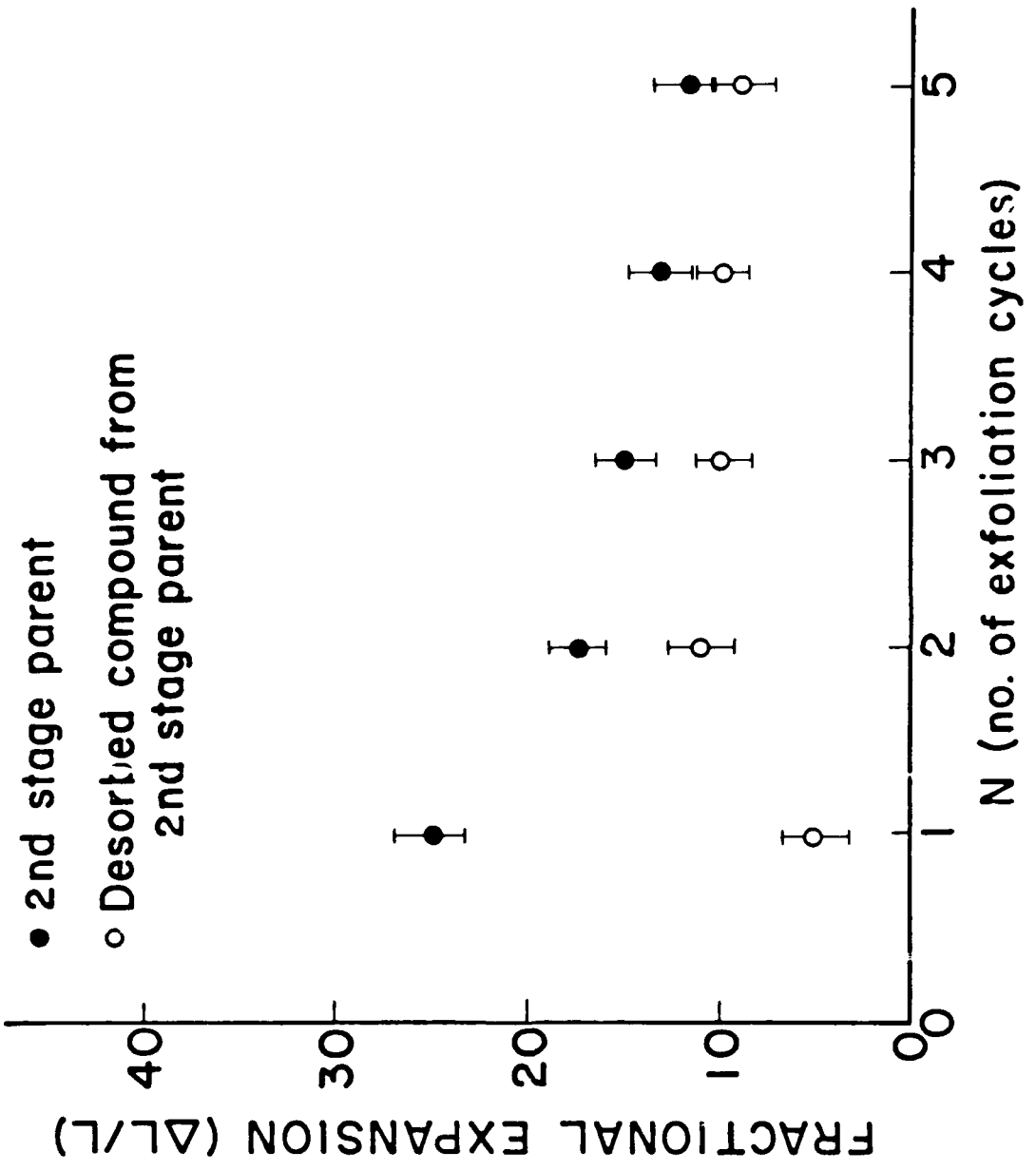
● 2nd stage parent
○ Desorbed compound from 2nd stage parent
FRACTIONAL EXPANSION (ΔL/L)
0
10
20
30
40
1
2
3
4
5
N (no. of exfoliation cycles)

Fig. 4

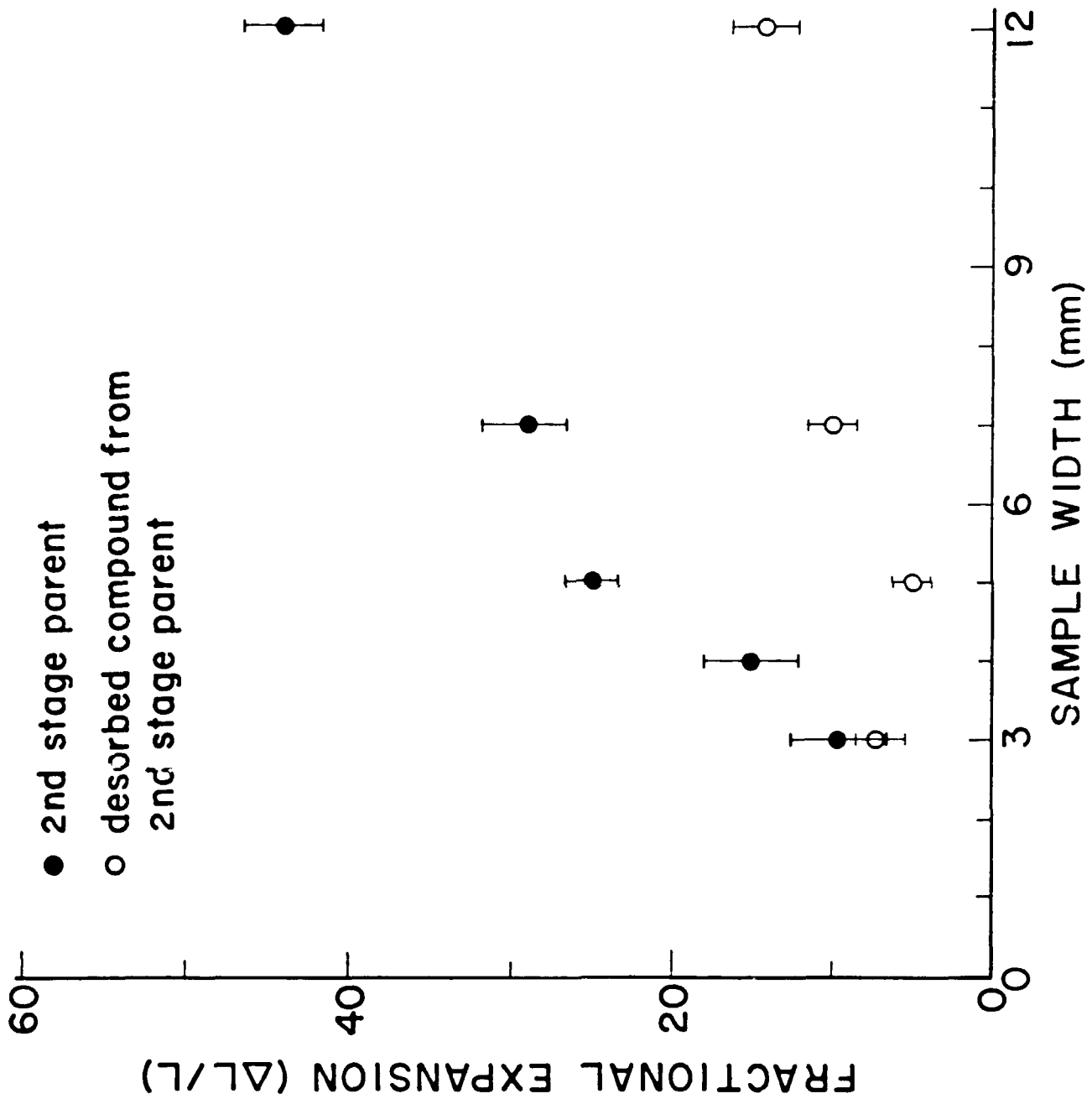
● 2nd stage parent
o desorbed compound from 2nd stage parent
FRACTIONAL EXPANSION (ΔL/L)
SAMPLE WIDTH (mm)
0
20
40
60
3
6
9
12

Fig. 6

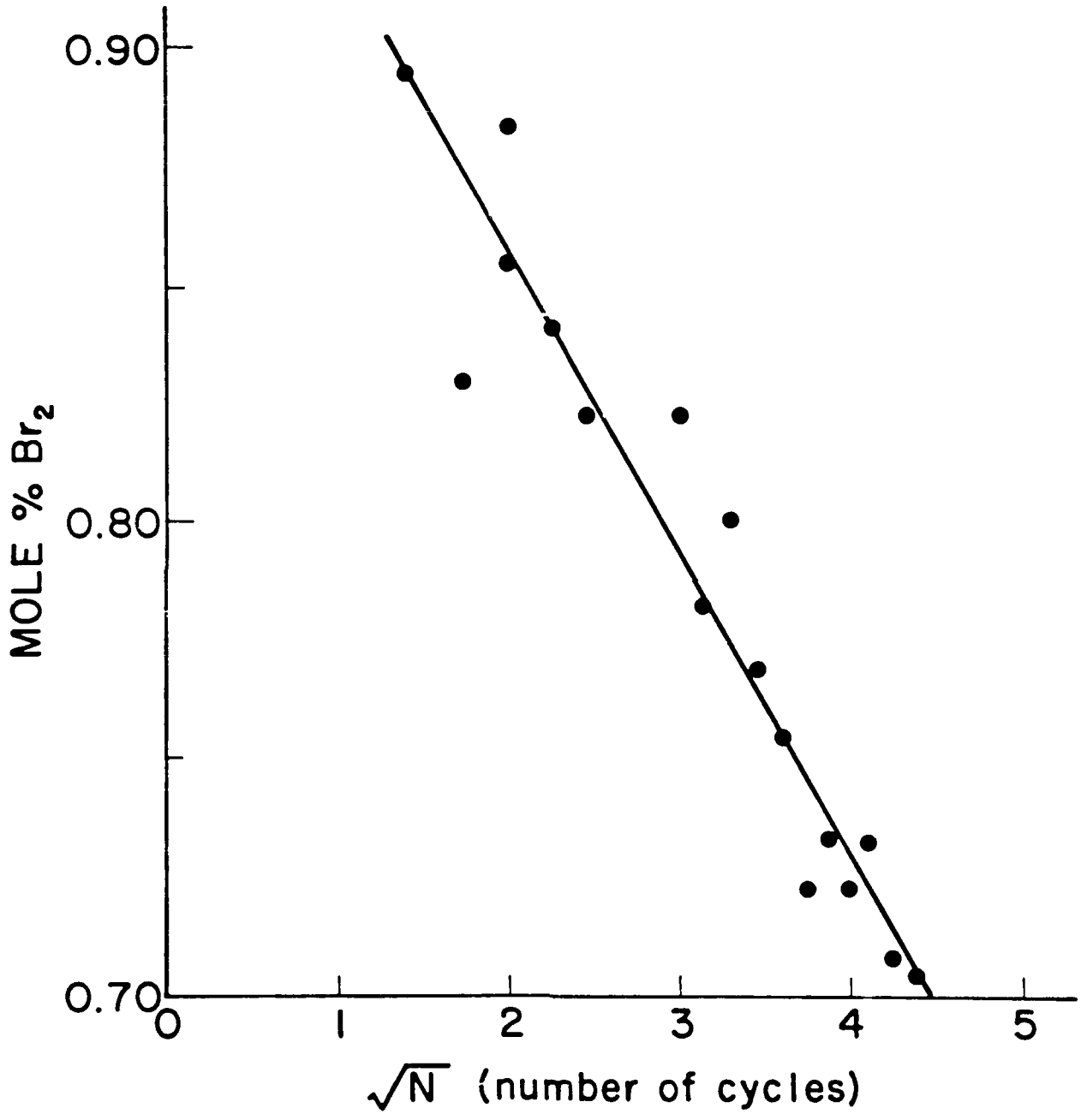

Fig. 5

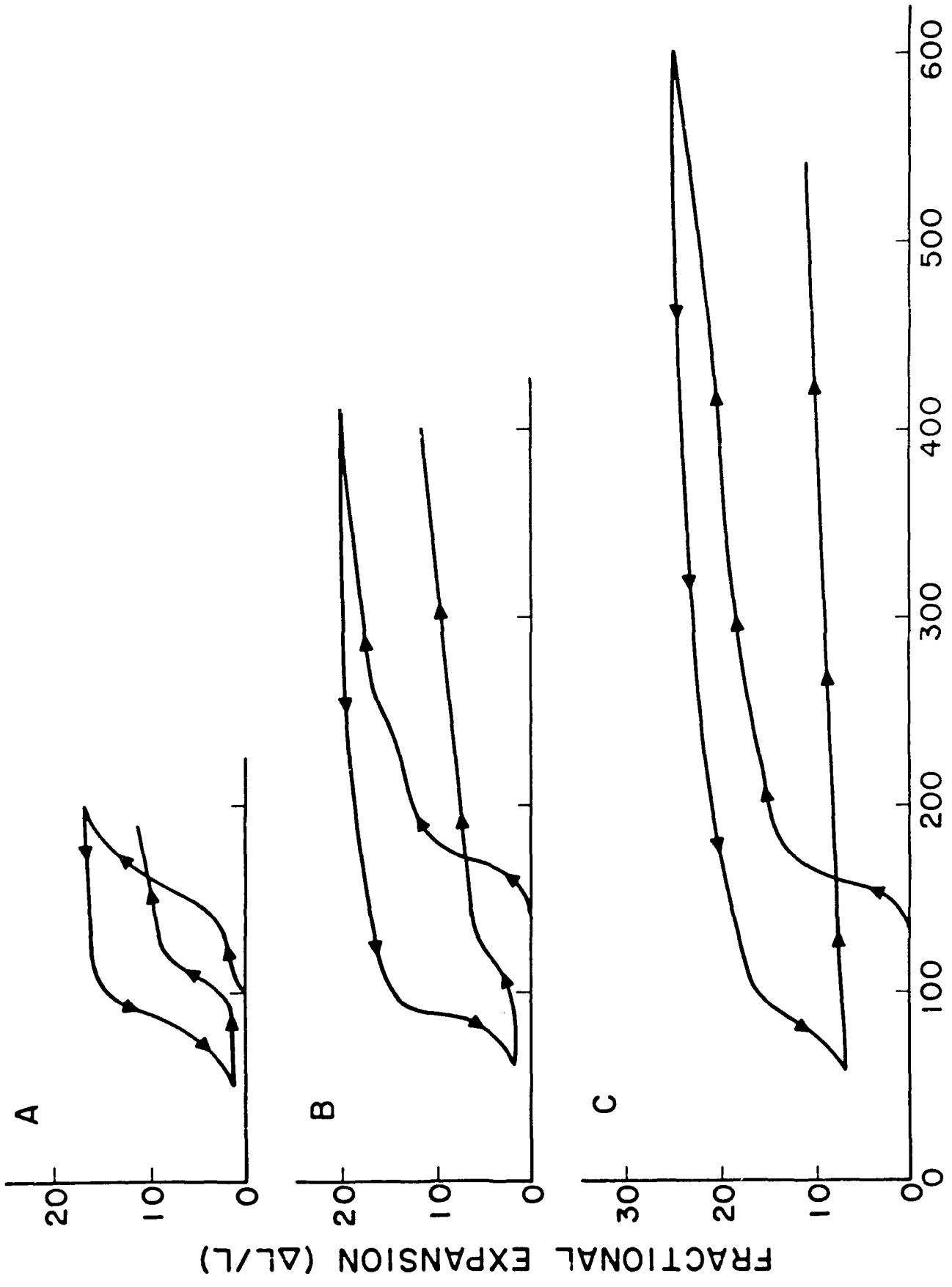
A
B
C
20
10
0
20
10
0
30
20
10
0
100
200
300
400
500
600
TEMPERATURE (°C)
FRACTIONAL EXPANSION (ΔL/L)

Fig. 7

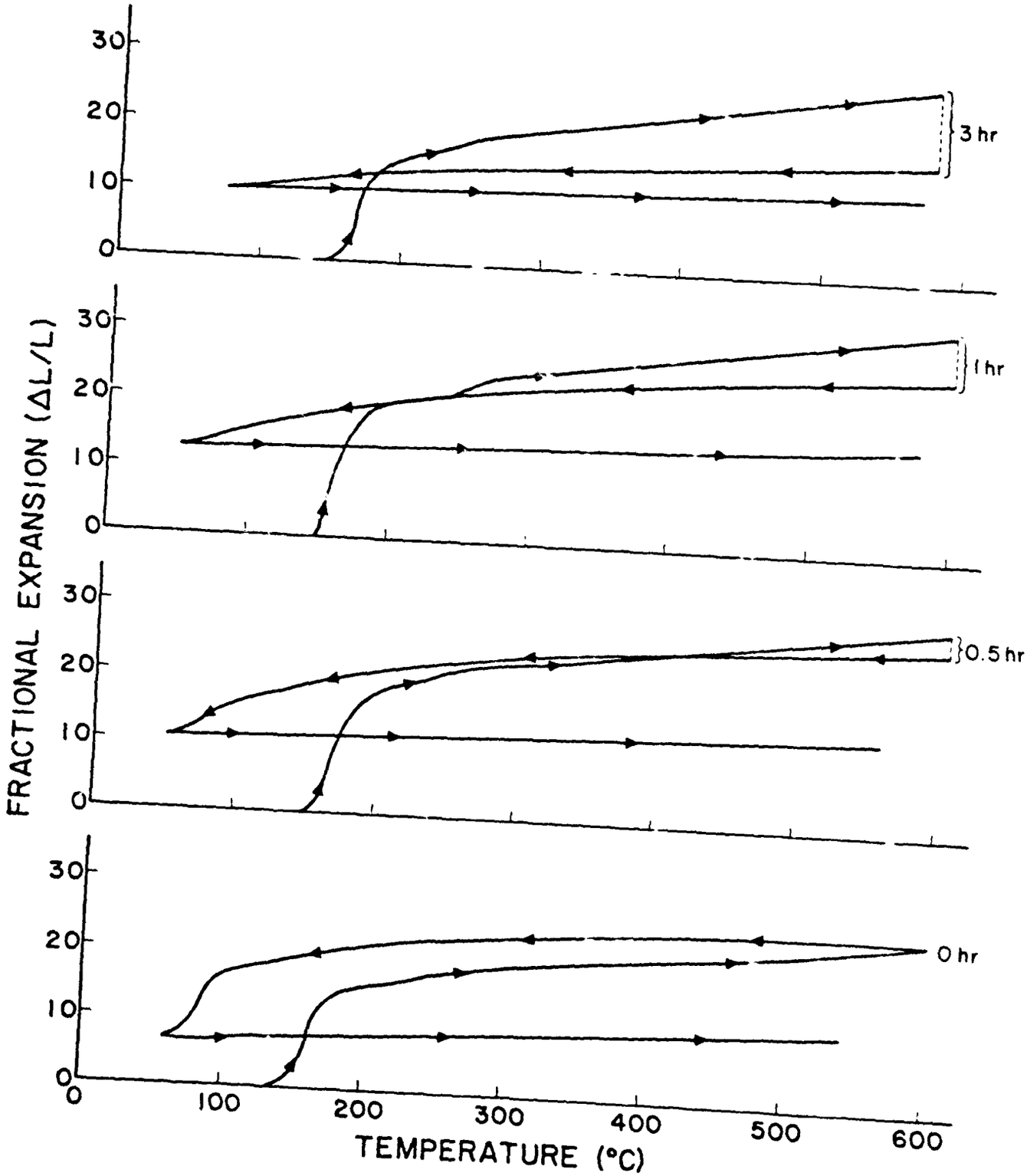
FRACTIONAL EXPANSION (ΔL/L)
30
20
10
0
3 hr
1 hr
0.5 hr
0 hr
0
100
200
300
400
500
600
TEMPERATURE (°C)

Fig. 8

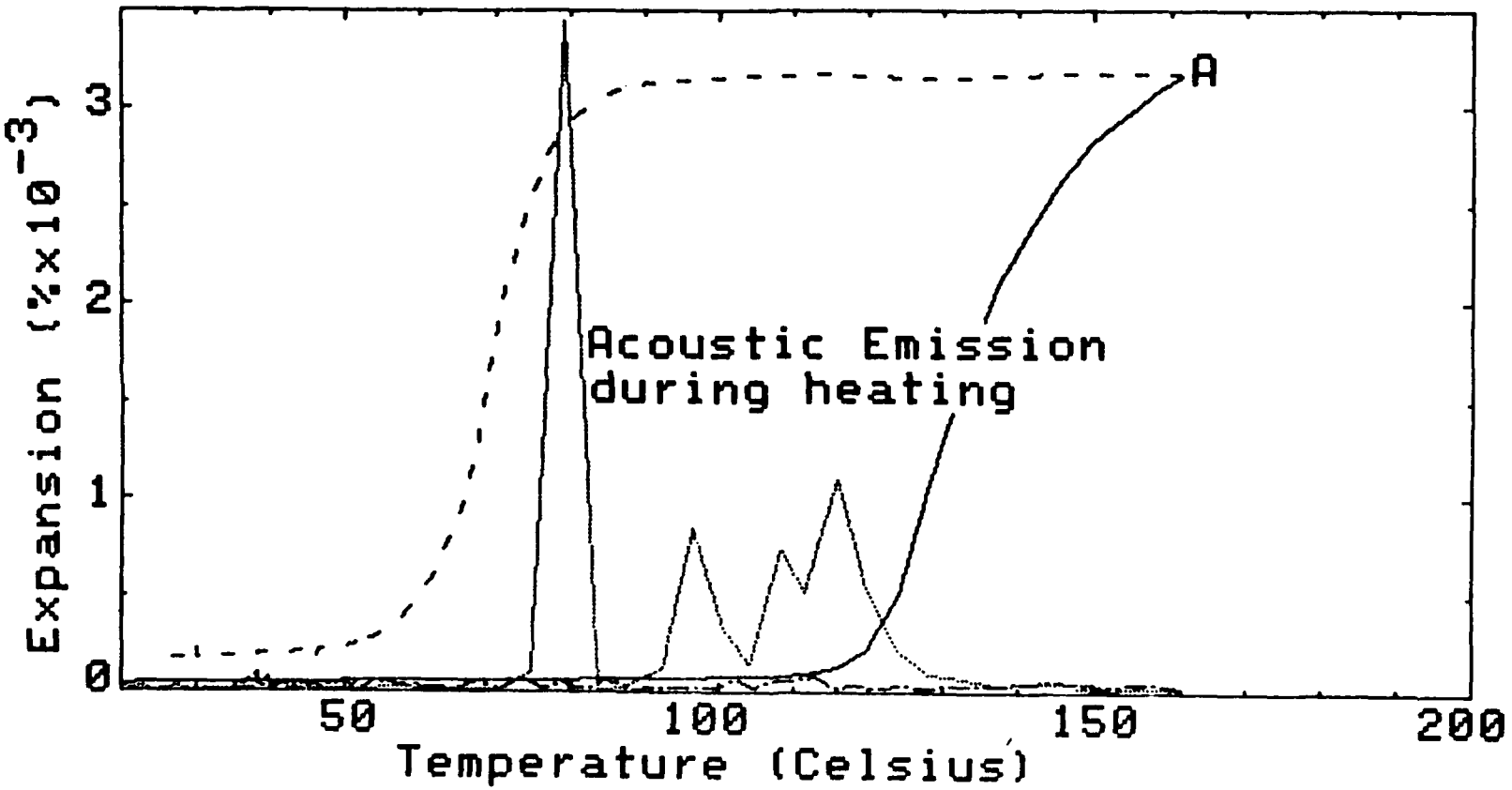
Expansion (%x10^{-3})
0
1
2
3
50
100
150
200
Temperature (Celsius)
A
Acoustic Emission
during heating

Fig. 9

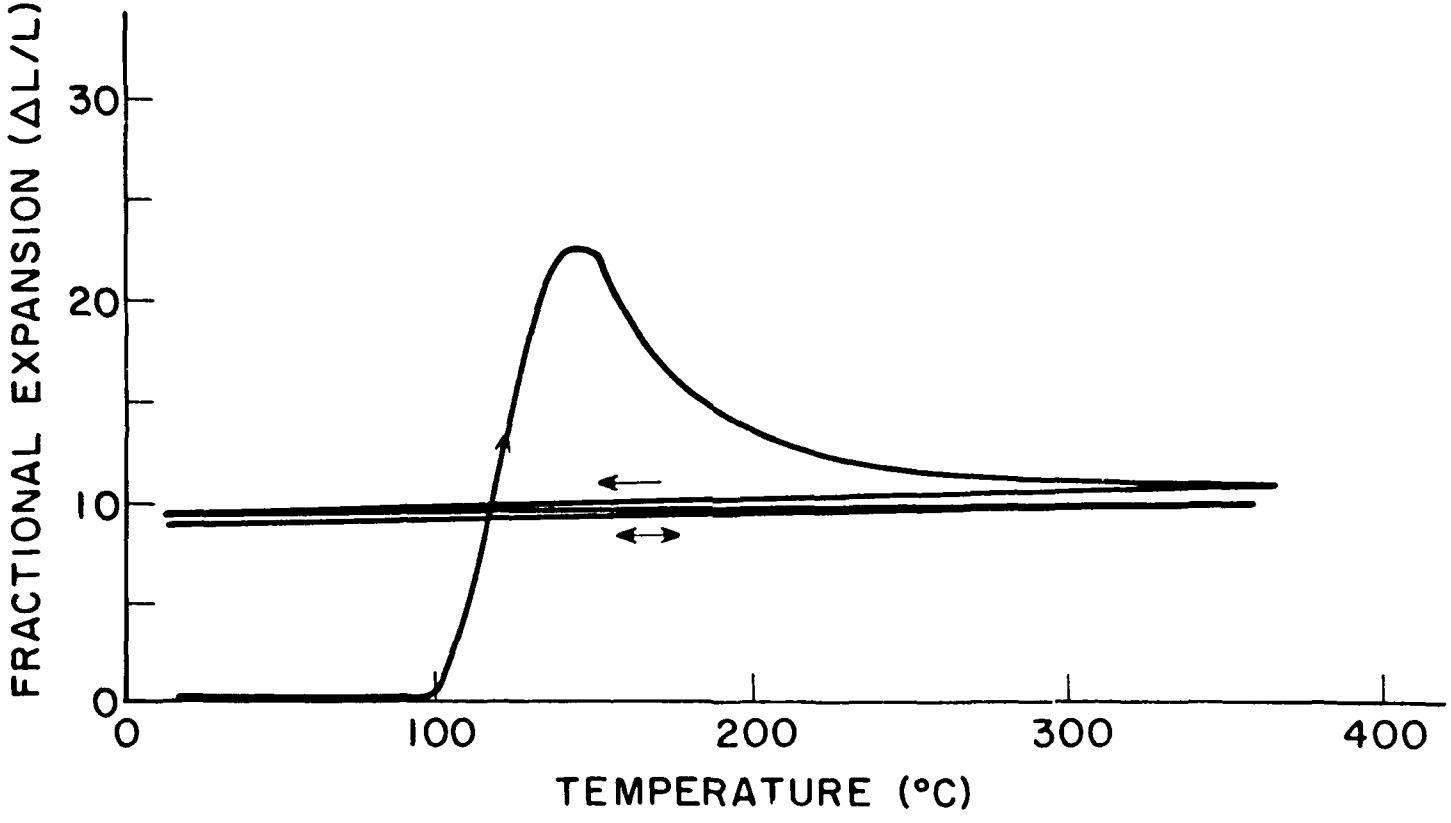
FRACTIONAL EXPANSION (ΔL/L)
30
20
10
0
0
100
200
300
400
TEMPERATURE (°C)

Fig. 10

PROFESSIONAL PERSONNEL

Principal Investigator:	D. D. L. Chung, Department of Metallurgical Engineering & Materials Science
Graduate Students:	S. H. Anderson, Department of Metallurgical Engineering & Materials Science
	R. Gangwar, Department of Physics

PUBLICATIONS

Published:

D.D.L. Chung "Exfoliation of Graphite," Proceedings of the 7th International Thermal Expansion Symposium, 1979.

S.H. Anderson and D.D.L. Chung, "Stage Evolution During Intercalation," Ext. Abstr Program -- Bienn. Conf. Carbon 15, 361 (1981).

S.H. Anderson, H.H. Lee and D.D.L. Chung, "Stage Dependence of the Exfoliation of Intercalated Graphite," Ext. Abstr Program -- Bienn. Conf. Carbon 15, 357 (1981).

D.D.L. Chung, "Thermal Analysis of Graphite Intercalated with Bromine " Thermal Analysis 7, Proceedings of the 7th International Conference on Thermal Analysis, 1982.

To be published:

S.H. Anderson and D.D.L. Chung, "Exfoliation of Intercalated Graphite," Synth Met.

S.H. Anderson and D.D.L. Chung, "Kinetics of Intercalation of Bromine in Graphite," Carbon.

R. Gangwar and D.D.L. Chung, "Intercalation of Iodine Monochloride in Graphite Fibers," Carbon.

INTERACTIONS

Spoken Papers

15th Biennial Conference on Carbon, Philadelphia, PA, June 22-26, 1981

S.H. Anderson, H.H. Lee and D.D.L. Chung, "Stage Dependence of the Exfoliation of Intercalated Graphite"

S.H. Anderson and D.D.L. Chung, "Stage Evolution During Intercalation"

TMS-AIME Fall Meeting, Louisville, KY, Oct. 11-15, 1981

S.H. Anderson and D.D.L. Chung, "Exfoliation of Intercalated Graphite"

11th Annual Conference of the North American Thermal Analysis Society, New Orleans LA, Oct. 19-21, 1981

S.H. Anderson and D.D.L. Chung, "Thermogravimetric Analysis of the Kinetics of Intercalate Desorption from Graphite Intercalation Compounds"

S.H. Anderson, H.H. Lee and D.D.L. Chung, "Thermal Acoustic Emission: Study of the Exfoliation of Graphite"

Annual Meeting of AIME, Dallas, TX, Feb. 15-18, 1982

S.H. Anderson and D.D.L. Chung, "X-ray Studies of the Kinetics of the Intercalation of Graphite"

General Meeting of the American Physical Society, Dallas, TX, March 8-11, 1982

D.D.L. Chung and S.H. Anderson, "Time-Temperature-Transformation Diagram for Stage Formation During Intercalation of Graphite with Br_2"

S.H. Anderson and D.D.L. Chung, "Exfoliation of Bromine-Graphite Intercalation Compounds"